University of Trento

Doctoral school in Cognitive and Brain Science (XXXI cycle)

Ph.D. Dissertation

Assessing functional connectivity in the newborn brain using fNIRS

Mariagrazia Popeo

Advisor: Angelo Bifone

Co-Advisor: Matteo Caffini

Submitted in partial fulfillment of the requirements for the degree of

Doctor of Philosophy in Cognitive and Brain Sciences

A.A. 2015-2018

Table of contents

Abstract

Functional connectivity represents a powerful approach to describe the intrinsic activity of the brain. It reveals the organization and correlations among anatomically separated regions supporting similar cognitive and sensory processes. Using functional Magnetic Resonance Imaging (fMRI), the recurrent spatial characteristics of these patterns have been extensively explored in the adult brain and their disruption has been found to be associated with psychiatric and developmental disorders. Unveiling the processes of emergence of resting state networks at a very early stage of life could shed light on the neuronal origins of these diseases. However, the study of the inception and development of functional connectivity in the newborn brain poses exceptional challenges, due to the complexity of dealing with non-compliant subjects. To this end, cortical activity at birth can be investigated using functional Near Infrared Spectroscopy (fNIRS) that represents a promising non-invasive neuroimaging method for developmental studies.

In the present thesis, I applied fNIRS to assess functional connectivity in term neonates. The first part of the dissertation is dedicated to investigating the maturation of a specific resting state network, the Default Mode Network, within the first 48 hours of life. The study aimed to examine its emergence, for the first time, using optical imaging on newborns immediately after birth. While the majority of fMRI literature focused on large-scale spatial patterns, I took a different approach measuring an intrinsic and localized fingerprint feature of the network, consistently detected in adult subjects.

In the second part of the dissertation, I aimed at improving the anatomical representation of brain connectivity, inferred only from signals collected at the scalp. Thus, I developed and validated a method for the reconstruction of spatially distributed functional signals on a dedicate template for term newborn subjects. The intent is to promote the shift from a *sensor space* description (one signal for each channel) to a *source space* representation in which the origin of the signal is reconstructed with better anatomical fidelity. The reliability of the reconstruction method was tested on synthetic and real data. In the former case, I simulated spatially correlated neural activity in the cortex, thus enabling assessment of the reconstructed images against a ground-truth map.

Analyses of functional connectivity in both sensor and source space showed that the Default Mode Network is still immature at birth, with a lack of homotopic correlation in the lateral parietal cortices, and no evidence of anticorrelation with the Dorsal Attention Network, a well established feature in the adult brain.

Overall the work presented in the thesis contributes to the understanding of functional connectivity in the infant's brain and provides useful tools for source-based connectivity analysis and for probe design and optimization.

Keywords: functional connectivity, fNIRS, image reconstruction, neonates, optical imaging.

Preface

The human brain can be depicted as a fascinating complex system consisting of functionally specialized regions continuously sharing information with each other. Unveiling the structure of these complex networks might provide a key to understand the functional organization of the brain and the interplay between functional segregation and integration. Since the 19th century, imaging techniques have been developed to explore and measure brain dynamics non-invasively, thus providing a new, powerful means of investigation. Considerable progresses have been made in this direction since the advent of functional Magnetic Resonance Imaging (fMRI) that paved the way to the description of the brain organization through the functional interactions between its components. Functional connectivity is defined as the temporal synchronization between spontaneous fluctuations of neuronal activity, registered at rest. Thus, in the absence of external inputs to the subject, the intrinsic brain activity can be captured. In this natural condition, as extensively demonstrated in numerous fMRI studies, correlations among anatomically separated regions emerge in the form of spatial patterns, which have been consistently described in adults. In healthy subjects, the resting state networks (RSNs) present recurrent characteristics while changes in their topology have been associated with the onset of various neurological or psychiatric diseases. Thus, the investigation of functional connectivity may prove to be important in order to understand the neural basis of certain disorders. In particular, there is a growing interest in the study of a specific RSN, the Default Mode Network (DMN), which has a potential role as a marker for developmental disorders, such as hyperactivity disorder or autism. For this reason, the exploration of the inception of functional connectivity at a very early stage of life - when the brain is highly plastic - may be decisive to plan early interventions. However, infants represent a challenging population to be investigated: most of the neuroimaging modalities employed in adults cannot be straightforwardly extended to non-compliant and non-verbal subjects. To this purpose, functional Near Infrared Spectroscopy (fNIRS) represents a promising option. This technique takes advantage of the relative transparency of human tissues to

light in the near infrared range (650 – 1000 nm) to investigate brain activity in a completely non-invasive way. Introducing light through the intact skull, optical imaging capitalizes on the absorption properties of the tissues to compute the localized variation in concentration of hemoglobin, in its oxygenated and deoxygenated form. These changes are associated with the vascular response to fluctuations in the underlying neuronal activity. During the measurement, sources are positioned adjacent to the scalp, introducing light through the intact skull. Detectors, placed few centimetres away from sources, register light that diffuses through the cortex. The pair of corresponding source and detector is referred to as channel. Considering the peculiar possibility to obtain measurements at the bedside and its non-invasiveness, fNIRS is extremely advantageous in developmental studies. However, especially in resting state studies in infants, functional connectivity is usually inferred only from signals collected at sensor position, one for each channel, resulting in a coarse description of the brain dynamics.

In my PhD project, I used fNIRS to explore functional connectivity in the neonates' brain from multiple perspectives. Firstly, I conducted a functional connectivity study on a sample of term newborns, recruiting subjects at the Rovereto's Hospital (Italy). Specifically, I investigated the inception of the DMN focusing on specific features of this network. Additionally, I developed methods to map functionally connectivity patterns on a finely-grained anatomical template, thus moving from a sensor-based analysis to a source-based representation with improved anatomical localization. Importantly, I devised a strategy, based on synthetic data, to validate my reconstruction approach against a ground-truth.

My thesis is organized as follows.

Chapter 1 is dedicated to introducing the concept of functional connectivity. Firstly, the structure and plasticity of the brain immediately after birth are briefly explained, in order to highlight the importance of this specific stage of development. Then, the approach of functional connectivity to explore the brain functional organization is presented. The focus is directed on the study of emerging resting state networks, and particularly of the DMN. The literature on the maturation of DMN at this stage of life is reviewed and discussed, to provide a framework to my work. Lastly, the tailored approach I chose to investigate the state of DMN at birth is described.

In Chapter 2, the fNIRS technique is introduced as an alternative neuroimaging methodology to fMRI for the study of functional connectivity in developmental age. The

physical principles of optical imaging and the different instruments in use are explained. The advantages and limitations of fNIRS in studies on neonates are illustrated through the comparison with other neuroimaging modalities. In this section, the problem of image reconstruction is illustrated, and the forward and inverse problems are mathematically described.

Chapter 3 is dedicated to presenting a resting state study I conducted using fNIRS on term neonates. The aim of the work was to investigate whether it is already possible to detect a mature DMN at birth. Specifically, all subjects were scanned within their first two days of life. We hypothesize the capability to identify the emergence of the network exploiting a localized feature consistently registered in adults. The areas of interest are probed with a sparse 20-channels array. In this chapter the experimental details of the study, as well as the results, are illustrated.

Finally, the study behind Chapter 4 arises from the opportunity to improve the description of functional connectivity, usually obtained in the sensor space, with a representation in the sources space. To this purpose, the reconstruction of spatially distributed functional signals is validated on a dedicated anatomical template with synthetic signals and real datasets, including the one presented in Chapter 3 and a second one provided by collaborators from University of Tokyo (Prof. Gentaro Taga and his research group). The process is tested under different experimental conditions, in order to establish the impact of various factors that are determinant during acquisitions on infants.

Finally, the future perspectives of my work are summarised and discussed.

1 Shedding light on the newborn's brain: a challenge

The very first stage of life is critically decisive for the development of the human brain. Due to its extreme plasticity, the neonate's brain undergoes rapid changes that may be determinant for the future growth of the individual. Understanding structure and organization of this biological evolving system during the first days and months of life remains a challenge. Recent advances in neuroimaging methodologies, such as Magnetic Resonance Imaging (MRI) or Near Infrared Spectroscopy (NIRS), provide a powerful means to acquire structural and functional information on the adult human brain *in vivo* and non-invasively. Extension of these methods to the study of the baby's brain holds considerable promise to discern the principles governing the brain development during the very early phase of life. A recent special issue of the Neuroimage Journal (Huang H., Huppi P., He Y., 2019) explored progresses and future perspectives in the baby brain imaging, demonstrating the increasing attention to the topic by the scientific community. This chapter is intended to present the state of art of newborns' brain investigation with neuroimaging methods, focusing on the emergence and development of its functional organization.

1.1 The infant brain, a complex and vulnerable system

The study of the human early brain development represents a fascinating as much as challenging research field. The postnatal brain can be conceptualized as an extremely complex system because of its continuous evolution and rearrangement. The formation of neural circuits effectively starts in the first trimester of pregnancy through intense neurogenesis and neural migration (Bystron, Blakemore, & Rakic, 2008). The process intensifies during the mid and late gestational period when an abundant synaptogenesis and axonal growth are the predominant mechanisms (Webb, Monk, & Nelson, 2001). By the end of pregnancy, the most of white matter connections have been settled, forming an

almost complete structural connectome. Synaptogenesis continues after birth, with a peak level of synapses reached at 2 to 3 years of age, followed by gradual and selective pruning (elimination of redundant synapses), a process that is thought to rebalance the excessive number of connections and to shape mature neural circuits (Keunen, Counsell, & Benders, 2017). Genetically programmed events, as well as external stimuli and experiences are responsible for the reshaping of the system architecture. Thus, different kind of processes contribute - within a constantly changing context - to the formation and organization of neural circuits (Stiles & Jernigan, 2010). The plasticity that characterizes the brain at this stage enables rapid structural and functional transformation, but at the same time makes it vulnerable to maladaptation (Gao, Lin, Grewen, & Gilmore, 2017), with the subsequent risk of a severe impairment of the normal growth of the system. Unveiling the principles of the brain organization in the infancy may be important to understand abnormal development. Indeed, it has been demonstrated that neuronal and psychiatric disorders, like Autism or Schizophrenia, may originate at early stages of brain maturation (Beardslee, Chien, & Bell, 2011): in such cases, recognizing the risk and being able to program an intervention during critical periods is of crucial importance (Figure 1.1).

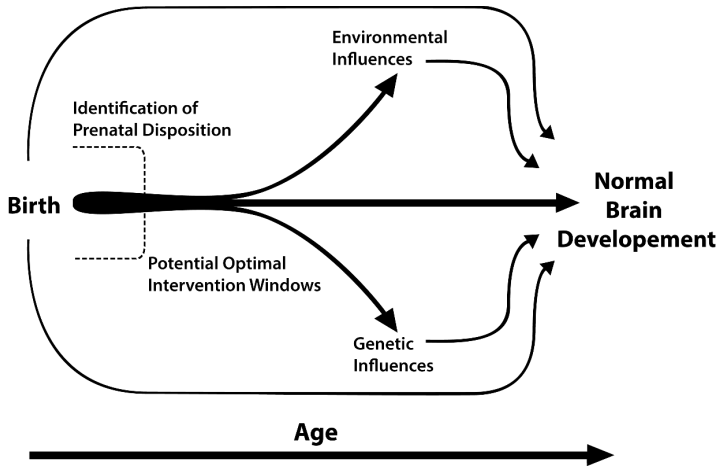

Figure 1.1 The illustration schematically emphasizes the strong dependence of brain development on gene-environment interaction, and highlights how an early intervention, in a narrow time window, could increase the probability for the subject to restore a normal trajectory of brain development. (The figure has been inspired by (Gao et al., 2017))

1.2 Functional connectivity approach to study the brain

Different imaging modalities can be applied to study function and structure of the brain. In particular, functional neuroimaging refers to a specific category of techniques able to measure localized physiological changes related to neural activity. Some of them take advantage of variation in cerebral blood flow to detect "activated" areas of the brain; on the contrary, some others rely on electrical or magnetic effects. In last decades, with technical advancements of imaging modalities (for instance, in terms of instrumentation, or of spatial and temporal resolution), it has been possible to gain precious insights into the formation and emergence of neural patterns and networks at different scales (Sporns, Tononi, & Kötter, 2005). At the dawn of imaging neuroscience, the attention focused on strengthening the theory about the centrality of functional segregation as a fundamental principle in brain organization. The segregation idea is grounded on specialization of anatomically separated brain areas for certain functions (Friston, 2011). Recently, the interest has shifted toward the comprehension of functional integration, to understand the connection between distinct areas and how they communicate with each other. The field has experienced a leap forward with the diffusion, in the last decades, of functional magnetic resonance imaging (fMRI). fMRI represents a powerful and non-invasive tool to investigate neural activity *in vivo*. Briefly, the method works under the assumption that regional variations in blood flow are linked to different levels of neural activity. As it will be explained later in section 2.2, the activation of a cortical area determines a local increment of blood flow, thus increasing the fraction of oxygenated hemoglobin over deoxygenated hemoglobin, with respect to baseline conditions. Exploiting the paramagnetic property of deoxyhemoglobin, fMRI uses the blood oxygenation level-dependent (BOLD) contrast to gain information on brain activity (Logothetis & Pfeuffer, 2004; Raichle & Mintun, 2006). Since its inception, fMRI has been instrumental for the mapping of task-related brain responses, i.e. region-specific activations evoked by specific stimuli. Here, instead, we will dwell especially on a more recent field of study opened by investigation of the brain "at rest" - in the absence of any external stimuli or task performance requests. In these cases, the subject lays still in the scanner for several minutes, without any presented stimulus, while fMRI signals are acquired on a continuous basis. In 1995 Biswal et al. (Biswal, Yetkin, Haughton, & Hyde, 1995) published the seminal observation that spontaneous fluctuations of the BOLD signal, recorded by fMRI

in the brain at rest, could not be classified as simple noise, but presented significant correlation between functionally related regions. This finding has paved the way to the study of the brain "functional connectivity" and its organization in distributed networks of functionally interconnected regions.

We generally refer to the expression "functional connectivity" (FC) to account for the estimation of the statistical interdependence of neuronal activity of anatomically separated brain regions (Friston, 2011). Thus, the study of functional connectivity enables mapping the large-scale cerebral organization and is thought to give information on the level of communication between cerebral areas. Interestingly, correlated spontaneous activity is organized in groups of anatomically separated brain regions. These emerging spatial patterns have been consistently observed in individuals and are usually referred to as resting-state networks (RSN) or intrinsic networks (Beckmann, DeLuca, Devlin, & Smith, 2005; Damoiseaux et al., 2006; De Luca, Beckmann, De Stefano, Matthews, & Smith, 2006; S. M. Smith et al., 2009; van den Heuvel & Hulshoff Pol, 2010). Functional connectivity studies have robustly identified a number of distinct resting-state networks in the adult human brain (De Luca, Smith, De Stefano, Federico, & Matthews, 2005). Furthermore, the description of homologous networks in other species, like rodents or monkeys, indicates that RSNs represent a core feature of the mammalian brain organization (Becerra, Pendse, Chang, Bishop, & Borsook, 2011; Vincent et al., 2007). Most of the observed functional RSNs overlap with activation networks involving areas with similar functions, simultaneously emerging during task-based experiments. Motor and visual networks, associated to analogous regions of the cortex, provide shining examples. Moreover, the pattern formed of the superior temporal insular and postcentral cortex consists of areas usually involved in auditory functions and the group of regions consisting of dorsolateral prefrontal cortex and superior parietal cortex are active together during memory tasks (Figure 1.2 illustrates the organization of some of the most studied RSNs). Contribution to the BOLD signal correlation is only given by low frequencies, in the range [0.01 – 0.1 Hz] and this explains the reason why we usually refer to "slow fluctuations" of spontaneous activity. In this way, noise due to scanner drifts ($<$ 0.01 Hz) and physiological components – like respiration ($\sim$ 0.3 Hz) and cardiac ($\sim$ 1.0 Hz) - are discarded.

Extraction of functional connectivity networks from resting state measurements is not

trivial, due to the absence of a task that could represent a reference for the analysis. Different approaches can be used to recognize the emergence of spatial patterns and infer the functional connectivity of the brain system. The most immediate is known as seed-based correlation analysis - or Region of Interest based-analysis (ROI) - and is based on the simple computation of correlation between the so called *seed*, which is the BOLD time course representative of a single voxel or of a small region, and all the other voxels or nodes of the brain. The resulting information is a map, showing regions of the brain that present coherent neural activity with respect to the chosen seed: we refer to these as functionally correlated areas. The connectivity matrix, which defines correlations between all possible seed regions in the brain, is widely used to explore global connectivity. The ROI-based approach was used to support the very first evidence of RSN (Biswal et al., 1995), and has been widely used in functional connectivity studies for its intuitive interpretation. However, its dependence on an *a priori* hypothesis (the choice of a specific region of reference) could represent a disadvantage. Indeed, the analysis allows to consider only one seed at time and to evaluate one network at time. Moreover, seed positioning may be affected by anatomical and functional differences among individual subjects.

Data-driven analysis methods, like Independent Component Analysis (ICA), offer the possibility to avoid an *a priori* choice and unveil the data structure (van de Ven, Formisano, Prvulovic, Roeder, & Linden, 2004). In this case, the signal is decomposed into statistically independent components, each one with an associated spatial map – the functional network - and a time course. In this way, the procedure allows to identify simultaneously all possible measurable spatial patterns. The origin of the coherence can have neural bases, be attributable to physiological noise or just represent a mere result of neuroimaging artifacts. Differently from seed-based methods, the ICA algorithm does not rely on specific hypothesis regarding the region of interest and can be used to identify and remove components related with noise. On the other hand, the interpretation of components is often not unique, and the identified networks may depend on input parameters, like the total number of components the algorithm should discern (Lv et al., 2018). ICA and ROI-based are not the only available approaches to the analysis of spatial connected patterns, but they are the most representative and widespread ones; the choice to specifically present them also depends on the necessity to illustrate and compare previous results in literature.

Spatial patterns measured at rest are strongly consistent among individuals and different analysis methods (Joel, Caffo, van Zijl, & Pekar, 2011), pointing out a solid functional interaction between anatomically separated brain regions (Figure 1.2).

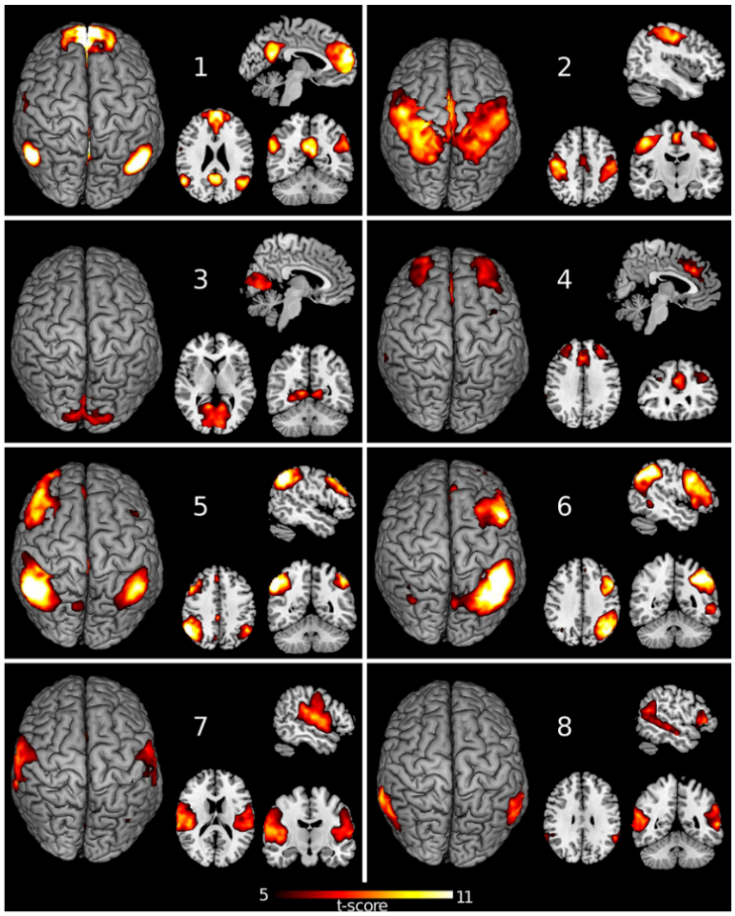

Figure 1.2 In figure, some of the most commonly described resting state spatial networks in literature are shown. Here, results from ICA analysis show: the Default Mode Network (1), the sensorimotor network (2), mesial visual network (3), executive control network (4), fronto-parietal networks (5-6), auditory network (7), temporo parietal network (8). The figure is taken from (Rosazza & Minati, 2011).

Hence, functional connectivity is a robust concept to describe architecture's cerebral organization in healthy subjects. Consequently, functional connectivity could also be a powerful tool to reveal alterations linked to neurological and psychiatric disease. Disconnectivity phenomena, in the form of decreases in correlation, have been registered within specific networks (M. D. Fox & Greicius, 2010). To name but a few, decreases in connectivity of the Default Mode Network have been measured in Alzheimer disease and schizophrenia (Supekar, Menon, Rubin, Musen, & Greicius, 2008)(Liang et al., 2006); aberrant connectivity within the Salience Network – composed of the anterior insula and

dorsal anterior cingulate cortex - has been shown in frontotemporal dementia (Seeley, Crawford, Zhou, Miller, & Greicius, 2009), and within the somatosensory network in multiple sclerosis (Lowe et al., 2002). Whether these alterations in functional connectivity are disease-specific and sufficiently robust and reproducible to represent a viable diagnostic or prognostic marker remains the object of active investigation.

1.3 Functional connectivity at a very early stage of development

An increasing number of studies highlighted the pivotal role of functional connectivity in developmental disorders. Various papers have focused on RSNs alterations in autistic subjects, finding weaker connectivity within the Default Mode Network (Redcay et al., 2013; Weng et al., 2010); on the other hand, in subjects affected by attention-deficit hyperactivity disorder (ADHD), alteration in Default Mode Network arises together with an increased connectivity in the salience network (Castellanos & Aoki, 2016; L. Wang et al., 2009). Hence, investigation of functional connectivity at an early stage of life and during early brain development may provide a key to interpret the neuro-functional mechanisms underlying these impairments and a tool to help planning interventions during the critical period.

In last years, significant insights into the development of resting state brain connectivity have been derived from research on both prenatal and post-natal life stage with fMRI methods. For instance, a few studies on healthy fetuses (Schöpf, Kasprian, Brugger, & Prayer, 2012; Thomason et al., 2013) revealed the emergence of bilateral functional networks since 24 weeks' gestational age, observing an increase of inter-hemispheric connections toward birth age, from a medial to lateral direction (Thomason et al., 2013, 2015). Research in prenatal period, implemented only recently, help to give some background to previous studies on postnatal age.

The first paper on functional connectivity in the early period after birth was published a decade ago (Fransson et al., 2007). Fransson and colleagues studied a small population of sedated preterm infants, scanned using fMRI methods, and were able to identify five functional networks (out of at least eight described in adults) in visual cortex, bilateral sensorimotor and auditory regions, precuneus area, lateral parietal and dorsolateral prefrontal cortex. Consistent results were found in a subsequent study on term, naturally sleeping, infants; even though the sedation seemed not to affect outcomes (Fransson et

al., 2009), it appears as a strong limitation of the technique. Later, in preterm infants scanned at term-equivalent age, a full repertoire of the major resting state networks in adults, including executive control and the most studied default mode network, was reported (Doria et al., 2010). Therefore, it emerged that functional patterns evolved from immature and fragmentary RSNs in preterm infants (Smyser et al., 2010a) into facsimiles – at different levels of similarity - of adult complex networks after *ex utero* brain development. Although contradicting results on bilaterality and symmetry of RSNs have been reported (Liu, Flax, Guise, Sukul, & Benasich, 2008), these works shed light on the evidence that several of the most recurrent resting state networks, already described in adults, start maturing during the last trimester of gestation, before the acquisition of cognitive competencies. However, the dynamics of growth differs from one network to another. Specifically, it appears that the development of functional networks is associated not only to already established genetic mechanisms (such as synaptogenesis or myelination), but also to the behavioural functions to which they are associated. As proof of this, networks involved in auditory or visual processes are fully matured at birth, revealing a structure comparable to the adult one, while networks linked to higher order functions could appear still fragmented at the end of the first postnatal year (Gao et al., 2014; Keunen et al., 2017). Even though studies presented above start delineating the general development within the first two years of life, the organization of functional connectivity immediately after birth – which represents the critical period window for interventions – has not been completely defined. In particular, we will focus on the Default Mode Network, one of the most observed RSNs in adults, which has been associated with developmental disorders (as highlighted at the beginning of the section). Surprisingly, the literature on this topic depicts an inconsistent scenario, thus prompting further research and exploration of new methods and tools.

1.3.1 Focus on Default Mode Network after birth

The Default Mode Network (DMN) was first identified as a group of brain areas that simultaneously decreased their activity (or "deactivated") during specific task conditions with respect to rest condition (Fransson, 2005; M. D. Greicius, Krasnow, Reiss, & Menon,

2003; Shine & Breakspear, 2018; Uddin, Clare Kelly, Biswal, Xavier Castellanos, & Milham, 2009). The definition, based on activation/deactivation mechanisms, depended on the close link of analyses and interpretations to a task-based reference model. After resting state fMRI methods were established, it appeared that this set of regions usually present correlated spontaneous activity, and may form a brain system *per se*. The anatomical configuration of the network is considerably consistent in literature, regardless of neuroimaging approaches or analysis methods used. It comprises the bilateral parietal cortex, precuneus/posterior cingulate cortex and lateral and medial prefrontal cortex (Raichle et al., 2001; van den Heuvel, Mandl, Kahn, & Hulshoff Pol, 2009).

DMN has been associated with spontaneous cognition and introspective thoughts. Indeed, regions involved in the network show increased activity during passive cognitive processes, but decreased activation during externally goal-directed activities (Buckner, Andrews-Hanna, & Schacter, 2008; Raichle et al., 2001). Subsequent studies have shown that a variety of situations involving active tasks engage the DMN areas. By way of example, recall of past events, imagination about the future (prospection) and conceiving the viewpoint of others (theory of mind) reflect the emergence of the set of regions classified within the DMN (Buckner & Carroll, 2007). The strength of connections between regions of networks decreases in deep sleep, as confirmed by Electroencephalogram (EEG) measurements, reflecting maybe alterations in consciousness (Horovitz et al., 2009). This suggests a strong relationship of detected DMN with intrinsic brain states.

Recently, neuroscience research is devoting closer attention to understanding the role of this network in the functional architecture of the healthy brain and the effects of diseases on its organization. In adults, evidences of disruption, abnormal reduction or increase in DMN connections have been found in schizophrenia, Alzheimer's disease and depression (M. Greicius, 2008). Moreover, the study of this network have an impact also on neurodevelopmental disorders. Nevertheless, for decades the majority of literature on DMN has focused on adult subjects. Reaching a deep comprehension of the stage of development at which the Default Mode Network emerges and how it evolves could provide insights into the explanation of neuronal origins of these disorder (Gao et al., 2009) and, more importantly, could help programming early intervention.

Even though the field is in its infancy, some studies have been conducted with the aim to unravel developmental mechanisms of functional connectivity in the very first years of

life (Gao et al., 2011, 2013; J. K. Smith et al., 2014). Nevertheless, to date, we still do not have a clear grasp of the state of DMN immediately after the birth. In one of the first whole-brain studies in newborns, Fransson and colleagues scanned a small sample of preterm neonates of 41 weeks of age (Fransson et al., 2007).

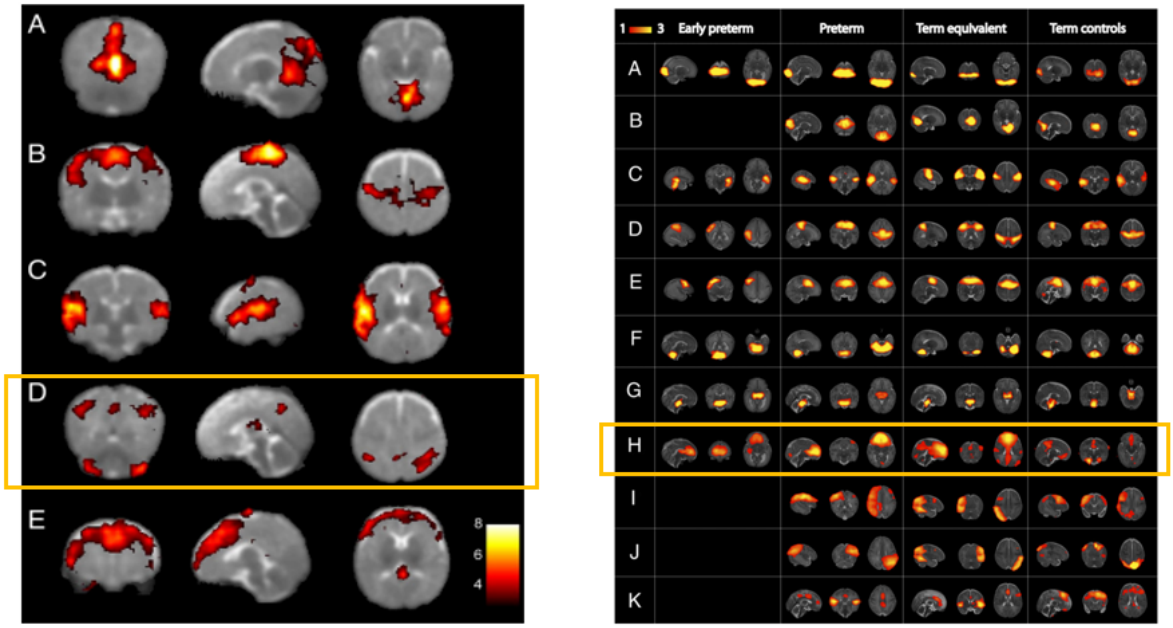

Figure 1.3 Results from different connectivity studies. On the left, a group analysis on early preterm neonates scanned at term equivalent age is reported (Fransson et al., 2007). ICA analysis revealed the presence of five main networks. The one (D) in yellow is considered a predecessor of DMN, because it partially resembles the spatial pattern observed in adults. On the right, Doria et al. (Doria et al., 2010) compared spontaneous activity patterns – corresponding to independent components from ICA – obtained in early preterm, preterm and term equivalent to those from term controls ones. They were able to detect several resting state networks: medial visual (A), lateral visual (B), auditory (C), somatosensory (D), motor (E), cerebellum (F), brainstem and thalami (G), default mode (H), dorsal visual stream (left and right components) (I and J), and executive control (K). The DMN (highlighted in yellow) varies with age, but shows a complete pattern in term equivalent and term controls subjects.

Their analyses of resting state data from slightly sedated and sleeping infants failed to discern a complete spatial pattern of Default Mode Network. However, strong functional connectivity between the bilateral parietal cortex and the precuneus/posterior cingulate cortex was detected. This configuration resembled in a certain way the posterior part of the pattern registered in adults and it was identified as a “proto” default mode network, to remark the incomplete similarity with the adult one (Figure 1.3).

This result was confirmed by subsequent work, in which the analyses were replicated on a larger set of term, naturally sleeping infants, to test the effects of the relative immaturity of the preterm brain (Fransson et al., 2009). Additionally, an incomplete pattern of DMN was observed in 2 weeks-old subjects, whereas a more complex and similar to adults network architecture was detected in 2 years-olds (Gao et al., 2009). This could support the idea that Default Mode Network is experience-dependent and matures gradually through infancy, in parallel with the development of cognitive competences. On the contrary, Doria and others (2010) suggested that the complex network of DMN may develop even before term (Figure 1.3). They collected BOLD resting-state fMRI data from infants at 29 to 43 weeks Post Menstrual Age (PMA) and divided them in three subsets (early preterm, preterm and term-equivalent). Data- and hypothesis- driven analyses demonstrated that DMN develops from an immature and incomplete network in preterm infants into a very similar version of the adult network at term (Doria et al., 2010). The discordant results could be due to a different analysis pipeline. Indeed, in their works, Fransson and others (2007, 2009) used probabilistic ICA without a precise time-resolved anatomical template brain, while Doria and colleagues performed accurate co-registration before ICA computation. In the latter case, the use of a 4D template for registration of correlation maps might have improved the ability to reliably delineate the development of the DMN.

1.3.2 A new approach to the study of DMN in neonate: motivation of the study

The state of art reveals a discordant scenario about the capability to detect a mature DMN at a very early stage of life and suggests the urgency of further investigation in the field. To date, almost all attempts to inspect the emergence of the network are directed at the investigation of a spatial pattern, which is well known from measurements in adults. However, the confounding scenario delineated before raises some doubts about the effectiveness of an investigation only based on the quest of a complete spatial pattern.
The core of the present thesis work revolves around the study of the DMN in term infants within two days from birth using functional Near Infrared Spectroscopy, a technique that measures a hemodynamic readout akin to the BOLD signal in fMRI, but is more amenable

to non-compliant subjects like the newborn baby. We hypothesize that exploration of DMN can be conducted through its interaction with other networks. We would take advantage of *a priori* information from adult subjects. Generally, positive correlations have been observed between functionally related brain regions, and negative ones between brain regions showing theoretically opposed functional roles (M. D. Greicius et al., 2003; Kelly, Uddin, Biswal, Castellanos, & Milham, 2008). More specifically, regions showing an increase of activity during attention-demanding tasks (task-positive regions) are positively correlated among themselves, and negatively correlated with regions that exhibit decreases in activity (task-negative regions) (M. D. Fox, Zhang, Snyder, & Raichle, 2009). Resting state fMRI studies (M. D. Fox et al., 2005; Fransson, 2005) highlighted a remarkable presence of anticorrelated spontaneous activity between these networks, even without any task. Specifically, negative correlations have been detected between DMN and dorsal attention network in adults at rest (Figure 1.4). The dorsal attention network (DAN) is bilaterally organized and includes the intraparietal sulcus (IPS) and the frontal eye fields (FEF) in each hemisphere (Corbetta & Shulman, 2002). While DMN is linked to internally directed processes, DAN controls cognitive functions linked to external attention-demanding stimuli.

The observed opposing relationship between spontaneous fluctuations is therefore coherent with the contrasting neural functions of the two networks (Corbetta & Shulman, 2002), and can be interpreted as an adaptive mechanism able to balance the switch between introspective and extrospectively oriented processes (Dixon, Andrews-Hanna, Spreng, Irving, & Christoff, 2016; M. D. Fox et al., 2005). The consistency and variability of this behaviour has been widely investigated (Dixon et al., 2016) in healthy adults (Keller et al., 2015) and in developmental period from childhood to young adulthood (Chai, Ofen, Gabrieli, & Whitfield-Gabrieli, 2014). The interaction between these networks in paediatric population has been addressed by only one study (Gao et al., 2013). Specifically, Gao and others analysed resting state fMRI data from a large cohort of paediatric subjects, divided by age in three subsets (3 weeks, 1-year and 2-years old). A seed-based analysis was conducted, using the posterior cingulate cortex (PCC) and the intraparietal sulcus (IPS) as seed regions for the Default and Dorsal networks, respectively. While the study failed in detecting negative network interactions in 3-week old subjects, synchronization between the networks was observed at 1 year, with a

remarkable increase in the second year of life. This result, consistent with previous findings (Gao et al., 2009), suggests that networks structure might be immature at birth.

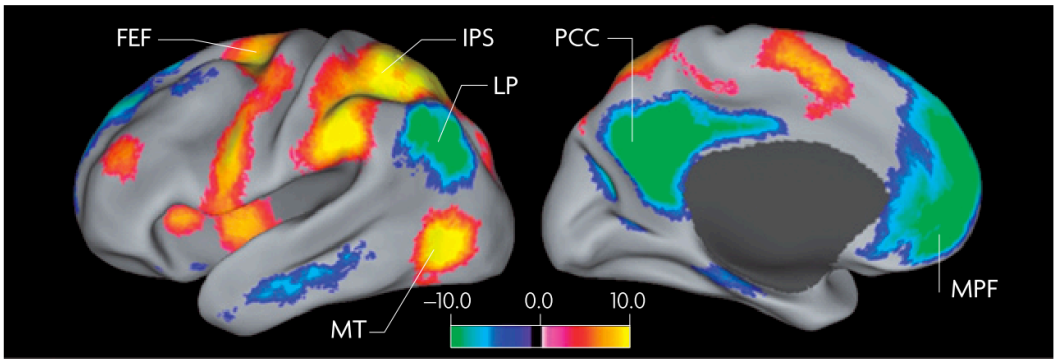

Figure 1.4 Negative correlations at rest between areas of dorsal attention network - which comprises the intra-parietal sulcus (IPS), frontal eye field (FEF) and middle temporal region (MT) – indicated with hot colours and areas of Default Mode Network – which comprises lateral parietal cortex (LP), medial prefrontal cortex (MPF) and posterior cingulate (PCC) - indicated with cold colours. Figure is taken from the review of (M. D. Fox & Raichle, 2007)

Alternatively, these patterns and their interaction may be present at birth in an embryonic form, but approaches based on mapping the spatially-extended networks in their entirety may not be effective in a pediatric population. Indeed, studies performed during the first two postnatal years show that the two networks (DMN and DAN) develop together, and so does their interaction, thus indicating a strong interdependence already at their inception. Hence, interactions between the systems underlying these networks may develop before mature, adult-like spatial patterns for the DMN and the DAN are observed.

To the best of our knowledge, no direct assessment in newborns has been performed yet. Indeed, functional neuroimaging studies in infant remain challenging. Neonates represent an extremely vulnerable and non-compliant population. While fMRI has been established as the “gold standard” for neuroimaging, ushering in a new era in developmental studies, it presents substantial disadvantages for the investigation of infants. To name but a few, the request of immobilization during the scan, obtained by restraint or sedation, loud scanner noise and safety issues in a non-verbal population represent important

limitations. All these factors, which will be tackled in detail below, motivate our choice of a different technique to probe at term neonates.

2 Principles of functional Near Infrared Spectroscopy

A promising alternative to fMRI for probing infants' brain is offered by functional Near – Infrared Spectroscopy (fNIRS). This recent technique exploits principles of optical spectroscopy to measure the hemodynamic response of the human brain to external stimuli. fNIRS uses optical fibres to inject (sources) and collect (detector) light to and from tissues. Light is introduced at the scalp and penetrates the skull and cerebrospinal fluid to reach cerebral cortex. Finally, it is registered, in a reflectance geometry, by a photodetector positioned at a fixed distance from the source. Physical effects due to the interaction with biological tissues will cause light attenuation, from which concentration changes of molecules involved in hemodynamic response process will be computed. With these basis, it is possible to non-invasively probe brain activity in humans (Bunce, Izzetoglu, Izzetoglu, Onaral, & Pourrezaei, 2006).

In the present section, the general history, theoretical principles and comparisons with other neuroimaging modalities will be overviewed, in order to present advantages and potential issues for the use of fNIRS in cognitive science, with an emphasis on developmental studies.

2.1 Optical imaging evolution

> "*On December 28, 1976 our family menu featured a grilled chuck roast, the poor academic's substitute for steak. This very American cut of beef still contains part of the shoulder blade of the steer, a flat piece of bone perhaps 3 or 4 mm thick, about the same as the human skull. […] We held the pink object up against the light and noticed that the shadow of a finger could easily be noted in the diffuse red light coming through the bone. If red light could, then certainly NIR light at the longer wavelengths would penetrate the human skull and provide access to the brain.*"
>
> *Jöbsis, 1979* (Jöbsis-vanderVliet, 1999)

As highlighted by Scholkmann in his review, the use of transmitted light through the body as a tool to probe human tissues started in the 1800 (Scholkmann et al., 2014). Halfway through the century, scientists were capable to describe spectra of oxyhemoglobin (HbO) and deoxyhemoglobin (HHb) (Perutz, 1995), which both play a central role in light absorption, as we will see in section 2.2. However, only in 1977, with the publication of his seminal paper (Jobsis, 1977), Jöbsis used the fundamentals of spectroscopy to lay the foundation for a new neuroimaging technique. The guiding principle relies on the relative transparency of biological tissues to light in the near infrared range of the optical spectrum - the so-called "biological window". Under this assumption, Jöbsis demonstrated the feasibility to record cerebral activity *in vivo*, from measurements of concentrations of oxyhemoglobin and deoxyhemoglobin. First evidences were obtained by trans-illuminating the head of an anesthetized cat and human adult voluntary hyperventilating (Jobsis, 1977): the era of near infrared spectroscopy (NIRS) applications had just started. Since 1980, first prototypes of NIRS machines (usually single-channel systems) were used to measure oxygenation and hemodynamic brain parameters in animals (Giannini, Ferrari, Carpi, & Fasella, 1982), human adults (Ferrari, Giannini, Sideri, & Zanette, 1985) and later newborn infants (Ferrari, de Marchis, & Giannini, 1986). Interestingly, in 1993, four studies on the application of NIRS principles to functional brain imaging were almost simultaneously published by different research groups (Chance, Zhuang, UnAh, Alter, & Lipton, 1993; Hoshi & Tamura, 1993; Kato, Kamei, Takashima, & Ozaki, 1993; Villringer, Planck, Hock, Schleinkofer, & Dirnagl, 1993). For the first time, a single-channel fNIRS was employed to probe cortical oxygenation changes (regularly registering an increase in HbO and decrease in HHb), in response to various cognitive tasks. Soon, the technique was extended to investigate more brain regions simultaneously, to obtain spatially resolved map of cerebral activity, for research and clinical purposes. Over time fNIRS instrumentations rapidly evolved, with a substantial increase in the number of available measurements channels. In parallel, a great effort was made to describe, from a theoretical and experimental standpoint, how the light spread in the brain. Studies on phantoms and simulated head models, combined with technological advances enabling production of high-density machines with hundreds of channels, paved the way to a tomographic approach and to the optical reconstruction of three-dimensional volumes. To date, wearable and wireless devices have further

enhanced the portability of the technique, strengthening the potential of optical imaging, which has been established as a popular neuroimaging tool in several research fields.

2.2 Measuring activity in the brain using fNIRS

Functional optical imaging exploits changes in optical properties of biological tissues that occur in response to external stimuli. In more detail: a certain amount of energy in the form of adenosine triphosphate (ATP) is necessary to support the sequence of physiological events localized in brain areas involved in stimulus processing. ATP is mostly produced by a mechanism that needs glucose and oxygen, constantly delivered to the tissues by blood supply. During neuronal activation, a considerable supply of energy is required to support the electrochemical processes; the greater amount of oxygen and glucose consumed determines a localized vascular response, with increases in cerebral blood flow (CBF) and cerebral blood volume (CBV). This process is driven by neurovascular coupling. The brain region engaged by the stimulation is provided, within a few seconds from the activation, by a supply of oxygen – transported by the hemoglobin – and glucose. It would be plausible to think that the demand of oxygen from blood cells leads to an increase in deoxyhemoglobin (HHb) concentration with a subsequent decrease in oxyhemoglobin (HbO) concentration. However, the quantity of total transferred oxygen is higher than that consumed in the process, with a net imbalance between the CBF and oxygen consumption (P. T. Fox & Raichle, 1986). This excess translates into a relative increase of oxygenated form of hemoglobin and a decrease of deoxygenated one, which characterizes in a recognisable way the hemodynamic response. The relation between physiological changes and neural activation is the guiding principle of some brain imaging methods (Buxton, Wong, & Frank, 1998). In the case of MRI, the magnetic properties of hemoglobin depend on the oxygenation state of its iron-containing heme group. As a result, the mismatch in magnetic susceptibility between the blood compartment and the brain tissue is different for oxygenated and deoxygenated blood. Hence, the activation-induced hemodynamic response modulates the local Magnetic Resonance signal: this is the basis of the blood oxygenation level-dependent (BOLD) signal measured from fMRI.

Optical imaging allows to determine the localized hemodynamic response from the computation of concentration variations in time of oxy- and deoxy- hemoglobin, which present different optical properties. The information is inferred from the attenuation of a beam of light, which is injected and subsequently detected at the scalp level. Light delivered into the biological tissue undergoes different processes. Photons interacting with the medium can be absorbed, e.g. depositing their energy in chromophores like the heme group of hemoglobin; alternatively, photons can be scattered (inelastically). The processes undergone by photons during their propagation into tissues depend on their wavelength and optical properties of the tissue. The human tissue turns out to be relatively *transparent* to near infrared light. Indeed, observing its absorption spectra (Figure 2.1), it appears that, in the near infrared spectral range (650-950 nm), absorption coefficients[1] are low, allowing light to travel for several centimetres in the tissue. Water, which is one of the most important constituents of biological tissue, shows strong absorption in the ultraviolet part of the spectrum, or at longer wavelengths, mostly in the medium and far infrared range. Among all absorbers in the near infrared, the chromophores of HbO and HHb are the most important ones, even if weak. Other absorbers include melanin and lipids, but we can safely assume that their concentrations and properties are not affected significantly by neural activation. Conversely, changes in relative concentration of oxy- and deoxyhemoglobin have an effect on the optical response of the tissue. A focus on the optical window reveals that, at its boundaries, HbO and HHb have opposite behaviours, except the so-called isosbestic point, at which they exhibit the same absorption coefficient. In order to differentiate their contributions, it is necessary to investigate the tissue with light at two wavelengths, chosen at opposite sides of the isosbestic point. From measurements of light attenuation, changes of concentration of the two chromophores can be calculated using the Modified Beer Lambert Law (MBLL) (section 2.3). Considering the characteristics of biological tissues, a major contribution to the photon path is represented by scattering events, which happen more frequently with respect to absorption, with an estimated proportion of 100:1 (Delpy & Cope, 1997). The capability of light to penetrate tissues guarantees the feasibility of optical imaging to

[1] Absorption and scattering coefficient defined optical properties of a medium. These quantities indicate, respectively, the mean free path travelled by the photon before being absorbed or scattered. They are expressed in mm^{-1}.

investigate *in vivo* brain activity: light injected at the scalp level travels a few centimetres deep into tissues passing through the skull and the cerebrospinal fluid (CSF) to reach cortical regions. Laser diodes or light emitting diodes are typically used as light sources, while photomultipliers or avalanche photo-diodes enable sensitive measurement of attenuated light diffusing back to the scalp. The penetration depth depends on the relative positions of source and detector – which form what is referred to as a *channel.* Photon migration models have been applied to estimate the value of penetration depth, approximatively from a third to half the distance between source and detector, in adults heads (Cui, Kumar, & Chance, 2005).

The definition of the optimal distance between source and detector is not trivial, because its choice is based on a number of factors, such as age of the subject or brain area to probe. Generally, in infants, this distance varies from 2 to 3 cm, while in adults usually increases -from 3 to 5 cm- due to different anatomical characteristics (e.g. the thickness of scalp and skull). Light travels through the scalp and diverse layers of tissues before reaching the cortex and on its way back to the detector. Thus, the signal collected contains hemodynamic response from the cortical arear, physiological and measurement noise, but also superficial physiological contributions. If the distance between coupled source and detector is less than 1 cm, the resulting signal does not contain cortical information anymore, but it is informative only of the physiological activity in the superficial layers of the head. On the contrary, an increase in the channel distance beyond the optimal separation induces a remarkable decrease in the signal quality (lower Signal To Noise Ratio value) (Calderon-Arnulphi, Alaraj, & Slavin, 2009).

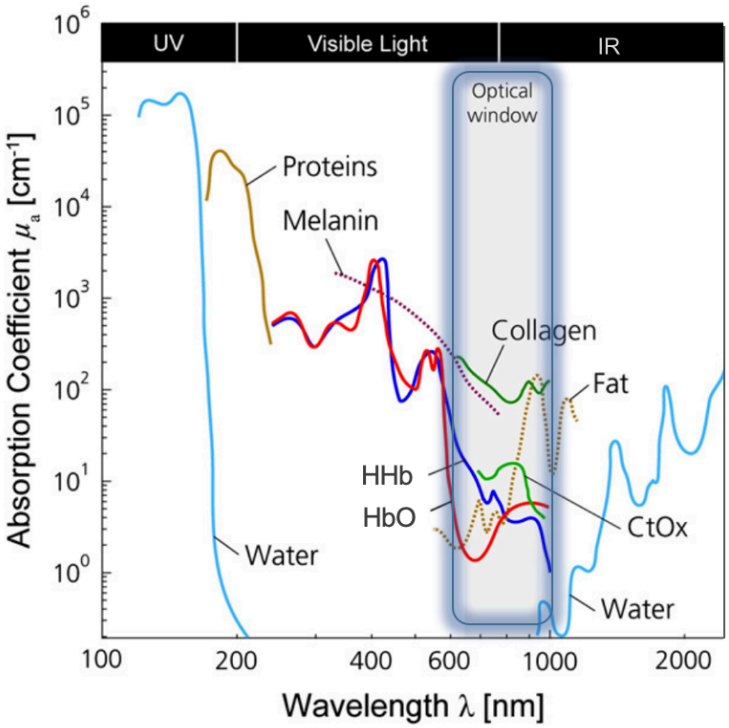

Figure 2.1 Absorption spectra of principal components of human tissue. In the highlighted optical window, oxy- and deoxy-hemoglobin are the most important absorbers. Indeed, collagen, lipid and melanin concentration are constant in time, while cytochrome oxydase is present in negligible quantities. Water, which is an important component of tissues, shows peaks outside the near infrared range. Figure has been adapted from (Scholkmann et al., 2014)

Because of scattering events, part of the photons injected at a point source is scattered backwards towards the scalp, where it can be detected, following a "banana-shaped" path (Figure 2.2). These photons can provide information on the tissue they pass through in their journey from source to detector.

More than one light source can be associated to each detector, enabling measurements in different regions or at different distances. The arrangement of all sources and detectors (forming the so-called optical probe) is usually bundled in a cap or strip, which is designed according to measurements needs and to fit the subject's head. The disposition of available optodes is crucial for the investigation of the right brain areas of interest.

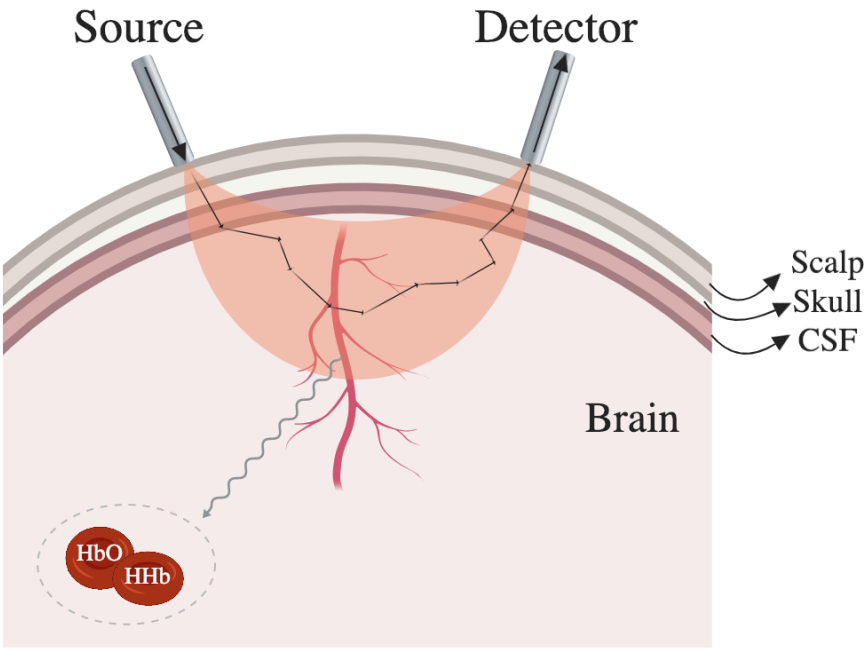

Figure 2.2 Light is introduced from a source at the scalp and travels through scalp, skull, CSF before reaching the brain. The figure shows events of scattering that affect the photon path (resembling a random walk path). Illustration, not in scale, highlights the interaction of HbO and HHb chromophores with light that will cause the attenuation recorded at the detector. The characteristic shape of the diffuse beam has been reproduced.

2.3 Modified Beer Lambert Law

Local changes in blood oxygenation can be informative about the neural activity and its evolution in time. After irradiating the tissue, optical imaging uses measurements of light that diffuses back to the scalp to compute the concentrations of oxy- and deoxy-hemoglobin. The Beer – Lambert Law relates the final attenuation of light to concentration of the chromophore and path travelled from the radiation in the tissue.

Let's imagine to illuminate a volume of a non-scattering medium (the chromophore) of thickness d using a beam of light with incoming intensity I_0. The medium partially absorbs the radiation, thus the attenuation of the outgoing intensity I can be modelled as follows:

$$I = I_0 e^{-\mu_a(\lambda)\cdot d} = I_0 e^{-c\cdot\varepsilon(\lambda)\cdot d} \qquad Eq.\ 1$$

where the absorption coefficient μ_a can be expressed as the product of concentration c of the illuminated chromophore and the molar extinction coefficient ε, which depends on

the wavelength in use. The distance travelled in the medium by the light represents the *optical distance*, indicated with *d*.

The attenuation, or optical density (OD), is the logarithm of the ratio between the intensity of light introduced I_0 and the intensity I detected:

$$OD = -log\frac{I}{I_0} = c \cdot \varepsilon(\lambda) \cdot d \qquad \textit{Eq. 2}$$

However, the biological tissue is a highly scattering medium; thus, it is necessary to take also into account the contribution of the diffusion process in light propagation. For these reason, Delpy et al. (Delpy et al., 1988) formulated the Modified Beer Lambert Law, which describes the relationship between attenuation, properties of the chromophore and both absorption and scattering events:

$$I = I_0 e^{-(\mu_a(\lambda)+\mu_s(\lambda))\cdot d} \qquad \textit{Eq. 3}$$

where $\mu_s(\lambda)$ indicates the scattering coefficient. By grouping separately the effects of absorption and scattering, it is possible to model the process:

$$OD = -c \cdot \varepsilon(\lambda) \cdot d \cdot DPF(\lambda) + G(\lambda) \qquad \textit{Eq. 4}$$

where *DPF* is the differential path-length factor, introduced to take into consideration the longer paths (with respect to source-detector distance) travelled by the photon due to scattering events. In fNIRS measurements, the latter process is responsible of the fact that a number of photons, after various scattering events, are scattered backwards toward the scalp, where they can be detected (reflectance geometry). Instead, $G(\lambda)$ is defined as the losses term and depends on $\mu_s(\lambda)$ and *d.*

In order to capture the changes of concentrations due to brain activity, the variation in time of *OD* has to be computed. For small physiological changes, $G(\lambda)$ and $DPF(\lambda)$ can be assumed constant. Calculating the difference between OD at time t_1 and t_2, the MBLL can be expressed as:

$$\Delta OD = OD_{t_2} - OD_{t_1} = \Delta c \cdot \varepsilon(\lambda) \cdot d \cdot DPF(\lambda) \qquad \textit{Eq. 5}$$

and consequently:

$$\Delta c = -\frac{\Delta OD}{\varepsilon(\lambda) \cdot d \cdot DPF(\lambda)} \qquad \textit{Eq. 6}$$

At the end, changes in concentration of the chromophore depends on the specific wavelength.

As explained before, within the "biological window", hemoglobin represents the main absorber in biological tissue, but it could be present in two different oxygenation states, with different absorption properties. Introducing HbO and HHb as specific chromophore references, MBLL equation can be written as:

$$\Delta OD = \left(\varepsilon(\lambda)^{HbO}\Delta[HbO] + \varepsilon(\lambda)^{HHb}\Delta[HHb]\right) \cdot d \cdot DPF(\lambda) \qquad \textit{Eq. 7}$$

In order to solve the problem and obtain the unknown variations of oxy- and deoxy-haemoglobin concentration, two wavelengths are necessary. In matrix form:

$$\begin{bmatrix} \Delta[HHb] \\ \Delta[HbO] \end{bmatrix} = d^{-1} \begin{bmatrix} \varepsilon(\lambda_1)^{HHb} & \varepsilon(\lambda_1)^{HbO} \\ \varepsilon(\lambda_2)^{HHb} & \varepsilon(\lambda_2)^{HbO} \end{bmatrix}^{-1} X \begin{bmatrix} \frac{\Delta OD(\lambda_1)}{DPF(\lambda_1)} \\ \frac{\Delta OD(\lambda_2)}{DPF(\lambda_2)} \end{bmatrix} \qquad \textit{Eq. 8}$$

Distance between source and detector d is well known while DPF are available from tabulations. Thus, concentrations of HbO and HHb at the two chosen wavelengths can be obtained using measurements of attenuated intensity obtained at the scalp.

2.4 fNIRS instrumentations

The different NIRS instrumentations on the market can be classified in three categories on the basis of the illumination scheme used: continuous wave (CW), frequency-domain (FD) and time-domain (TD) modality. Potentialities and limitations of each modality will be briefly described.

2.4.1 Continuous wave fNIRS

The most common CW technique injects light of constant intensity and measures the attenuation of transmitted light. To date, continuous wave instrumentations represent the majority of the available devices on the market, due to their ease of use, portability and affordability. Systems are equipped with a variable number of sources (laser diodes or LED's) and detectors (avalanche photodiodes). The sampling rate usually varies in a range between 5 and 10 Hz (even though in same cases can reach hundreds of Hz) and a multiplexing technology – in time and/or frequency- allows discrimination of signals from different sources and at different wavelengths. In the first case, diodes are switched on and off in specific time intervals; in the second, light is modulated with different frequencies when all diodes are turned on (Scholkmann et al., 2014). However, assuming the contribution of scattering constant in time, in continuous wave modality only changes in concentration of HbO and HHb can be computed (see Eq. 8). A complete overview of the development of CW devices is reported in (Ferrari & Quaresima, 2012).

2.4.2 Frequency-domain fNIRS

The peculiarity of frequency-domain systems is the use of intensity-modulated light sources (sinusoidal, 10 – 100 MHz). From the computation of the attenuated mean intensity, the modulated amplitude and the phase shift of the light collected at detector position, absolute values of absorption and reduced scattering coefficients can be estimated using multidistance systems.

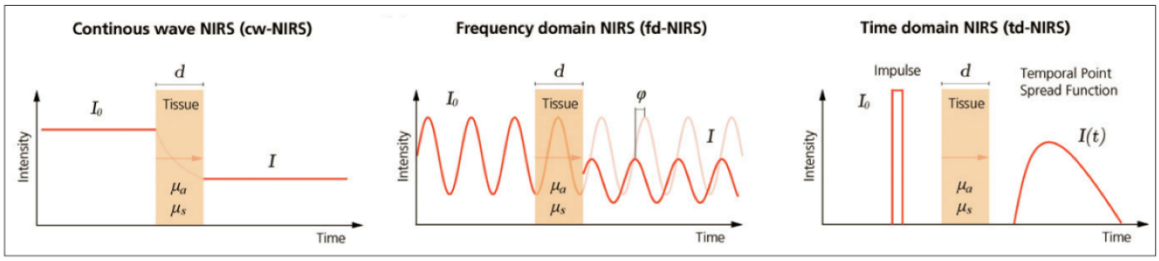

Figure 2.3 Schematic illustration of different modalities of fNIRS. Light is injected (I_0) in a medium of width d characterized by optical properties characterized by absorption $\mu_a(\lambda)$and scattering $\mu_s(\lambda)$coefficients. Intensity of emitted light I is detected in reflectance geometry. In frequency domain also phase delay φ is measured. The figure is taken from (Scholkmann and Wolf, 2012).

Thus, one of the advantages of FD modality is the capability to differentiate the information on optical properties: the absorption coefficient provides information about constituents of the media, while the scattering coefficient informs on its structure. Using the resulting values, it is possible to compute absolute values of the chromophores concentrations (Fantini, 1995; Wolf et al., 2008a). FD systems are able to provide more parameters with respects to CW machines, with a better signal SNR. However, it should be considered the impact of the higher cost and, sometimes, of the fewer available channels that could determine a worsening in experimental conditions with respect to CW instrumentations (see description of ISS Imagent machine in section 3.3.1).

2.4.3 Time-domain fNIRS

Spectroscopy in the time domain relies on the measurement of the photon time of flight distribution (or temporal point spread function, TPSF). After the introduction into the tissue of a very short pulse of light (~ 100 ps, generally using lasers), the shape of time of flight distribution of the photons contains information about the interaction between light and medium. Absorption is responsible for the attenuation, while scattering broadens the TPSF (Torricelli et al., 2014). In this way, absolute values of absorption and reduced scattering coefficient can be computed, similarly to multidistance FD-fNIRS systems. Moreover, studying the time of arrival of the photons gives information about the penetration depth: photons arrived later have undergone more scattering events, so they have a higher probability to have investigated deeper areas of the brain. On the contrary,

photons arriving early more likely carry information about the superficial tissue layers. The approach guarantees high sensitivity (due to the photon counting modality) and direct information on depth penetration; however, relatively expensive and less portable instrumentations may represent significant disadvantages for its use in a clinical environment.

2.5 Neuroimaging techniques for infant brain: why optical imaging?

The main interest guiding the present thesis work is the investigation of functional connectivity in the infant brain at rest. The choice of the most suitable method to conduct studies in this field is not taken for granted as much as one could think. Indeed, several neuroimaging techniques are available for resting state studies on adults, but many of them cannot be straightforwardly applied to infants (Aslin & Mehler, 2005; Aslin, Shukla, & Emberson, 2015). Briefly overviewing the peculiar technical specifications of most popular neuroimaging approaches will help to point out relative fNIRS advantages and limitations.

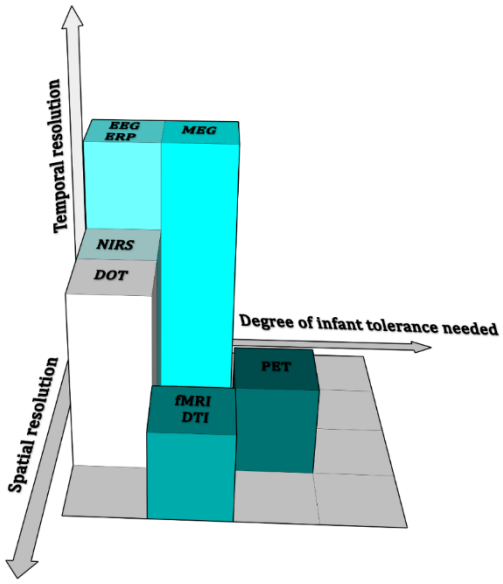

Figure 2.4 Representation of a qualitative comparison between different neuroimaging methods in use, on the basis of various technical parameters. With a low degree of tolerance required from the infant subject and a good trade-off between spatial and temporal resolution, fNIRS represents a promising alternative to the most popular fMRI and EEG for developmental studies. The figure has been inspired by (Lloyd-Fox et al., 2015)

Generally, measurement of cerebral activity can be conducted directly, using electrical or magnetic fields generated by neurons- in the case of EEG and magnetoencephalography (MEG) or indirectly measuring the hemodynamic response, like fMRI and fNIRS, or the metabolic response, like positron emission tomography (PET).

In the last decade, a considerable number of resting state studies in newborns has been conducted using fMRI. This methodology enables non-invasive measurement with good spatial resolution (~ mm) and has understandably become the reference standard for the neuroscience community. With a robust and reproducible signal, this

technique is capable to simultaneously map multiple networks, thus providing a rich description of spatially distributed whole brain activity. However, a limited acquisition rate determines a lower temporal resolution for fMRI compared to fNIRS that, on the contrary, acquires data up to hundreds of Hertz (Huppert, Hoge, Diamond, Franceschini, & Boas, 2006). This produces a more detailed temporal description of hemodynamic response in optical imaging. Furthermore, fMRI presents disadvantages during acquisition that should not be underestimated, in particular for conducting studies involving human paediatric population. Firstly, fMRI necessitates the baby to remain still and restrained for at least 20 min. In many studies (Souweidane et al., 1999; Yamada et al., 2003), sedation is used to complete the measurements and this condition is not always acceptable, especially in healthy infants. Acquisitions in such a vulnerable population are usually conducted during natural sleep of subjects, that could be disturbed by the acoustic noise generated from MRI machine gradients (Mohammadi-Nejad et al., 2018). Moreover, it is problematic to manage the safety issues regarding the MR scanner in non-verbal subjects. Sudden movements are frequent during the newborns' sleep; dealing with these movement artifacts is difficult, also because of the limited tolerance of available motion correction algorithm to head displacements in resting state scans (Aslin et al., 2015). Finally, availability of research MR scanners in paediatric wards is extremely limited, and transportation of the subjects to radiological division represents a challenge for preterm and term newborns (White, Liao, Ferradal, Inder, & Culver, 2012). Thus, the technique is not completely suitable for studies included in a standard screening program or for frequent and repeated measurements on the same infant.

PET belongs to the family of indirect techniques, like fMRI, but is definitively more invasive. Indeed, it requires the injection in the body of a radioactive tracer and, exploiting the decay process, measures photons that are emitted. It is in general used for clinical studies - only one paper on early newborns has been reported (Thorngren-Jerneck et al., 2001) - and is not appropriate at all for investigating paediatric healthy population.

On the other hand, due to its non-invasiveness and high temporal resolution (~ ms), EEG is widely used for developmental studies especially in awake children, while still less employed for resting-state functional investigations at birth (Orekhova et al., 2014; Tokariev, Videman, Palva, & Vanhatalo, 2016). Cerebral communication is regulated by electrical signals between neural cells. EEG directly monitors the electrical brain activity by a number of electrodes placed at the scalp and distributed following specific

anatomical references. EEG measurements modality resembles the fNIRS procedure and guarantees harmless and comfortable acquisitions. However, the low spatial resolution represents the essential drawback of the technique: at the scalp the total contribution from thousands of neuronal electrical signals is registered. Thus, the capability to localize the cortical origin of brain activity is limited.

Ultimately, a word on MEG. This technique measures the feeble magnetic fields generated by electrical currents associated with neuronal activity, similarly to EGG, a direct measurements of brain activity. Despite the better spatial resolution, MEG, like fMRI, requires a high level of subject's tolerance and suffers from high cost of the recording instrument (Lloyd-Fox et al., 2015; Mohammadi-Nejad et al., 2018).

To sum up, with its good trade-off between spatial and temporal resolution, relative low-cost and ease of use in a non-compliant population, fNIRS represents a promising alternative for probing infants at a very early stage of life. As any other technique, some limiting factors are present. Above all, spatial resolution of ~2-3 cm is lower than fMRI (~ mm) and the depth of penetration depends on the thickness and specific optical properties of superficial tissues (Fukui, Ajichi, & Okada, 2003). For most devices the number of channels is modest (typically tens) and a sparse array hampers the ability to explore extended networks. Moreover, fNIRS can only detect activity from the surface of the cortex, leaving out of range all medial-brain regions (like the hippocampus). In addition, the fNIRS signal is contaminated by non-neural contributes from scalp, skull and superficial veins that are crossed twice by the detected photons (Aslin et al., 2015). Lastly, it is not always possible to obtain a subject specific co-registered anatomical image. Considering the lower spatial resolution and the difficulty to cover and explore the whole-brain dynamics, fNIRS is unlikely to replace the versatility of fMRI for basic research, but offers substantial advantages for large screening studies in vulnerable populations. First, it is silent and portable. This is fundamental for measurements on preterm and term newborns because allows comfortable bedside acquisitions in neonatal unit care, without any acoustic noise (White et al., 2012). From a practical point of view, the cap fixes sources and detectors to the scalp without requirement of rigid head stabilization, thus enabling measurement with fewer constrictions on subjects than fMRI. This consents long-time continuous measurements (monitoring) and repeated acquisitions within short intervals (Wolf et al., 2008b). fNIRS can also estimate concentration changes in both oxy- and deoxy-hemoglobin, adding further information to the BOLD fMRI signal.

Moreover, infants are very suitable for fNIRS techniques because of their smaller head size, thinner skull and minimal hair, all of which increase sensitivity compared to adults. Technological advances in instrumentations ensure the possibility to obtain a dense probe with higher number of channels enabling multiple source-detectors measurements. High-density arrays of diffuse optical tomography (DOT) allow the regression of contributions of superficial layers, with a more reliable resulting signal, and the computation of volumetric images providing informative maps of hemodynamic activity. As qualitatively evidenced in Figure 2.4, spatial resolution is higher with respect to the typical fNIRS systems and almost comparable to fMRI (Eggebrecht et al., 2012; Hassanpour et al., 2014). DOT presents all advantages of optical imaging and is optimal to probe infant brain functions at bedside, in regular nurseries or intensive care units (Ferradal et al., 2015; White et al., 2012); nevertheless, DOT systems in use often cannot guarantee a complete coverage of the head because of difficulties to manage the ergonomics of the cap.

2.6 Image reconstruction problem in optical imaging

As highlighted in section 2.5, one of the major drawbacks of optical neuroimaging is the lack of anatomical reference and a subsequent non-immediate reconstruction of cortical origins of the signal. However, using a reference anatomy and with the information provided by multiple channels, it is possible to produce images of estimated cortical activations. In the first place, the process requires the ability to describe how light propagates in tissues, starting from a specific arrangement of sources and detector onto the scalp. The process of modelling light transmission from sources to detectors is defined as *photon migration*. After having established the conditions that model the phenomenon, we can predict variations in measurements at each channel, given a localized change in a baseline set of optical properties. The relationship between change in optical properties and change in measurements can be linearly approximated by a sensitivity matrix that is computed from the photon migration models (*forward model*). Image reconstruction can be performed by solving the *inverse model*, which describes the relationship between changes in detected signals and changes in optical properties of the tissue, and is generally regarded as an ill-posed problem.

2.6.1 Modelling light propagation: the forward problem

The simplified method previously illustrated (section 2.3) can be considered valid under the assumption of constant scattering in a medium that therefore is approximated as homogeneous. Unfortunately, the human brain, constituted of various layers with different optical properties, cannot be straightforwardly assumed as homogeneous. The description of photon migration in the tissue is a complex problem that requires some approximations. The process could be accurately modelled using the transport theory, a more direct approach with respect to the Maxwell's equations (Vilain, 2014). To this purpose, the Radiative Transport Equation (RTE) represents a realistic physical model based on energy conservation (Lihong V. Wang & Wu, 2009):

$$\frac{1}{c}\frac{\partial L(\boldsymbol{r},\boldsymbol{s},t)}{\partial t} = -\boldsymbol{s}\cdot\nabla L(\boldsymbol{r},\boldsymbol{s},t) - (\mu_s+\mu_a)\cdot L(\boldsymbol{r},\boldsymbol{s},t) + \mu_s\int_{4\pi} L(\boldsymbol{r},\boldsymbol{s}',t)\cdot P(\boldsymbol{s}',\boldsymbol{s})d\Omega' + S(\boldsymbol{r},\boldsymbol{s},t) \qquad \textit{Eq. 9}$$

The term at the left side of the equation describes the energy change over time, with c indicating the speed of light and $L(\boldsymbol{r},\boldsymbol{s},t)$ the radiance at position $\mathbf{r}$ oriented as the unit vector $\mathbf{s}$; the term $-\boldsymbol{s}\cdot\nabla L(\boldsymbol{r},\boldsymbol{s},t)$ is due to energy flow; $-(\mu_s+\mu_a)\cdot L(\boldsymbol{r},\boldsymbol{s},t)$ indicates the loss of energy due to absorption and scattering contributions; $+\mu_s\int_{4\pi} L(\boldsymbol{r},\boldsymbol{s},t)\cdot P(\boldsymbol{s}',\boldsymbol{s})d\Omega'$ is an increase of energy from radiation scattered in the direction $\mathbf{s}$ with the term $P(\boldsymbol{s}',\boldsymbol{s})$ representing the phase function, thus the probability that a photon coming from the directions $\mathbf{s}$ is scattered in the direction $\boldsymbol{s}'$ into a solid angle $d\Omega'$; lastly, $+S(\boldsymbol{r},\boldsymbol{s},t)$ is the contribution from a source in the volume at the position $\mathbf{r}$. However, the RTE equation is still too complex and requires an onerous computational effort to be solved.
In the case of biological tissues, under the assumptions of albedo[2] ~ 1 and radiance almost isotropic after a small number of scattering events, light propagation can be modelled by the diffusion approximation of the RTE equation. Here, truncating the expansion in spherical harmonics of the radiance at the first order it is possible to obtain:

[2] The albedo indicates the ratio between scattering coefficient and the sum of scattering and absorption coefficient.

$$L(\boldsymbol{r}, \boldsymbol{s}, t) = \frac{1}{4\pi}\Phi(\boldsymbol{r}, t) + \frac{3}{4\pi}\boldsymbol{J}(\boldsymbol{r}, t) \cdot \boldsymbol{s} \qquad \textit{Eq. 10}$$

where $\Phi(\boldsymbol{r}, t)$ is the photon fluence and $\boldsymbol{J}(\boldsymbol{r}, t)$ is the photon flux (energy flow per unit area per unit time). In a highly scattering medium like biological tissue, changes in photon flux are small during the transport mean free time, and the photon flux can be described using Fick's law:

$$\boldsymbol{J}(\boldsymbol{r}, t) = \frac{1}{3(\mu_{s\prime} + \mu_a)}\nabla\Phi(\boldsymbol{r}, t) \qquad \textit{Eq. 11}$$

where $\mu_{s\prime}$ is the reduced scattering coefficient, depending on the scattering coefficient and anisotropy value.

Assuming this and indicating $D = \frac{1}{3(\mu_{s\prime}+\mu_a)}$, after the substitution of the terms in RTE the diffusion equation (DE) has the form:

$$\frac{\partial\Phi(\boldsymbol{r}, t)}{c\partial t} + \mu_a\Phi(\boldsymbol{r}, t) - D\nabla^2\Phi(\boldsymbol{r}, t) = S(\boldsymbol{r}, t) \qquad \textit{Eq. 12}$$

In the presence of very simple geometries, DE can be solved through analytical methods, using Green's functions. However, the human head is a complex multi-layered object, for which the solution of light propagation models needs numerical methods. A representative example is the Finite Element Model (FEM), which approximates solutions for a volumetric finite mesh, subdividing the whole object of interest into subsets – the finite elements – modelled by simpler equations (Arridge, Schweiger, Hiraoka, & Delpy, 1993). Various other methods have been described in literature, such as the boundary element method (BEM) (Arridge et al., 1993) or finite difference method (Pogue, Patterson, Jiang, & Paulsen, 1995) and automatic software solvers have been developed.

Alternatively, statistical methods like Monte Carlo can simulate the path travelled by single photons into the medium, without any assumption on diffusion (Fang, 2010). For this reason, this method is highly reliable, in particular way in correspondence of tissues boundaries or regions with very low scattering (such as CSF). The only disadvantage is the computational cost that can be highly demanding (Fang & Boas, 2009).

2.6.2 Inverse problem

According to Arridge (Arridge & Schweiger, 1997), the forward problem in optical imaging is expressed as follows:

Given a distribution of light sources $\boldsymbol{q}$ *on the boundary* ∂V *of an object V and a distribution of optical parameters* $\boldsymbol{p}$ *within V, find the resulting measurement set* $\boldsymbol{M}$ *on* ∂V.

$$\boldsymbol{M} = F(\boldsymbol{p}) \qquad \textit{Eq. 13}$$

where F is a nonlinear mapping operator which allows to move from the space of optical parameters (referred to as source space) to the space of measurements (or sensor space). Specifically, F is the model of photon propagation, which allows the prediction of measurements in the forward model process once given a well-known set of optical parameters.

In a similar way, the inverse problem can be stated as follows:

Given a distribution of light sources $\boldsymbol{q}$ *and a distribution of measurements* $\boldsymbol{M}$ *on* ∂V *derive the optical parameters distribution* $\boldsymbol{p}$ *within V.*

$$\boldsymbol{p} = F^{-1}(\boldsymbol{M}) \qquad \textit{Eq. 14}$$

where the nonlinear operator F^{-1} here allows the mapping from the measurements space (signals collected at the scalp) to the tissue parameters one.

With a perturbative approach (Arridge & Hebden, 1997), if we have an estimate solution $\boldsymbol{p}_0$ that is close to the searched solution $\boldsymbol{p}$, Eq. 13 can be expanded in a Taylor series in $\boldsymbol{p}_0$:

$$\boldsymbol{M} = F(\boldsymbol{p}_0) + F'(\boldsymbol{p}_0)(\boldsymbol{p} - \boldsymbol{p}_0) + (\boldsymbol{p} - \boldsymbol{p}_0)^T F''(\boldsymbol{p}_0)(\boldsymbol{p} - \boldsymbol{p}_0) + \cdots \qquad \textit{Eq. 15}$$

where F' and F'' are the first and second order derivatives, respectively. In the discrete case, these derivatives are represented by the *Jacobian matrix* $\mathbf{J}$ and the *Hessian matrix* $\mathbf{H}$. Setting $\Delta\mathbf{M} = \mathbf{M} - \mathbf{M}_0 = F(\boldsymbol{p}) - F(\boldsymbol{p}_0)$ and $\Delta\boldsymbol{p} = \boldsymbol{p} - \boldsymbol{p}_0$:

$$\Delta \boldsymbol{M} = J\Delta \boldsymbol{p} + \Delta \boldsymbol{p}^T \boldsymbol{H} \Delta \boldsymbol{p} + \cdots \qquad \textit{Eq. 16}$$

Neglecting higher order terms, a linear approximation of the forward problem can be performed. At this point, solving the inverse problem consists in the inversion of the Jacobian matrix (or sensitivity matrix):

$$\Delta \mathbf{p} = \boldsymbol{J}^{-1} \Delta \boldsymbol{M} \qquad \textit{Eq. 17}$$

Assuming only absorption variation related to changes in hemoglobin concentration, $\Delta \boldsymbol{p}$ can be reduced to $\Delta \boldsymbol{\mu}_a$ (variation of absorption coefficient).

Considering small spatial variations of the absorption coefficient, the non-linearity of the diffusion absorption equation can be overcome using the Rytov approximation (Madsen, 2013). Thus, the perturbation in photon fluence, collected at detector *d* if only source *s* is turned on, is given by:

$$\Delta OD(\boldsymbol{r_s}, \boldsymbol{r_d}) = \frac{1}{\Phi_0(\boldsymbol{r_s}, \boldsymbol{r_d})} \int_V \Phi_s(\boldsymbol{r_s}, \boldsymbol{r}\,)\, \Delta \boldsymbol{\mu}_a(\boldsymbol{r}) \Phi_d(\boldsymbol{r}, \boldsymbol{r_d}) d\boldsymbol{r} \qquad \textit{Eq. 18}$$

where $\boldsymbol{r_s}$ and $\boldsymbol{r_d}$ represent, respectively, positions of light source and detector in the 3D volume of the head. The Monte Carlo method is used to obtain the fluence $\Phi_0(\boldsymbol{r_s}, \boldsymbol{r_d})$ estimated when only source s is on (Fang & Boas, 2009). The product of the fluence distribution $\Phi_s(\boldsymbol{r_s}, \boldsymbol{r_d})$ from the position of the light source and the fluence distribution $\Phi_d(\boldsymbol{r}, \boldsymbol{r_d})$ from the position of the detector is given by the three-points Green's function of diffusion absorption equation:

$$G(\boldsymbol{r_s}, \boldsymbol{r}, \boldsymbol{r_d}) = \Phi_s(\boldsymbol{r_s}, \boldsymbol{r}\,) \Phi_d(\boldsymbol{r}, \boldsymbol{r_d}) \qquad \textit{Eq. 19}$$

where $\boldsymbol{r}$ represents the position of a generic point in the 3D volume of the head. From now on, we will refer to the above Green's function as the *sensitivity profile,* which is computed for each source-detector pair.

With the previous assumption on absorption perturbation $\Delta \boldsymbol{\mu_a}$, the forward problem can be discretized and linearized. For a volume of N voxels (index *n*), S sources (index s) and

D detectors (index *d*) placed onto the scalp, the variation in photon fluence, registered at detector *d* if only source *s* is on, is given by:

$$\Delta OD_d^s = \frac{1}{\Phi_{d,0}^s} \sum_{n=0}^{N} G_{d,n}^s \Delta\mu_{a_n} \qquad \textit{Eq. 20}$$

When all S sources are turned on, the total change in fluence collected at detector *d* will result from the sum of all perturbation contributions.

Eq. 20 can be rewritten in the linear matrix form (Tremblay et al., 2018):

$$\underset{(m \times 1)}{\mathbf{\Delta OD}} = \underset{(m \times n)}{\mathbf{J}} \quad \underset{(n \times 1)}{\mathbf{\Delta\mu_a}} \qquad \textit{Eq. 21}$$

where $\mathbf{\Delta OD}$ is the optical density vector of measurements, for every *m* channel, and $\boldsymbol{\Delta\mu_a}$ is the absorption coefficient variation in the volume of *n* voxels. Each element of the Jacobian **J** matrix, known also as *sensitivity matrix*, is computed by combining all the Green's functions.

At this point, the only missing step to complete the inverse model is the computation of the inverse of the Jacobian matrix $\mathbf{J^{-1}}$. Since **J** matrix is far from being square, the inverse cannot be directly obtained. In order to invert the **J** matrix, it is necessary to use some regularization procedures (Engl, Hanke, & Neubauer, 1996)(Engl et al., 1996; Neumaier, 1998). The most common used approach is the Tikhonov regularization (Tikhonov, Goncharsky, Stepanov, & Yagola, 1995) applied to the Moore-Penrose pseudoinverse definition. In this way, the estimated $\Delta\hat{\mu}_a$ is:

$$\Delta\hat{\boldsymbol{\mu}}_a = \mathbf{J}^{\mathrm{T}}(\mathbf{J}\mathbf{J}^{\mathrm{T}} + \mathrm{k}\boldsymbol{\sigma}^2_{\mathbf{\Delta OD}})^{-1}\mathbf{\Delta OD} \qquad \textit{Eq. 22}$$

where k is a scalar regularization parameter and $\boldsymbol{\sigma}^2_{\mathbf{\Delta OD}}$ is the measurements covariance matrix, assumed to be diagonal (Caffini, 2009). The number of sources is usually largely superior to the number of sensors, thus the inversion problem still remains strongly ill-posed.

In order to solve the inverse problem, a detailed knowledge of the optical properties and anatomy should be provided (Boas & Dale, 2005; Guven, Yazici, Intes, & Chance, 2005).

The model reliability is then dependent on two main factors. First, geometric features of the object in which photon path is simulated, for instance when the Monte Carlo approach in used. In this case, models required for simulations consist in voxelized or volumetric mesh-based objects. Second, the goodness of the registration of sources and detectors position onto the object. Here, the challenge is the production of rigorous multilayers head models in which properties of different layers reflect the structure and optical characteristics of a real *in vivo* brain. An efficient option is to realize volumetric mesh-based models starting from subject-specific MRI structural images. Especially for infants studies these structural models are usually not available and optical head models are usually obtained from MRI atlases that are used to produce segmented 3D meshes.

2.7 Open issues

In conclusion, this chapter aimed to present principles and technical characteristics of optical imaging, and to describe its advantages, as well as limitations, in the investigation of neonates' brain. The good spatial and temporal resolution trade-off, as well as some practical aspects related to dealing with a vulnerable and non-compliant population, are decisive benefits. Indeed, the possibility to obtain long-term and silent measurements makes the technique ideal to perform functional connectivity studies at a very early stage of life.

In Chapter 3, the emergence of Default Mode Network is explored in term newborns with a frequency-domain fNIRS instrument. Subjects are scanned bedside within the first 48 hours of life. In our approach, we focused only on a specific part of the DMN (section 1.3.2) - without the need of a full coverage of the brain - and its anticorrelation with adjacent elements of the Dorsal Attention Network. Functional connectivity is examined through a correlation channel-based analysis. Indeed, typically fNIRS signals, collected by optodes at the scalp, are analysed directly. Almost all the few studies on infants – immediately after birth - reported in literature, provide a similar course-grained description of functional connectivity. Therefore, the interpretation of brain connectivity relies on a two dimensional description, obtained from channels acquisitions distributed onto the head (*sensor space*). Thus, the question arises – how to enrich the above picture, and improve anatomical localization of brain activity?

As highlighted in section 2.6, even though optical imaging does not provide anatomical information, the process of image reconstruction allows the definition of internal optical properties of tissues from intensity measurements acquired at the scalp. In lay terms, the method gives the opportunity to enhance the two dimensional description, with a three-dimensional map of the origins of hemodynamic response (*source space*). To date, only two resting-state fNIRS studies in newborns shifted the analysis from sensor to source space. White et al. (White et al., 2012) used DOT measurements in preterm and term infants to reconstruct functional connectivity maps. Using a high-density instrumentation, with 106 channels, they investigated primarily the occipital cortex. The method showed great potential also for clinical applications. Indeed, image reconstruction reliably reflected lesions due to occipital stroke that fMRI, acquired for the whole sample, revealed in one subject. A few years later, a different study on full term infants used an arrangement of almost 300 channels to probe a more extended brain area, which included occipital, temporal and parietal regions (Ferradal et al., 2015). As in the previous work, each participant was scanned using DOT and, subsequently, fMRI methods. The high degree of spatial agreement between connectivity maps – obtained respectively from fMRI and reconstructed DOT data of term newborns -confirmed the reliability of the process. However, in both works mentioned above, realistic head models were realized from subject-specific structural MRI images. This procedure is impracticable for large monitoring studies and undermines the benefits of the portability of fNIRS. Moreover, even if the fMRI technique represents the reference point for functional neuroimaging, it should be recognized the lack of a ground truth for functional connectivity patterns, and it remains unclear to what extent the resulting correlation map is influenced by different factors occurring in fNIRS measurements. To tackle this problem, I developed an approach based of the reconstruction of functional connectivity in the source space that is described in Chapter 4, alongside with its validation with synthetic and real data.

3 Investigation of functional connectivity in the neonate's brain using functional Near Infrared Spectroscopy

Aim of the present chapter is to present a functional connectivity study on neonates, scanned within their first two days of life. In particular, the work focused on the investigation of the emergence of the Default Mode Network using optical imaging. The DMN is anatomically distributed, and comprises regions, like the Precuneus, that are hardly accessible to fNIRS. Here, we have developed a probe that covers symmetrical regions of the parietal cortex. We aim to assess the presence of significant interhemispheric correlations between the left and right Lateral Parietal (LP) cortices, key components of the DMN. Moreover, we entertained the hypothesis that anticorrelations between LP and the Intra-Parietal Sulcus, an element of the Dorsal Attention network, may already exist at birth. This feature is consistently described in adults, and its observation would provide evidence of a mature functional connectivity structure of the DMN in our group of subjects. To this end, we explicitly account for negative correlations, often discarded in the analysis of resting state data. In this chapter, we report an analysis in the space of channels, to compare our results to previous studies. An extension of the analysis to the source space is reported in Chapter 4.

3.1 Introduction

The non-invasive use of light to probe the brain with fNIRS is a novel and promising methodology for studies in developmental age. As extensively discussed in Chapter 1, fNIRS instrumentation is silent and portable, allowing measurements in neonatal unit care without strict requirements on baby compliance. Moreover, neonate subjects are peculiarly suitable for optical imaging because they have a thinner scalp and less hair than adults, and bone calcification of the skull is still incomplete thus increasing the amount of

light that reaches cortical tissues (Engstro et al., 2009).

Previous studies, conducted both in adult and infant subjects, assessed the capability of optical imaging to efficiently describe resting state connectivity. Initially, functional connectivity in motor and visual areas have been registered with fNIRS in a small sample of healthy adult participants (White et al., 2009). Using seed-based correlations, the authors observed symmetrical functional responses, reflecting spatial characteristics of maps previously described with fMRI (Damoiseaux et al., 2006; De Luca et al., 2005). These results were later confirmed by Lu and others (Lu et al., 2010) in a study that probed the same areas. Data- and hypothesis-driven analyses at the group level confirmed the capability of fNIRS to reproduce the expected interhemispheric correlations and its feasibility for resting-state brain network detection. In addition to seed-based correlation, independent component analysis (White et al., 2012; Zhang et al., 2010) and whole-brain correlation analysis (Sasai et al., 2012) highlighted the consistency of fNIRS spatial patterns of correlating regions with fMRI maps extracted from the same areas.

As discussed in Chapter 1, fMRI is, to date, the reference neuroimaging technique for the inference of functional connectivity. Therefore, a valid strategy to test the reliability of the resting state fNIRS method is the comparison of its outcomes with fMRI-based studies, using both methods to acquire the same data (Niu & He, 2014). Particularly, the well-known network of Default Mode, as well as Dorsal Attention Frontoparietal Control, emerged from simultaneous fNIRS/fMRI acquisitions over the frontal, temporal and occipital cortices (Sasai et al., 2012). The experimental agreement, validated from different techniques, confirmed that resting state fNIRS signals are able to reflect spontaneous hemodynamic fluctuations from cortical regions and can be used as a valid tool to investigate dynamics of brain activity.

The demonstration of the feasibility of fNIRS for functional connectivity studies in adults is encouraging for the extension of the technique to the investigation of resting state in newborns. Exploring brain dynamics of sleeping term infants, Taga and others (Taga et al., 2000) measured spontaneous fluctuations in the cerebral oxygenation state. With a successful observation of functional connectivity at rest, they paved the way to measurements at different stages of development (Homae et al., 2010). Indeed, the analysis of fNIRS data from a cohort of neonates, 3-months and 6-months old subjects, revealed the capability of optical imaging to capture changes in cortical organization during development. Specifically, some cortical regions, as the temporal, parietal and

occipital, showed an increase of functional connectivity from birth to 6 months. On the other hand, regions such as the frontal areas, revealed a decrease in regional correlation, likely due to pruning of connections during development. Moreover, thanks to its portability, fNIRS has a potential as a bedside clinical tool because it allows measurements to be carried out in the nursery or in neonatal intensive care units (Ferradal et al., 2015; White et al., 2012). This enables the acquisition of scans on both term and preterm infants in their personal cradles while sleeping, within the very first few days or even hours of life, which is a substantial improvement compared to other available techniques.

Here, we used fNIRS to investigate the inception of DMN in the developmental brain. Indeed, its investigation at an early stage of life may provide important insights into the neuro-functional mechanisms underlying developmental disorders (Castellanos & Aoki, 2016; Redcay et al., 2013). The network has been described extensively in adults – both healthy subjects and patients - and explored in adolescences (McCormick & Telzer, 2018). However, whether a DMN-like network exists at birth remains controversial and the subject of active investigation. The majority of studies on resting state connectivity in early infants – with particular attention to the inception and evolution of DMN – have been performed using fMRI, in the attempt of registering the same spatial pattern already defined in adults. In this study, we tested the hypothesis of an effective existence of DMN at term age, avoiding the research of a recurrent spatial pattern and proposing an alternative approach, based on an *a priori* information of the relationship between DMN and task-positive networks. In fact, functional connectivity inferred at rest unveils an interaction between DMN and, Dorsal Attention Network (DAN) in the form of negative correlations (M. D. Fox et al., 2005), suggesting an inverse temporal modulation (M. D. Fox, Corbetta, Snyder, Vincent, & Raichle, 2006).

Under these assumptions, we focused on the capability to detect a signature of DMN immediately after birth. Further, we hypothesized that negative correlations, like those observed between DMN and DAN in adults, may already exist at a very early stage of life. Therefore, the detection of interhemispheric homotopic correlations between the symmetrical parietal regions of DMN, coupled with the finding of an intrahemispheric anti-correlation involving IPS within the DAN (and a consequent interhemispheric correlation between respective IPS), could account for the presence of DMN in an early post-natal brain. If confirmed, this study could provide evidence of the emergence (or lack thereof) of a DMN in the newborn brain.

To date, to the best of our knowledge, no resting state fNIRS studies on infants have yet focused precisely on the exploration of default mode network at this very early stage of development, specifically in the first two days of life. Here, we present and discuss results from a functional connectivity study on a sample of neonates subjects, all of them scanned within the first 48 hours of life, in a period which falls into the critical window for early intervention.

3.2 Choice of participants

The recruitment of the infant subjects, which we personally carried out, represented the most challenging and time-consuming factor of the present study and lasted approximately nine months. Considering the critical age of participants, the ethics commission of the University of Trento approved a rigid protocol for this study. The protocol dictated that no direct contact with future parents could be made before the hospitalization in the maternity ward. For this reason, the cohort could be recruited only after birth. Before presenting aims and methods of the study to the family, we performed a check of the medical records. First, we evaluated the Apgar score of the infant. The Apgar index quantifies the health of a neonate from the evaluation of five criteria (**A**ppearance, **P**ulse, **G**rimace, **A**ctivity, **R**espiration) and can vary from a minimum of 1 to a maximum of 10. The test is repeated 1 minute (Apgar 1) and 5 minutes (Apgar 5) after birth. A low value indicates that the neonate needs additional medical attention (Apgar, 2015). Only healthy newborns with normal Apgar Scores (7 and above) were selected. We also excluded mothers who experienced a high-risk pregnancy and / or serious pathologies (for instance, entailing intake of antibiotics).

Thirty healthy full-term infants were scanned in the nursery of Santa Maria del Carmine Hospital, in Rovereto (Italy). However, this number does not include recruited subjects on whom it was impossible to perform the measurement (for instance, because of a prolonged state of awakening, or continuous crying for discomfort, possibly induced by the fNIRS cap). In the next paragraphs, the reasons behind the exclusion of a consistent part of the scanned participants will be introduced.

3.3 Probe design and data collection

The intent of the work is to investigate of the DMN in newborns studying the emergence of a localized feature. Therefore, we defined a specific arrangement of sources and detectors with the aim to make the best use of the limited number of available channels, in order to ensure extended and homogeneous coverage of parietal areas and IPS. Sources and detectors were arranged in 2 hexagonal modules (

*Figure 3.1*a):this geometric disposition provided an optimal coverage of an almost rectangular area (White et al., 2012). Twenty channels in total, 10 for each hemisphere, probed regions of interest. The distance between coupled sources and detectors was fixed at 20 mm. We considered the 10-20 EEG system as reference for probe positioning (Jurcak, Tsuzuki, & Dan, 2007). Sources 2 and 16 were placed, respectively, coincident with C3 and C4 points while detectors 2 and 4 as close as possible to P3 and P4 points (

*Figure 3.1*b), following the correspondence of 10-20 system points to cortical areas in infant brain (Kabdebon et al., 2014). We inserted source and detector fiber bundles in a custom-built elastic cotton bonnet. Using the head of a realistic doll as model, we manually realized different prototypes of the cap before sewing the final one (
Figure *3.2*). The shape of the cap was inspired by a typical EEG cap for infants. Optodes were inserted in holes that we cut in the fabric, and cap's seams have been designed in order to not coincide with sources and detectors positions.
The imaging cap circumference of 34 cm reflected the average size of a term (40 week PMA) neonate head. A bigger version (36 cm) and a smaller version (32 cm) of the cap were also realized, to adjust to different sizes of the baby's head. The elastic material enabled us to easily adjust to the variability we experienced in head circumferences. We used holes over the ears and the Cz point as references for a standard positioning of the cap for measurements. A silicon strip attached in the frontal region of the cap facilitated fixing and prevented any slipping of the fabric on the hairless baby forehead.

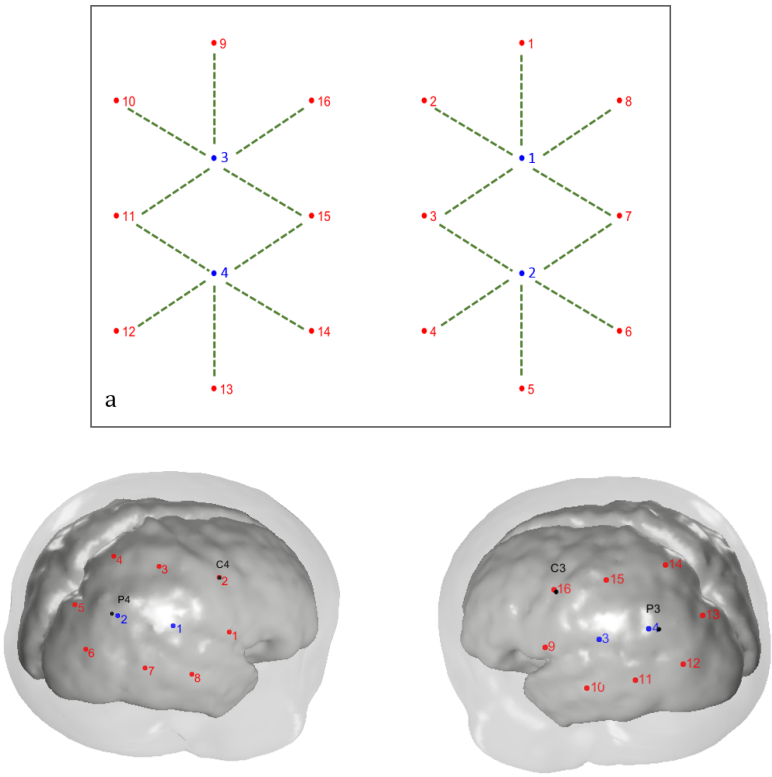

Figure 3.1 Planar representation of the hexagonal geometry, ideal to maximize coverage of a rectangular area. The sixteen sources are drawn in red, while the four detectors in blue. The central position of the detectors maximizes the number of channels available for measurements. Green lines indicate connection of sources and detectors to define a channel (a). Projection of the planar arrangement onto the scalp of a dedicated Atlas. Proportions are realistic because the Atlas used refers specifically to a 40 weeks neonate head (b).

Resting state data were recorded in the maternity ward of the Rovereto Hospital, preferably within one hour after feeding. Total scanning duration ranged from 7 minutes to 15 minutes, depending on the infants' compliance. In general, subjects were scanned while sleeping in their cradles in a dimly illuminated room, to create the most comfortable environment for their rest. We acquired measurements on neonates in a quiet or active sleep; acquisitions were interrupted as soon as the subject showed signs of wakefulness. Even though we did not directly monitor the sleep state (using, for example, quantitative EEG measurements), sleep patterns were controlled based on behavioral criteria. According to the scoring system for states of sleep in infants (Grigg-damberger, 2016; Stefanski et al., 1984), different stages of sleep are recognizable by the eyes being closed, small body movements – like jerky startles – and occasional sucking or chewing; rapid eye movements could be observed.

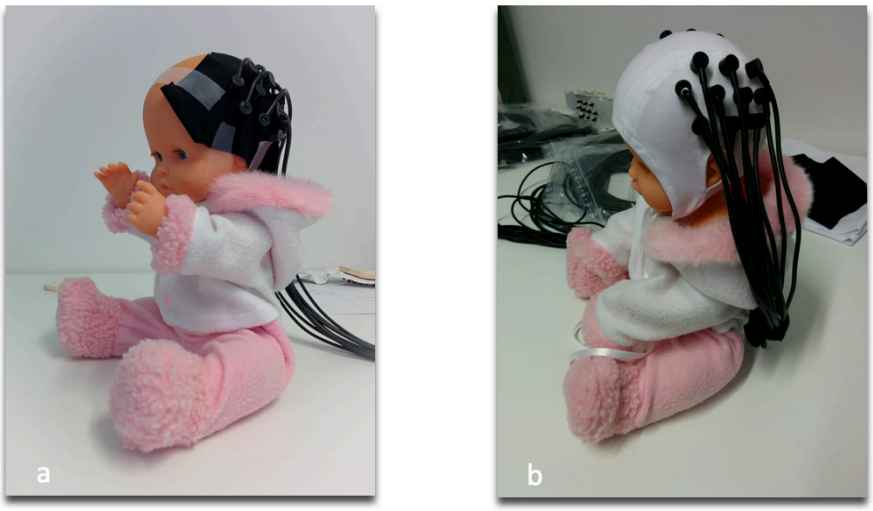

Figure 3.2 Different phases in the process of imaging cap building, from a preliminary prototype realized in an exploratory stage (a) to the final imaging cap (b). The head doll is consistent with the average head size of a typical full-term newborn. The model we used for acquisitions has been realized on the base of an EEG cap.

A state of wakefulness is instead observable in subjects (at rest or active) with eyes open and alert aspect, regardless of body movements. Based on these criteria, acquisitions were stopped if subject showed half-open or open eyes.

No medical sedation was administered. Moreover, a camera pointed toward the subject's face allowed an online monitoring of the acquisition, recording video and audio of the acquisition in place. Later inspection of recorded videos confirmed potential participant's awake state or the presence of environmental noises, which were critical criteria for subject exclusion from the study.

In general, during the newborn's sleep, sudden movements are frequent and this condition could cause an uncoupling between cap and scalp. In order to prevent movement artifacts, an operator held the cap for the entire duration of the acquisition (Figure 3.3). Indeed, the designed cap was equipped with thin, non-elastic side-ties. However, we verified that tying the strings together under the chin was an inefficient solution to guarantee a good quality acquisition as well as a risk factor for the subject. In order to avoid influencing the sleep state and, consequently, the resting state measurement, we excluded the possibility that a parent or the operator hold the infant. This would have introduced an affective touch component in the study, compromising its replicability. Although in literature there are no studies on the correlation of affective

touch and functional connectivity patterns measured in newborns, for good measure our experimental setup involved minimum physical contact with the subject.

A curtain separated operator and subject from the rest of the room. Infant's parents could monitor the scanning through online video recording, remaining silent during the entire duration. Each measurement required at least two operators, for direct monitoring of the infants and for the control of instrumental parameters.

Figure 3.3 Setup of a resting state measurement. The subject rests in his/her cradle while one operator holds the cap during the entire acquisition period, trying to follow possible head movements. This helps to prevent the head-cap uncoupling that causes movement artifacts. Neonates' brain activity is recorded in a dimly lit room. The only source of light (artificial) comes from a screen on the side of the cradle and enabled video recording from a camera placed above the screen and directed toward the baby's face. Infant's parents signed the consent to the use of the picture.

3.3.1 fNIRS instrumentation

For this study, we recorded hemodynamic activity using a frequency-domain NIRS system (ISS Imagent™, Champaign, Illinois) with 16 laser diodes – emitting at 690 and 830 nm - and 4 photomultiplier tubes[3]. The system operates with a sample frequency of 15.625 Hz, registering three different components of the signal detected at the scalp: AC and DC components and the phase shift. Light sources are modulated at high frequency (110

[3] The instrumental impossibility to realize multidistance measurements prevented us from the computation of absolute optical parameters.

MHz). Moreover, alternately switching "on/off" cycles on light emitters ensures a correct recognition of the signal coming from each source. Generally, the user can choose the number of sources simultaneously emitting light, considering that each set is "on" for 20 ms. In our case, using the machine option "switch-16", two sources emit light simultaneously while the four detectors acquire signal.
It can be useful to specify that for the analyses we used DC signals.

3.4 Data quality assessment: evaluation of noise sources

In order to define a reliable dataset for functional connectivity analyses, we established rigid criteria for evaluation of data quality. First of all, we individuated possible influences of noise on measured signals. In general, different sources of noise can contaminate the time series, hindering the identification of the hemodynamic response. Noise due to instrumentation, physiological oscillations or head movements can affect data quality.
Physiological noise represents the main contribution to the signal recorded with optical imaging systems. Cardiac pulsation, respiration, slow and very-slow fluctuations are detectable in the scalp and all the cerebral tissues crossed by the incident light. However, the technique is more sensitive to physiological oscillations from superficial layers (which are also traversed twice, in and out). These confounding components of the signal should be removed, in order to disclose the hemodynamic response. On the other hand, physiological parameters to which fNIRS is sensitive can be exploited to assess data quality. We considered the presence of heart beat in the raw signal as a sign of the reliability of data and, if this does not happen, a sufficient reason to exclude the single measurement from the sample (an example is reported in Figure 3.4). In addition, we employed a second criterion to evaluate the acceptance of the data: in frequency domain fNIRS machines, a low standard deviation of the phase data confirms the preservation of the lock-in mechanism, providing a further evidence of the accuracy of the acquisition.
All data incorporate a component of noise, which includes both instrumental and experimental contributions (Huppert, Diamond, Franceschini, & Boas, 2009). High frequencies characterizing machine noise can be removed using a low pass filter (this aspect will be discussed in section 3.6). Moreover, experiments were performed in a poorly-lit environment to mitigate contamination from other sources.

Motion artifacts represent another important source of uncertainty in the data. In optical imaging, artifacts usually occur when a movement of the head causes a temporary uncoupling of sources and detectors to the scalp, or a displacement of the probe on the head, thus introducing a net discontinuity in the time series. Involuntary and sudden movements characterize neonates sleep and this, combined with the difficulty of guaranteeing perfect fixing of the optodes to the head, increases the chance of an imaging cap shift. Motion artifacts result in rapid changes in the signal (Figure 3.4) and, in general, involve simultaneously almost all channels. In order to assess data quality, we visually inspected raw time series and extracted, periods - at least 5 minutes long - with no evident artifacts. Despite the operator's attention in following the baby's movements, we had to discard irreversibly damaged data, due to repeated movement artifacts – with too short "clean" periods – or due to the loss of a consistent number of channels after the movement. In the latter case, the uncoupling persisted until the end of acquisition. Moreover, considering the probe arrangement geometry, the misplacement of one detector determined the loss of half of channels for hemisphere, so the rate of discarded data was quite high.

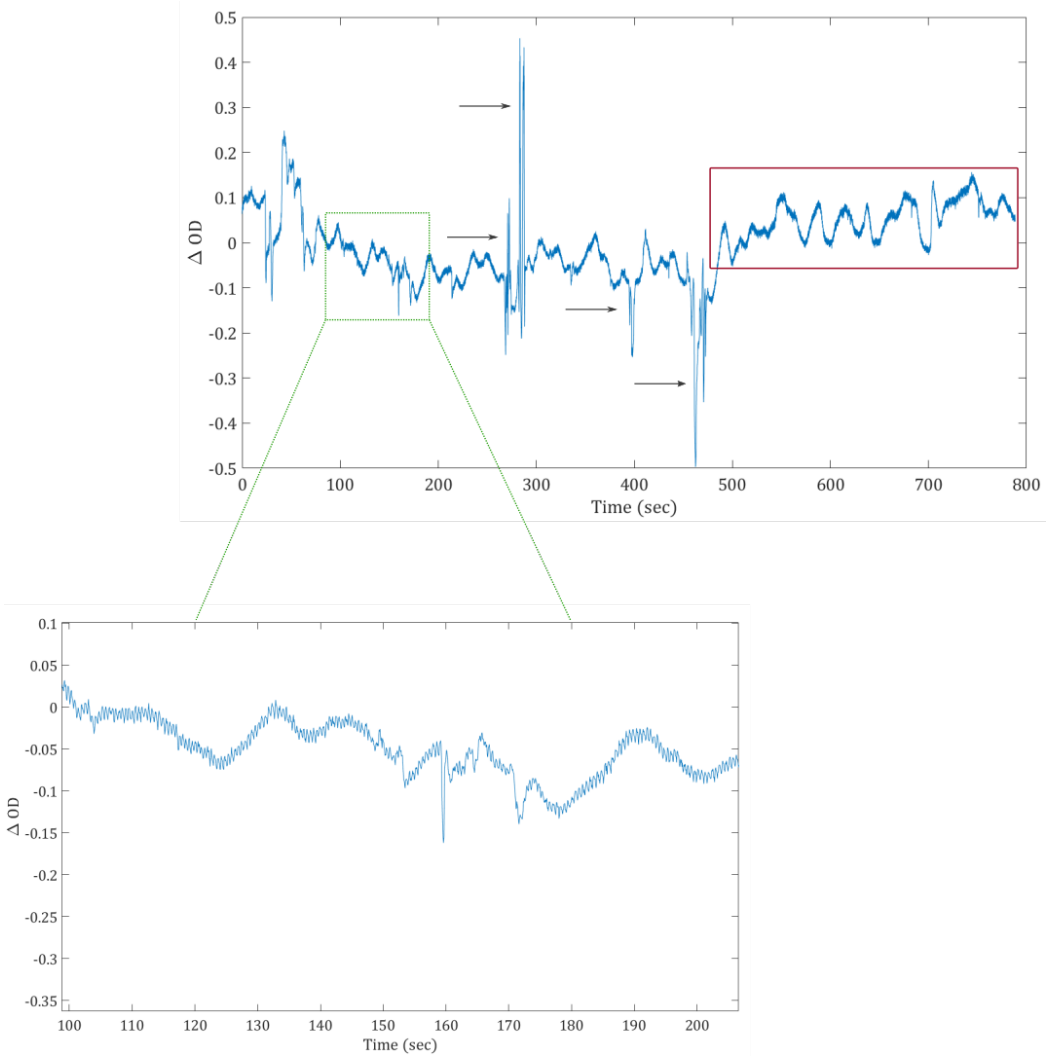

Figure 3.4 Example of non-filtered time series (subject 23) affected by several movement artifacts, appearing as sudden changes. Black arrows indicate artifacts. The red square encloses the period of the signal considered clean and accepted for further analyses (~ 5 min). Zooming of a random section of the time course highlights a clear presence of the heartbeat.

3.5 Definition of the final dataset

The first ten – out of thirty - acquisitions had to be discarded due to an insufficient securing of the cap to the subjects' head. Indeed, the final procedure, illustrated in section 3.3, was the result of numerous attempts, before we found a reliable and reproducible method.

Eight - out of the remaining twenty - subjects showed sufficient quality according to the criteria we had fixed, and were included in the final analyses (6 males, 2 females, 39.8 ±

1.1 average weeks Post Menstrual Age - PMA)[4]. From the final dataset (twenty subjects), we excluded twelve participants due to several reasons: heavy movement artifacts (n = 7), noisy environment that affected the rest of subjects (n = 2), evident twilight sleep (n = 2) or incorrect probe positioning (n = 1).

In Table 1, available information about the clinical and demographic history of included neonates are reported. Each subject was scanned once within the first two days of life. All neonates' mothers were in good health and non-smokers. Moreover, informal consent was obtained for each neonate and signed by at least one parent prior to the acquisition. Following the protocol, the data of the subjects were anonymized and linked to demographic information only through a code.

Table 1 – Demographic and clinic subjects' information

Id	Sex	GA (weeks)	GA (days)	Head (cm)	Weight (g)	AP 1/ AP 5	CA (h:min)	Delivery
14	M	38	6	33.5	2970	9 / 10	21:18	C
15	M	41	1	36.5	3960	8 / 9	17:01	C
23	F	39	3	34.5	2970	10 / 10	20:03	C
24	F	41	1	33.0	3120	9 / 10	14:07	V
26	M	39	2	35.0	3500	10 / 10	22:14	V
27	M	38	6	33.0	3360	9 / 10	47:26	V
29	M	39	1	34.0	3050	10 / 10	42:34	V
30	M	41	1	33.5	3230	9 / 10	20:18	V

Id = subject identification code; GA = gestational age; AP = Apgar score; CA = chronological age; Delivery indicates caesarean section (C) or vaginal (V) birth.

[4] In literature, an extensive terminology is used to determine postnatal age of an infant and the awareness on the correct definition is necessary to the interpretation of the dataset. With the expression "gestational age" it is usually indicated the time between the first day of the mother's last menstrual period and the day of the birth of the baby. It is generally expressed in weeks and days. Instead, the expression "post-menstrual age" referred to gestational age plus the time elapsed after birth (which is known as "chronological age") (*PERINATAL CARE PERINATAL CARE Seventh Edition Guidelines for Guidelines for*, 2012).

3.6 Pre-processing and functional connectivity analysis

We used the Modified Beer-Lambert Law (MBBL, discussed in section 1.6) to compute hemoglobin concentration signals from attenuation of light recorded (Cope & Delpy, 1988). We used tabulated values for molar extinction coefficients (Prahl, 1999). At wavelength 830 nm $\varepsilon_{HBO} = 415$ and $\varepsilon_{HHb} = 2141.8$; at 690 nm $\varepsilon_{HBO} = 1008$ and $\varepsilon_{HHb} = 778$ (molar extinction coefficients are expressed in $l \cdot cm^{-1} \cdot mol^{-1}$). Differential path length factors were obtained from a dedicated study on newborn infants (Duncan et al., 1995): 4.64 at 830 nm and 5.41 at 690 nm.

In order to remove cardiac ($\sim$ 2 Hz in infants) and respiration ($\sim$ 0.6 Hz in infants) contributes from the total signal, we filtered resulting concentration data to the frequency band of 0.01 – 0.1 Hz. This choice of range of frequencies, which is typical for resting state studies, allows discarding confounding physiological contributes and also high frequencies due to instrumental noise, while retaining the low frequency fluctuations that define functional connectivity. In order to perform further comparisons, channels' time series were transformed into z-scores subtracting the mean value and then dividing by the standard deviation.

Finally, for functional connectivity analysis, we considered z-scored time series of the filtered oxy-hemoglobin and deoxy-hemoglobin. The duration of individual measurements depended on the degree of infant tolerance and quality of sleep. We registered a high variability in length of good data quality sections, ranging from 4701 time points ($\sim$ 5 min) to 9001 ($\sim$ 10 min). In an attempt to compare time courses of different durations without discarding any information, we temporally concatenated z-scored signals of the respective channels from the eight subjects. This approach is usually employed in fMRI to investigate functional connectivity using Independent Component Analysis (ICA) (Cole, Smith, & Beckmann, 2010), but it have been used also for different group-level statistical analyses on fNIRS time series (S Tak, Uga, Flandin, Dan, & Penny, 2016; Sungho Tak & Ye, 2013; Tong, Bergethon, & Frederick, 2011). Thus, concatenating oxy-hemoglobin (or deoxy-hemoglobin) z-scored signals, we obtained 20 representative time series, one for each channel, respectively. Lastly, correlation matrices were computed from the r Pearson's correlation coefficient between all the resulting channels' time series pairs (r varied in the range [-1,1]), for both HbO and HHb, to describe the group-level dynamics of functional connectivity. Each row (or column) of the matrix

returns the r-value of correlation between the time course of a single channel and the time course of all the remaining channels.
In addition, we reported a second popular approach, which exploits the average behavior of the subjects' set of interest (Cai, Dong, & Niu, 2018; J. Wang, Dong, & Niu, 2017). To obtain a coherent sample, we extracted from each signal a clean portion of exactly 4701 time points, which corresponds to the shortest clean portion of a time series. In this way, we obtained eight time series with the same length for the eight subjects. Here, group-level functional connectivity was calculated from the average of Fisher transformed correlations for each subject.
Bearing in mind the research question focused of the opposite relationship between two networks, we considered both positive and negative correlation values, without applying a threshold.

3.7 Results

In this section, we report results from correlation analyses on the subset of eight subjects that met the rigid exclusion criteria. The 20-channels probe, used for acquisitions on neonates, was designed to cover the LP cortices, part of the DMN, and the IPS, which is part of DAN. The measurements aimed to test the presence of homotopic positive correlations and negative correlations between the two ipsilateral areas of interest.
In previous resting state fNIRS studies, only variation in HbO were presented, due to a better quality of the signal with respect to HHb (Homae, Watanabe, Nakano, & Taga, 2007). Here, for the sake of completeness, we show results for both signals.
First, we reported results of analyses on concatenated HbO time series (Figure 3.6). For an easier interpretation, we referred to channel numbering illustrated in Figure 5, which is coherent with the matrices' digits. The correlation matrix showed a clear differentiation of behavior for hemispheres. The first 10 channels (in the right hemisphere) exhibited positive intrahemispheric temporal correlations. The resulting dynamics within the hemisphere was almost uniform, with strong correlations between two different channel pairs (10-4 and 6-3 channel), with values of 0.87 and 0.85 respectively.

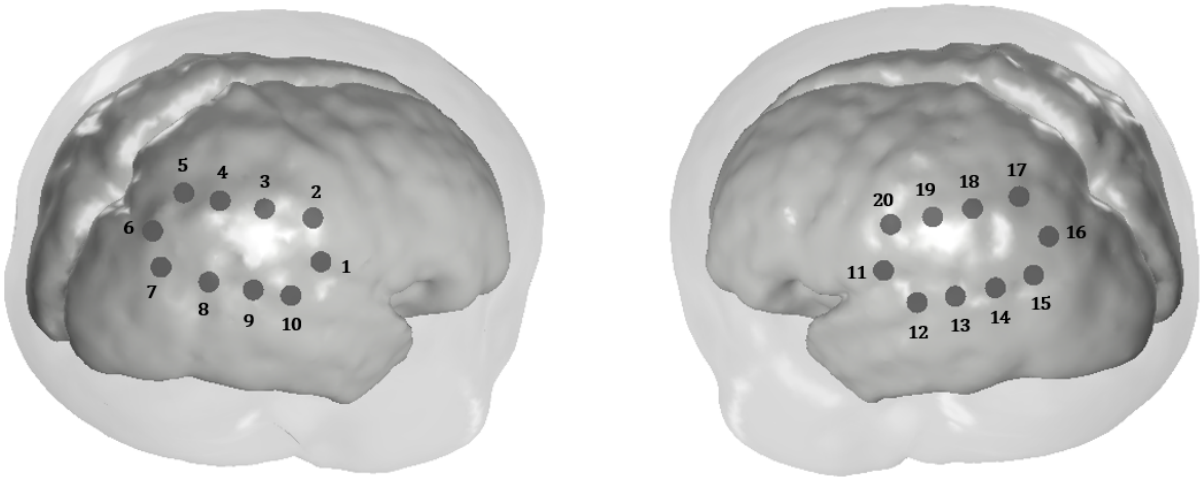

Figure 3.5 Channel disposition for right and left hemisphere. The grey circles indicates positions halfway between source and detector coordinates onto the scalp, in correspondence of the highest depth penetration. Channels 2-3 and 19-20 are positioned, respectively, over the right and left IPS area; pairs of channels 7-8 and 14-15 cover, the respective LP regions.

The left hemisphere exhibited an equally uniform behavior, with positive correlations (except for channels pair 18-15 that showed a low negative correlation of -0.16). Interestingly, the correlation values registered between channels 16 and 13 and channels 20 and 14 were both very high (respectively of 0.91 and 0.84). However, the two pairs of channels that showed high correlation within the left hemisphere did not correspond to those previously cited for the right side. Despite similar dynamics, a paired sample t-test confirmed a significant difference ($p < 0.001$) between the mean left and right hemisphere intrahemispheric correlations in oxy-hemoglobin signal. Interestingly, no differences at specific channels level have been found.

Global distribution of r values, represented in the histogram, confirmed the presence of very weak negative correlations (minimum value at $r = -0.23$), which characterized predominantly the interhemispheric communication. Interestingly, analyses did not highlight homotopic interhemispheric correlations. Moreover, we did not register any competitive relationship between the two distinct areas of interest, within the same hemisphere. In order to point this effect, we visualized results of the seed based correlation analysis (Figure 3.6). We chose to employ the most representative channels as seeds – basically, those ones probing the underlying areas corresponding to C3, C4, P3 and P4 reference points (see

Figure *3.1*). Here, the separation of dynamics between the two hemispheres is clearly highlighted.

We repeated the same analyses on concatenate z-scored deoxy-hemoglobin time courses. Results, in Figure 3.7, are in complete agreement with those already showed for oxy-hemoglobin signals. Registered negative correlation remained weak (- 0.33) and the emerging pattern accurately reflected the ones from HbO. In the average description of the phenomenon, we lost the effect of negative correlations, which appeared strong at individual level in the majority of subjects (Figure 3.8 and Figure 3.9).

The additional analysis on time series with the same number of time points corroborates previous observations (Figure 3.10).

3.8 Discussion

In the present study, we aimed to assess aspects of the DMN in neonates in a subgroup of subjects selected according to strict quality criteria, to minimize the risk of spurious correlations arising, e.g., by motion or physiological noise. The understanding of the stage of development at which the network emerges could provide insights into the evolution of functional connectivity and contribute to explain neuronal origins of diseases related to its disruption (de Lacy, Doherty, King, Rachakonda, & Calhoun, 2017; Gao et al., 2009; Padmanabhan, Lynch, Schaer, & Menon, 2017). Our research is based on the assumption that the existence of DMN in newborns is connected to the capability of detecting a landmark of the network, already consistently observed in older populations (M. D. Fox et al., 2005, 2009). In general, in adults, positive correlations have been registered between functionally related brain regions, as well as negative between brain regions showing theoretically opposed functional roles (M. D. Greicius et al., 2003) (Kelly et al., 2008). Specifically, positive homotopic correlations have been observed in interhemispheric parietal areas, while spontaneous anti-correlated activity have been reported between specific areas of DMN and DAN (Corbetta & Shulman, 2002) at rest. The reliability and variability of this behavior have been widely investigated in healthy adults (Dixon et al., 2016; Keller et al., 2015; Vincent, Kahn, Snyder, Raichle, & Buckner, 2008) and in the developmental period from childhood to young adulthood (Chai et al., 2014).

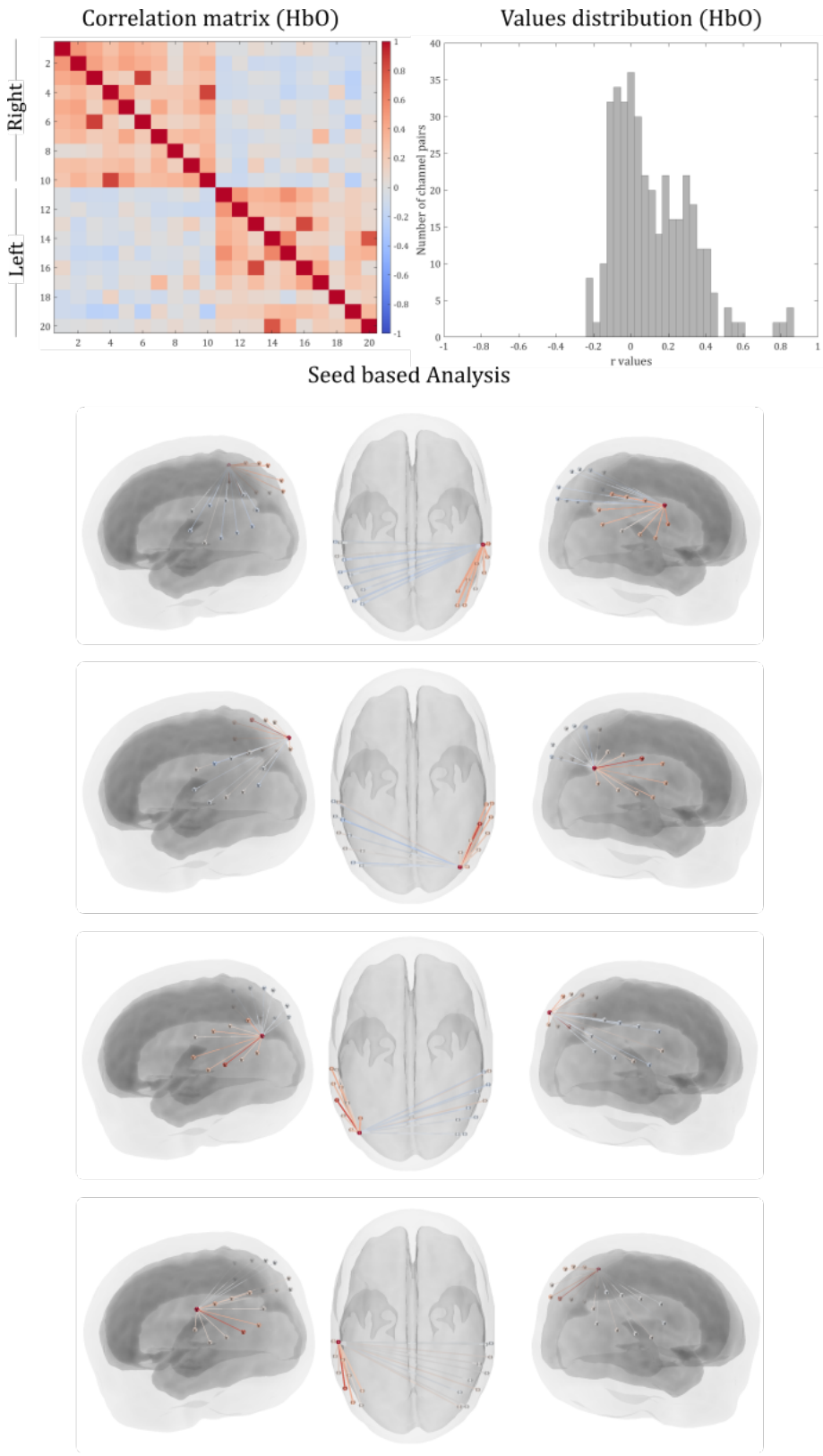

Figure 3.6 Correlation analyses on concatenated time course obtained from oxy-hemoglobin signals. Correlation matrix (left) and correlation values distribution (right) are reported on the top. Digits indicated in the matrix represent measurement channels: from 1 to 10 on the right hemisphere, from 11 to 20 on the left hemisphere. Values of correlation vary in the range [-1, 1] and are represented with a divergent scale map. Diagonal values were excluded from the correlation values distribution. Below, lateral and top views of the brain illustrate seed based correlation results. Chosen seeds are, in order: channel 2, channel 6, channel 16, channel 20.

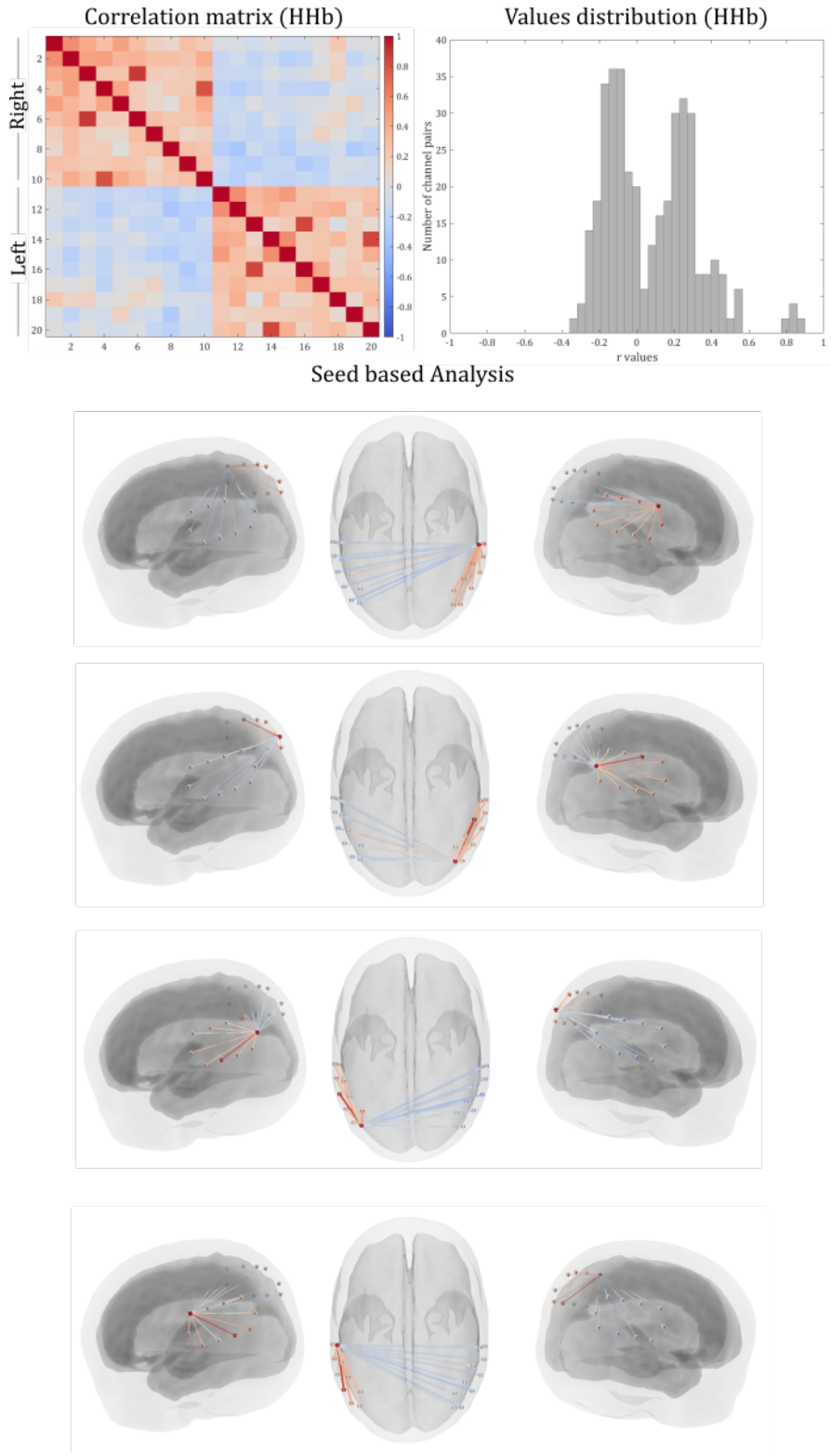

Figure 3.7 Correlation analyses on concatenated time course obtained from deoxy-hemoglobin signals. Correlation matrix (left) and correlation values distribution (right) are reported on the top. Digits indicated in the matrix represent measurement channels: from 1 to 10 on the right hemisphere, from 11 to 20 on the left hemisphere. Values of correlation vary in the range [-1, 1] and are represented with a divergent scale map. Diagonal values were excluded from the correlation values distribution. Below, lateral and top views of the brain illustrate seed based correlation results. Chosen seeds are, in order: channel 2, channel 6, channel 16, channel 20.

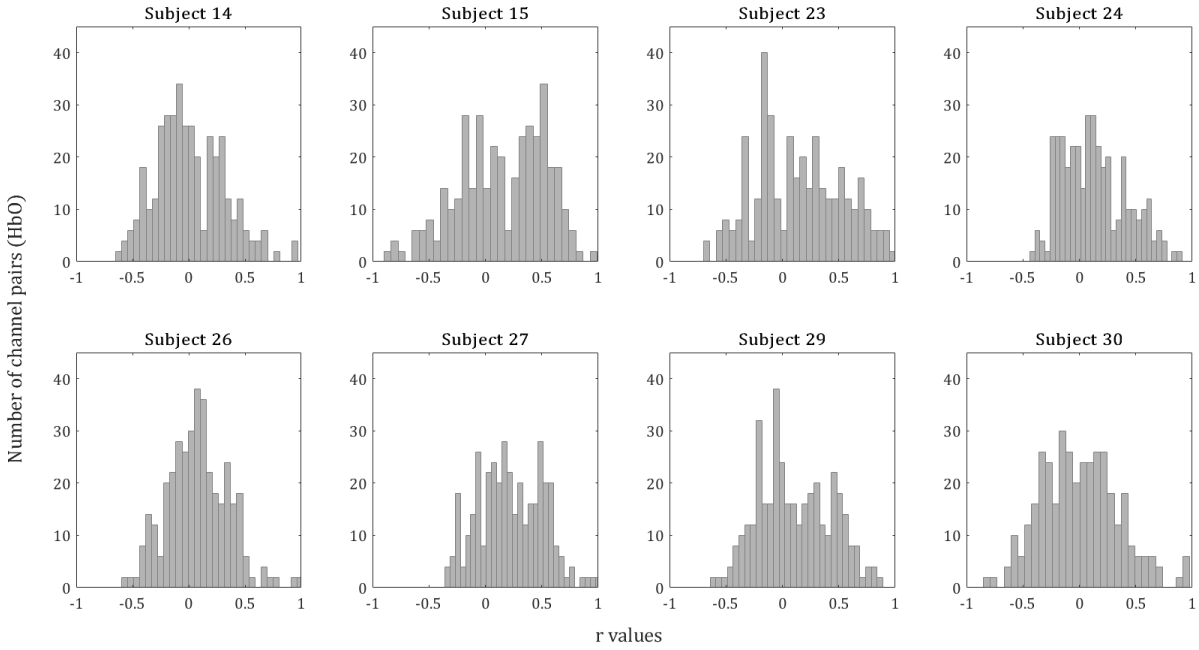

Figure 3.8 Correlation values distributions calculated from oxy-hemoglobin signals for each of the 8 subjects included in the analysis. Diagonal elements of the correlation matrix were excluded from the representation of correlation values distribution.

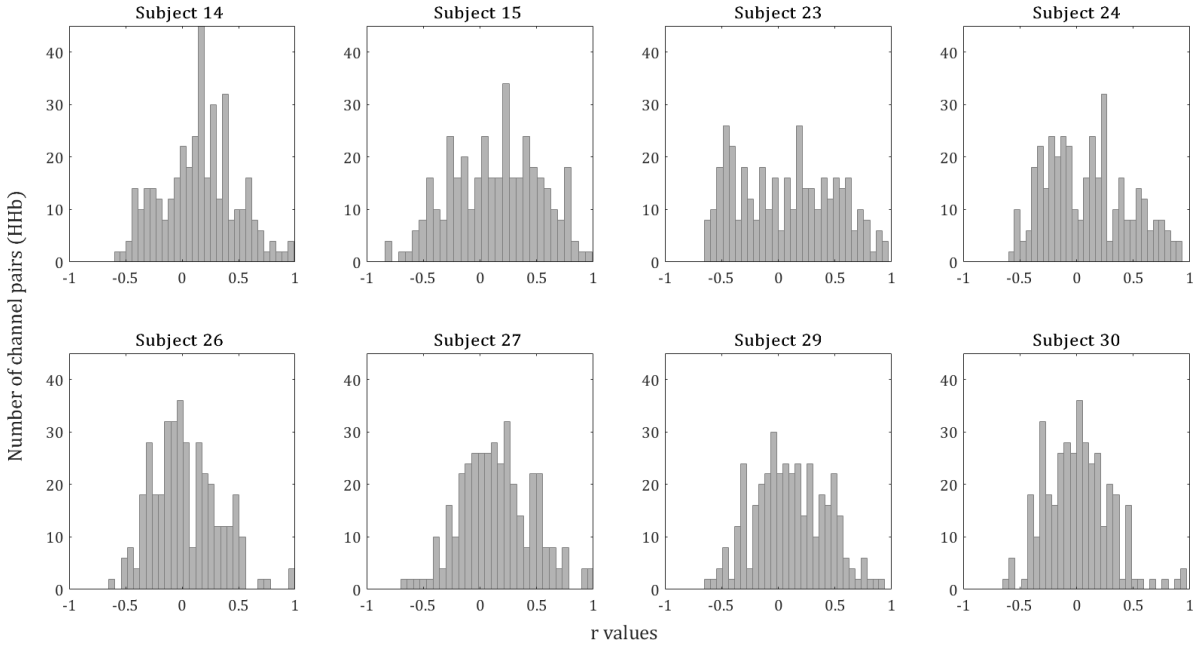

Figure 3.9 Correlation values distributions calculated from deoxy-hemoglobin signals for each subject. Diagonal elements of the correlation matrix were excluded from the representation of correlation values distribution.

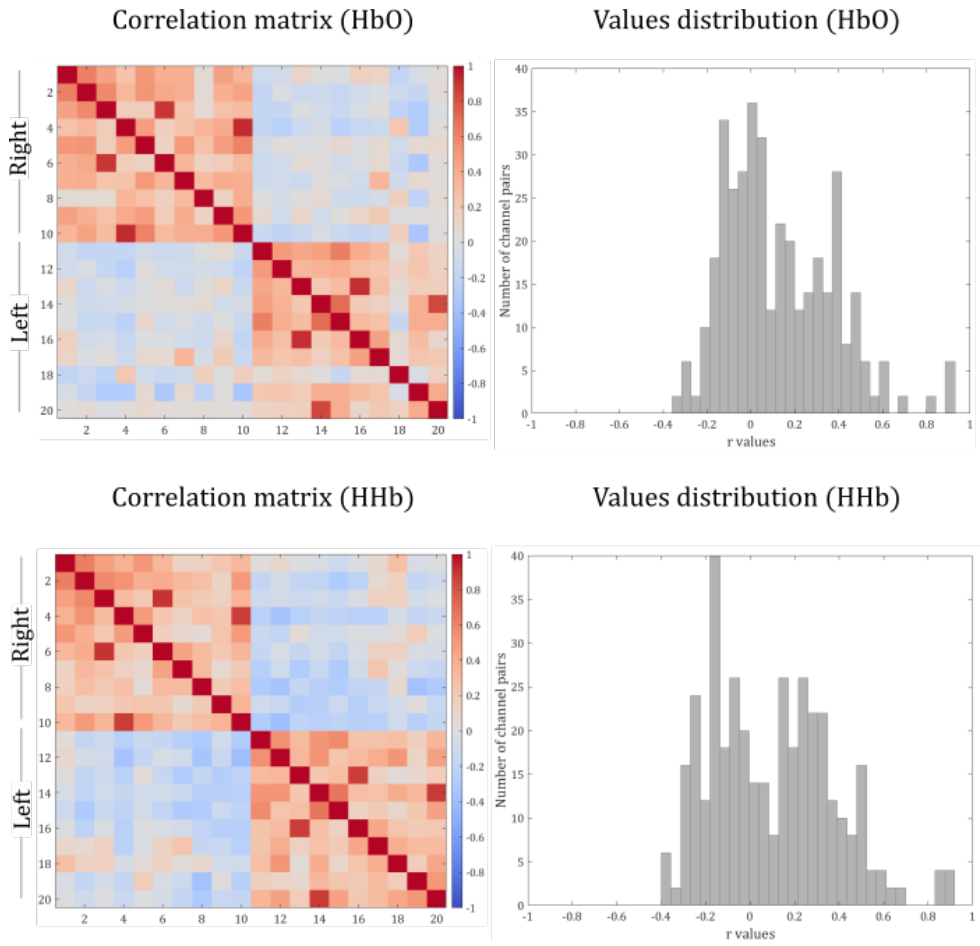

Figure 3.10 Correlation analyses obtained averaging the Fisher's z score of the single subjects. To represent matrices, we computed the inverse transformation from Fisher's z to Pearson's r-value. Diagonal values were excluded from the representation of the correlation values distribution.

Hence, we hypothesize that, if a mature DMN is already present at this stage, we should observe interhemispheric correlation between homotopic parietal regions, and intrahemispheric anticorrelations between components of the DMN and DAN covered by our probe. We did not find evidence of either in our dataset, at least at the level of channel-based analysis.

Some resting state studies have recently raised concerns about the interpretation of negative correlations. It has been suggested that anti-correlations could appear as a consequence of a specific pre-processing method, commonly used in fMRI analyses (Buckner et al., 2008; Murphy, Birn, Handwerker, Jones, & Bandettini, 2009). The debate on their explanation is based on the possibility to link the emergence of anticorrelations to artifactual effects induced by the global signal regression (GSR) (M. D. Greicius et al.,

2003; Murphy et al., 2009; Uddin et al., 2009). This procedure removes the spontaneous fluctuations of the BOLD signal that are common to the entire brain and that are referred to as *global signal* (M. D. Fox et al., 2009). The main contributions to global signal come from physiological non-neuronal confounds, but components with neuronal origin can also be present. The existence of a shared global component is reflected in an excess of positive correlations in raw fMRI data. Thus, the effect of Global Signal Regression (GSR) consists in the shifting of correlation distributions towards negative values and after the pre-processing the resulting Pearson's distribution appears centered at zero (Murphy & Fox, 2017). Therefore, negative correlations are strengthened and their effect is enhanced even in group-analyses. There is still an on-going discussion and further studies will help to clarify the goodness of the method. In order to avoid the potential pitfalls of this procedure and to describe genuinely anti-correlated processes, in our work we studied the emergence of anti-correlated activity without using a GSR method.

Analyzing the average cerebral dynamics of the sample, we did not detect strong negative correlations within or between hemispheres - to be exact between LP areas of DMN and IPS in DAN. The lack of specific interactions between the two networks could refer to an immature development of one or both patterns or even to an immaturity of their interaction. In literature, the majority of works on the inception and maturation of the whole brain functional connectivity come from fMRI-based measurements. Nonetheless, delineating a coherent evolution trajectory for the DMN spatial pattern is not trivial, due to contrasting descriptions of its state at birth. While some studies reported the capability of detecting a complete spatial pattern in term newborns (Doria et al., 2010), in other seminal works (Fransson et al., 2009, 2007) a new terminology had to be introduced – *proto DMN* - to indicate the only partial resemblance of the neonate pattern to the adult one.

The state of the networks could also be interpreted taking into account the underlining behavior, generally associated with neural activity. Indeed, the competitive correlation between the DMN and DAN, respectively, is considered as a "recurring switch between an introspective versus an extrospectively oriented state-of-mind" (Fransson, 2005). In this regard, the first behavioral evidences of an interconnection between internal and attention processes have been noticed after 3 months of age (Rothbart & Posner, 2001). Indeed, the strategy to calm the weeping of infants (a mechanism associated to DMN) by distracting them with an external stimulus (related to attentional processes), like a toy,

worked only from the reported age. In this case, the negative correlation results in an inhibitory process, from a behavioral approach.

Ultimately, our results are in accordance with a previous fMRI study (Gao et al., 2013). The authors explored the evolution of the interactions between DMN and DAN in 2 weeks, 1 year and 2 years old infants and found its appearance only at the first year of age. To sum up, to date, no resting state fNIRS studies have yet focused precisely on the exploration of default mode network at this stage, specifically in the first two days of life. Our study confirmed previous findings on the absence of an opposite relationship between the two networks under investigation. However, the lack of a consensus in literature on the maturation of DMN at birth precludes a direct connection of the outcomes with the level of development of the network.

In addition, our study finds no evidence of homotopic interhemispheric functional connectivity in the parietal areas covered bilaterally by our probe. This result is consistent with previous observations from a longitudinal resting state fNIRS study on 4 days old neonates, 3 months and 6 months old infants (Homae et al., 2010). By probing the frontal, temporal, parietal, and occipital areas with 94 channels at a fixed distance, those authors found no evidence of bilateral organization of functional activity at very early stage and starts to emerge only at three months. On the other hand, bilateral correlations between homotopic counterparts have been detected with optical imaging in both preterm and term subjects in the visual cortex (White et al., 2012) and in the middle temporal and auditory areas (Ferradal et al., 2015). These results, consistent with some fMRI findings (Fransson et al., 2009, 2007), have been obtained using diffuse optical tomography. DOT makes use of a large number of channels, thus affording higher spatial resolution and, in general, better filtering of superficial noise. Indeed, the inclusion of source-detector pair with a short separation distance, thus only sensitive to superficial tissues, enables the removal of confounding effects of scalp hemodynamics. However, it should be noted that, for the latter process, the optimal short-separation distance, measured in term infants, is only 2.15 mm (Brigadoi & Cooper, 2015). To date, the instruments on the market are still unable to satisfy this condition, therefore scalp contaminations cannot be completely removed, even though DOT may provide more accurate depth information thanks to the use of overlapping channels.

Furthermore, we detected a surprisingly uniform dynamics within each hemisphere. The result may be attributed to a course-grained description of the functional connectivity

with a channel-based analysis. It appears as if the discrete grid of channels could hinder, to some extent, details of functional information. This raises the question: can we enrich the channel-based characterization of resting state connectivity? Of course, the inverse reconstruction of cortical origins of hemodynamic signal is well established in high-density optical systems. However, to what extent the procedure is affected by experimental conditions in functional connectivity studies is an open issue that will be discussed in the next Chapter.

The present study would benefit from further improvements. Firstly, it would be important to increase the number of participants. Certainly, the sample we investigated is small: as often happens in infant studies, the drop out rate is very high, involving in average at least the 40% of the initial data set (Lloyd-Fox, Blasi, & Elwell, 2010). In addition, we included only subjects that satisfied rigid inclusion criteria, to avoid introducing spurious correlations in our analyses. Thus, results can be considered reliable even if a higher statistics is necessary to consolidate our conclusions. Moreover, monitoring of the sleep stage through simultaneous EEG measurements may help to reduce the variability among subjects.

4 From sensor to source space: a validation study

Resting state studies conducted with fNIRS often limit the description of the functional dynamics only to a sensor-based analysis. This approach results in coarse-grained maps of connectivity. In the present Chapter, we validate the process of reconstruction of spatially distributed signals. The method has been tested on synthetic and real resting state datasets, simulating the variation of experimental factors, such as probe (size and geometry), original pattern of correlations and level of noise in the signal.

4.1 Introduction

Despite the numerous technical advantages of fNIRS application to functional connectivity developmental studies, optical imaging comes with multiple challenges. One of the most critical issues concerns the definition of an optimal probe design. Ideally, in order to comprehensively describe the global dynamics, the full coverage of the brain should be provided. To this purpose, a high number of optodes, organized in densely packed arrays is necessary. Recently, extended geometries allowing the overlapping of measurement channels have been achieved in studies on adults (Eggebrecht et al., 2014, 2012), thanks to the advantages of diffuse optical tomography (DOT) (Joseph, Huppert, Franceschini, & Boas, 2006; Koch et al., 2010; Zeff, White, Dehghani, Schlaggar, & Culver, 2007). This method exploits long and short distance measurements to improve depth-sensitivity and to separate the confounding superficial contributions from the deep cortical component of the signal, collected at the scalp (G. E. Strangman, Li, & Zhang, 2013; White & Culver, 2010). To date, high density caps, ensuring whole-brain coverage, have been used for monitoring cortical hemodynamic in an early preterm (Galderisi et al., 2016) and a term newborn (Singh et al., 2014) - testing in both cases, only one patient. However, the very few functional connectivity studies that focused on such a specific population did not guarantee the investigation of the entire brain. For instance, arrays

with limited spatial extension, but formed of multidistance overlapping channels, have been employed to explore connectivity in small cohorts of preterm and term infants, at first only in occipital regions (White et al., 2012) and later, also in temporal and inferior parietal cortices (Ferradal et al., 2015). Alternatively, available sources and detectors can be distributed in sparse arrangements, with fixed channel distance. This approach have been employed to inspect frontal, temporal, parietal and occipital regions in preterm newborns (Fuchino et al., 2013), term neonates and infants of 3- and 6-months old (Homae et al., 2010) during natural sleep with an almost comprehensive coverage of brain. In these works, the connectivity is usually inferred from fNIRS signals collected by sources and detectors distributed onto the scalp. The functional analysis conducted in the sensor space typically results in a coarse-grained description of activity distribution, which represents a critical limiting factor. However, with an acceptable spatial resolution, usually achieved using DOT configurations, it is possible to recover a global description of absorption variations and to reconstruct the information for each node or voxel of a digital reference brain. Thus, the analyses can be shifted in the so-called *source space*, where the hemodynamic response has its origin. In resting state studies, the process allows the definition of three-dimensional functional connectivity visualizations, similar to those obtained from fMRI data. These maps could complement the channel-based description, informing in a comprehensive way on the anatomical localization of activations and facilitating the interpretation of the results.

In order to obtain a three-dimensional image reconstruction, it is firstly necessary to define a model of photon migration capable of simulating the light propagation through the head. A forward model allows the prediction of changes in scalp measurements assuming a prior knowledge of changes in optical properties of the head, thus relating source space to sensor space. Different discrete approaches, such as Finite Element Method or numerical Monte Carlo simulation, can be used to solve the photon migration problem (Arridge & Schotland, 2009; Boas, Culver, Stott, & Dunn, 2002; Fang & Boas, 2009). However, the accuracy of the forward solution strictly depends also on the accuracy of the geometry used to model the real head and on the relative set of optical properties associated to each brain tissue. The optimal choice would consist in a subject-specific, multi-layered anatomical structure, obtained via Magnetic Resonance Imaging (MRI), where to individuate sources and detectors positions (Boas & Dale, 2005; Perdue, Fang, & Diamond, 2012). However, this approach is often unrealistic for vulnerable

populations, such as infants. In addition, the request of individual MRI acquisitions would cancel the practical advantages of optical imaging that make the technique preferable in specific conditions. For these reasons, in most cases atlas head models represent a good compromise. Given all these elements, the image reconstruction process can be obtained by solving the inverse problem: changes in optical properties of the head are computed from changes in measurements collected at the scalp level. This leads to a mathematically ill-posed inverse problem that necessitates of regularization methods to be solved (see section 2.6.2). This process has been implemented and widely applied to reconstruct oxygenation changes, especially in adult head (Cooper et al., 2012). However, the potential of this procedure has not exploited extensively in functional connectivity studies. Understanding the impact of external factors on the method is useful to assess the reconstruction of the information in the source space, in particular for research on infants, which are the most suitable subjects for resting state fNIRS investigation.

In this Chapter, we present work on the validation of the reconstruction of spatially distributed functional signals on a dedicated anatomical template, applied to functional connectivity studies in infants. The aim is to assess the reliability of a source-based functional connectivity representation, able to enrich the popular sensor-based analysis approach. Specifically, we studied the impact of different experimental factors, like probe size and geometry, and Signal-to Noise ratio (SNR) on the inverse reconstruction of optical data acquired on infants. This analysis provides guidance to optimize probe design, and to appreciate the factors that determine the reliability of the method. However, the assessment of the quality of the reconstructed spatial patterns is challenging, due to the lack of a benchmark. To this purpose, we simulated absorption changes at the cortical level in order to define a ground-truth. Specifically, we generated a synthetic pattern of correlated activity fluctuations resembling the Default Mode Network (DMN), in the presence of various levels of noise. In addition, we explored the influence of the presence of negative correlations on the reconstruction process, introducing in the analyses the contribution of anticorrelations to the synthetic spatial pattern. After this introductory validation, we applied the implemented tool to reconstruct two real functional connectivity datasets.

4.2 Computational validation

4.2.1 Anatomical Model

The first step for a definition of the inverse reconstruction process is the choice of an appropriate head model, able to reflect cerebral structures and properties of the sample under investigation.

Our entire research is focused on the study of neonates. However, at this very early stage of life, the cerebral structure evolves quickly. Thus, working with an atlas that reproduces the anatomical characteristic of brain, referring to a narrow period of time after birth, is a great advantage. To this purpose, we used a 4D atlas (Brigadoi, Aljabar, Kuklisova-Murgasova, Arridge, & Cooper, 2014), a tool particularly suitable to studies on infants. The atlas was produced using MRI images recorded on 142 infants from 29 weeks to 47 weeks PMA (post menstrual age) (Kuklisova-Murgasova et al., 2011), thus reflecting the structural changes occurring in this time window. Therefore, for each week PMA, the package provides:

- a multi-layered tissue mask, segmented into 6 tissues: extra-cerebral tissue (ECT, including scalp and skull tissues), cerebrospinal fluid (CSF), gray matter (GM), white matter (WM), cerebellum and brainstem. For each layer, absorption and scattering coefficient values are available;
- a high-density, volumetric, tetrahedral multi-layered mesh;
- surface meshes for the ECT, GM and WM layers;
- cranial landmarks, corresponding to inion (Iz), nasion (Nz) and left and right pre-auricular points (ALAl and ARAr).
- 10-5 EEG system coordinates (Oostenveld & Praamstra, 2001) on the scalp surface. Usually, this EEG-based system is also used in fNIRS studies as reference for sources and detectors positioning (Jurcak et al., 2007).

Here, the 4D age-matched optical head geometry represents the ideal anatomical model for image reconstruction in the sample of interest. For testing the reliability of the reconstruction in a consistent population, in this study we employed the 40th weeks Atlas that reflects the characteristics of typical term newborns (Figure 4.1).

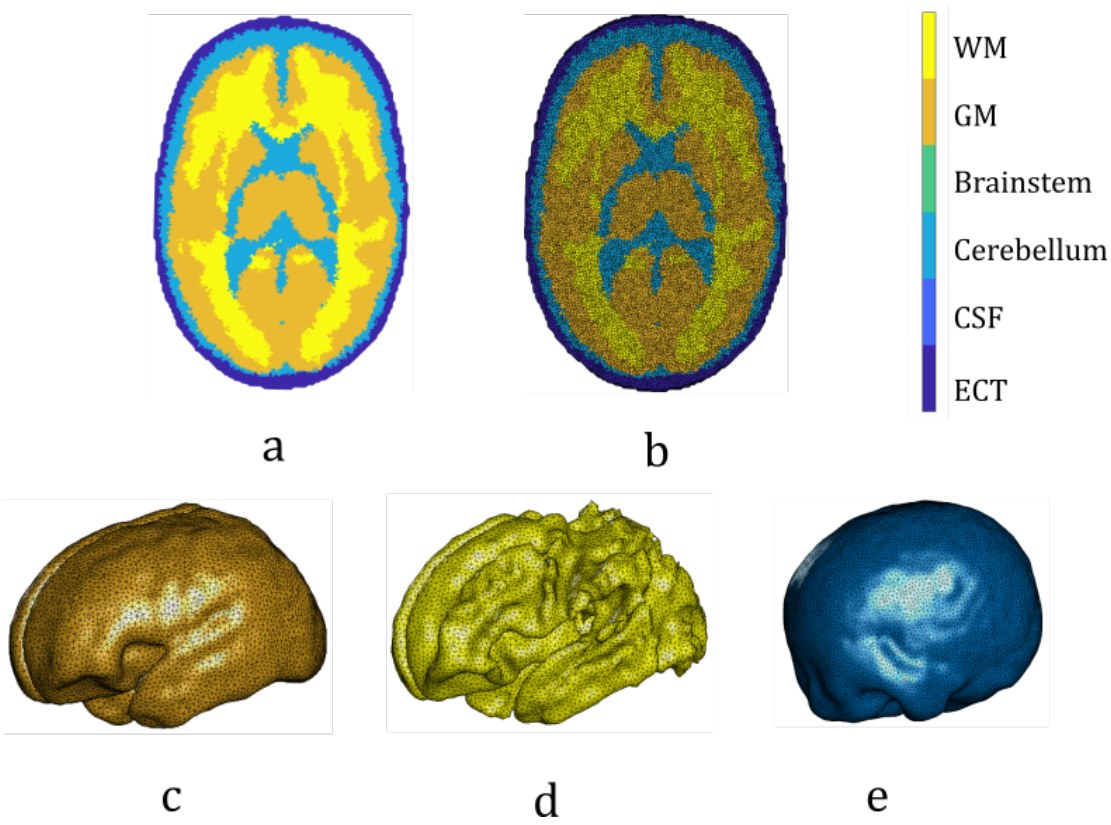

Figure 4.1 Features of the dedicated 4D Atlas used for simulations. In this panel, components of the atlas at 40 weeks are reported: a) the multi-layered tissue mask, b) multi-layered tetrahedral volumetric mesh, c) surface mesh for grey matter, d) surface mesh for white matter, e) surface mesh for scalp.

4.2.2 Probe design

Considering as reference the scalp of the 40th week's Atlas, we designed four different optical probe configurations to explore conditions and constraints that influence the final reconstructed image.

First, a full coverage of the head has been mimicked with an extended and dense probe to provide a reference for more restricted probes. This ideal configuration was defined by placing sources and detectors in correspondence of the 10-5 EEG system points (Oostenveld & Praamstra, 2001). At first, we associated a source to the Cz point; starting from Cz, we distributed alternatively detectors and sources towards both nasion (Nz) and inion directions (Iz). Once completed the central curve, allocation of simulated optodes

continued from the center to right and left directions, following the reference curves. We excluded points below T7 and T8 because not useful to our exploration. As follows, we obtained a large probe of 124 sources and 133 detectors, symmetrically arranged between hemispheres. By definition, distances of adjacent reference points, in 10-5 system, correspond to the 10% and 5% of the total distance of the curves defined onto the scalp, in front-back or right-left directions. Therefore, the final mesh fence was not a uniform structure with fixed distance values between optodes. From all possible pairs, we selected only channels with source-detector distance in a realistic range of [18-28 mm]. Eventually, 997 channels formed the resulting configuration (Figure 4.3). This probe is definitely unrealistic because, to date, no instrumentation is able to guarantee such a high number of channel for the investigation of newborns' brain activity (Ferradal et al., 2015). Nevertheless, the resulting configuration aimed at illustrating the effect of a compact and extended coverage of the scalp in the image registration process, simulating the best-case possible scenario.

The second arrangement was obtained from a specific subset of the first one. We maintained the geometry of the largest probe. Here, we chose a subgroup of 12 sources and 12 detectors – placed symmetrically through the hemispheres – capable of covering the parietal areas. Such areas are supposed to be involved in the emergence of DMN. Considering only pairs in the above-cited range of distances, we defined a probe of 32 channels. The first two optodes arrangements were simulated in order to test the impact of the size of the array on the final reconstruction, provided an ideal geometry – with a large number of overlapping measurement channels.

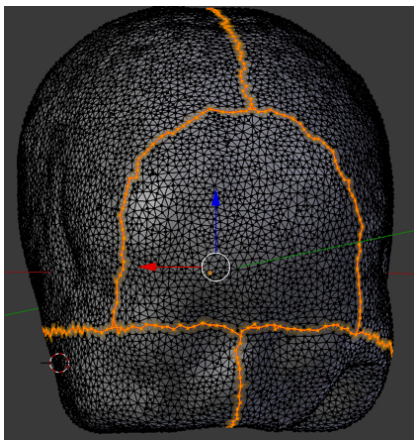

Figure 4.2 Picture of a step of planar probe projection process onto the scalp mesh, using Blender. We worked with the two hexagonal components of the probe (one for hemisphere) separately. Scalp was segmented and the projection involved only lateral regions.

The remaining configurations were reproduced starting from sources and detectors arrangements already used for the acquisition of real resting state datasets on newborns. The geometry of the third probe was initially designed for the study previously described in Chapter 3, in order to investigate parietal areas of DMN with twenty channels at our disposal. Sources and detectors were arranged in two hexagonal geometries, with 10 channels for each hemisphere, at a fixed source – detectors

distance of 20 mm. First and second probe configurations were created choosing points with well-known coordinates (all 10-5 points coordinates onto the scalp are included in the Atlas). In this case, the planar distribution of the optodes was defined beforehand and then the two-dimensional geometry was mapped onto the curved 3D surface of the scalp using Blender software. Blender is a free and open-source software for computer graphics. It is used for creating video games, animated film and 3D printed models and includes toolsets for UV unwrapping, texturing and 3D printing (to name a few) [5]. Even if the software is not dedicated to neuroimaging purposes, it is highly versatile and allows the mapping of 2D flat objects on volumetric meshes. The advantage of Blender, with respect to other available tools such as AtlasViewer in Homer2 (Aasted et al., 2015) is the request of only 2 points for the projection. We produced two distinct hexagonal arrangements and mapped one hemisphere at a time (Figure 4.2). Four symmetric optodes were anchored to C3, P3 of 10-5 EEG system (Jurcak et al., 2007)– and, on the opposite hemisphere, to C4 and P4 – and a dedicated wrapping algorithm has been applied.

Finally, the last configuration reflected the probe used in a different resting state investigation on 4-days old term neonates by (Homae et al., 2010). Frontal, temporal, parietal and occipital areas of each hemisphere were investigated with a sparse probe of 94 channels, characterized by a source-detector distance fixed at ~2 cm. In this case, the coverage of the brain is certainly more extended, with only a gap in the center. Considering the average age of the sample, also in this case the 40th week of 4D Atlas can be considered a highly representative head model. Sources and detectors coordinates onto the head mesh were provided from the authors of the work and are illustrated in Figure 4.3.

[5] More information on the website: www.blender.org.

4.2.3 Choice of optical properties

The assignment of appropriate optical properties to each node of the mesh is a crucial step to guarantee a reliable computational model. Optical features referring to distinct layers of tissues vary according to the nature of the sample used to measure them (Choi et al., 2004). Of course, *in vitro* (or post mortem) and *in vivo* measurements return dissimilar values due to a number of physiological factors, such as the variation of blood content, structural changes or difference in temperature. From a technical point of view, even though continuous wave instrumentations are widely diffused for near-infrared studies, they are not feasible to determine absolute and separated values for absorption and reduced scattering coefficients. Thus, hemoglobin concentrations, from which optical properties will be derived, are generally estimated through multi-distance, frequency-domain or time-domain approach. However, despite the vast amount of available literature on fNIRS cognitive studies on infants, a limited number of papers have focused on the assessment of in vivo optical properties of the newborn's head. Moreover, some of these works produced a single average value of absorption and reduced scattering coefficients for the neonate brain (Zhao, Ding, Hou, Zhou, & Chance, 2005; Zucchelli et al., 2017) that does not fit with our need of a detailed description of each layer of the head (corresponding to the different components of the atlas segmentation). Another aspect to be reckoned with is the age of the subject: values obtained from an early preterm population (Ijichi et al., 2005), would not be representative in our case. In view of this, we used optical properties obtained by measurements at a single wavelength (800 nm) (Fukui et al., 2003) and already reported in other studies (Brigadoi et al., 2014; Dehaes et al., 2013).

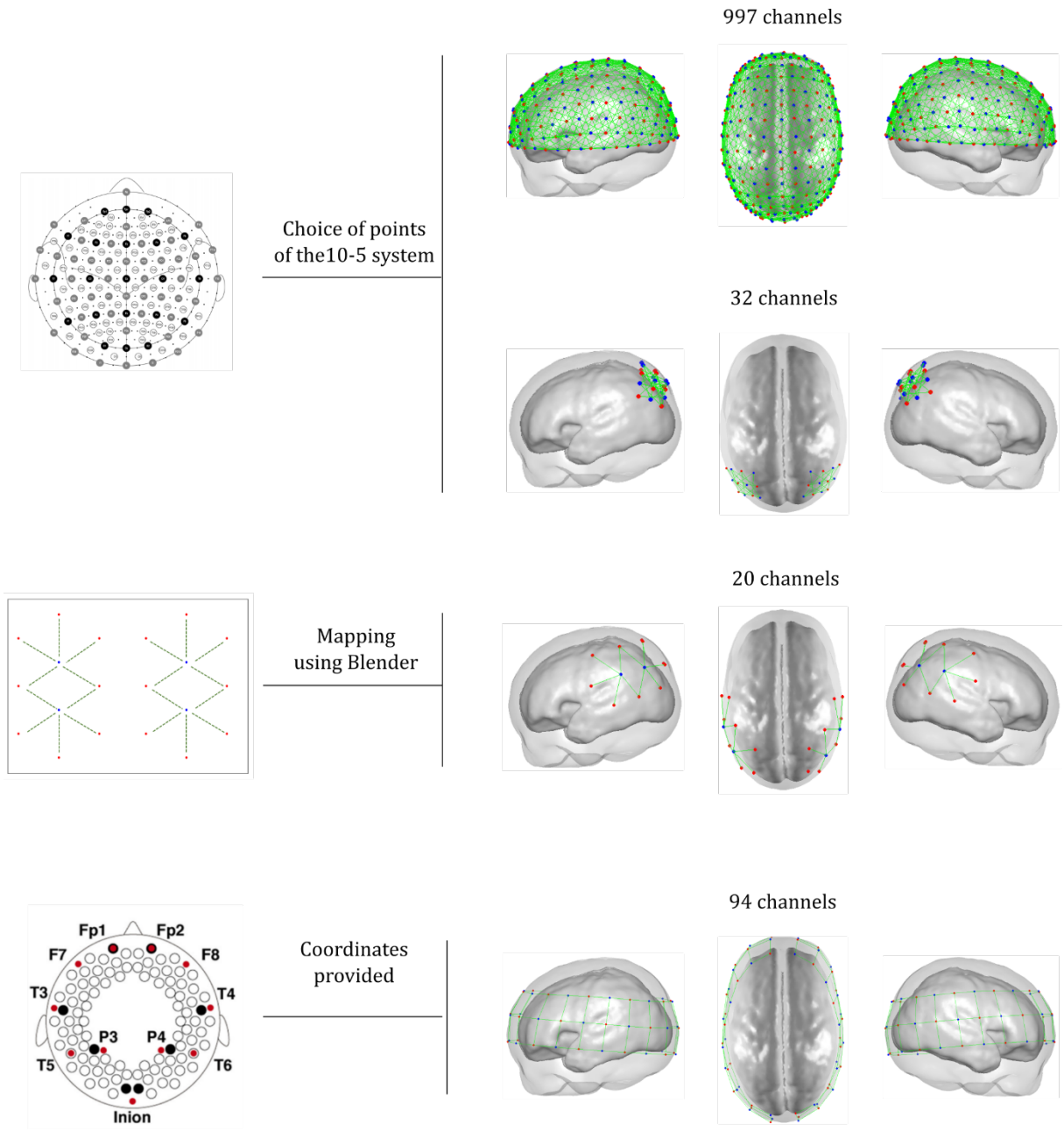

Figure 4.3 Probes construction for simulations. The large extended probe (997 channels) and its subset (32 channels) were defined from the 10-5 reference coordinates, associating alternatively a source (in red) or a detector (in blue) to well-known points of the system. Optodes positions for the first realistic configuration (20 channels) were obtained after a mapping of a linear geometry onto the Atlas scalp. Coordinates of the last arrangement were provided by the authors of the study (Homae et al., 2010). Green lines connect only those pairs of source-detector at a distance in the range [18-28 mm], indicating the presence of a channel. It should be noted that the last two probes were characterized by a fixed source-detector distance (20 mm).

Optical features assigned to each layer of the Atlas head mesh are reported in Table 1. We averaged scalp and skull properties to obtain a unique ECT value. The same refractive index (n = 1.3) and anisotropy coefficient value (g = 0.9) – parameters required from Monte Carlo simulations - were assigned to each different tissue. Brainstem and cerebellum properties were approximated to the white matter values.

Table 2 – Optical properties assigned to the six layers of the head model and used for the photon migration simulations.

	μ_a (1/mm)	μ_s (1/mm)	g	n
ECT	0.017	17.50	0.9	1.3
CSF	0.004	0.32	0.9	1.3
Gray matter	0.048	5	0.9	1.3
White matter	0.037	10	0.9	1.3
Brainstem	0.037	10	0.9	1.3
Cerebellum	0.037	10	0.9	1.3

4.2.4 Photon migration simulations

In order to simulate how light spreads in the brain, we generated the statistical distribution of photons in the human head model, with a Monte Carlo method (Wilson & Adam, 1983). Using Monte Carlo, we were able to obtain the probability distribution by modelling a large number of photons trajectories in a multi-layered medium and keeping track of their paths, one by one. Monte Carlo follows a basic algorithm, which is repeated until certain conditions are satisfied (Fang & Boas, 2009). To start, direction of the photon and the initial position have to be defined. Light is injected perpendicularly to the head surface through optodes, modelled as pencil beams. Therefore, the initial position corresponds to sources and detectors coordinates onto the surface of the volumetric head mesh (Figure 4.1, b). Being a tetrahedral mesh, it is organized in nodes, element and faces. At first, the algorithm recognizes the element enclosing the light source. When the photon enters the medium passing through the first element, the length travelled before the next scattering event (scattering length) and a scattering angle are computed on the basis,

respectively, of an exponential distribution and the Heyney–Greenstein phase function (describing the probability of scattering at a specific angle) (L. Wang, Jacques, & Zheng, 1995). The absorption acts by reducing the weight of the photon – at the beginning set at 1– with the Beer-Lambert Law, where the absorption coefficient is the one associated to the current element. The resulting photon weight is distributed to the nodes of the element enclosing the photon. Along its trajectory, the photon will move from one element to another until the entire scattering length has been travelled. The subsequent scattering event determines a deviation in the trajectory of the photon. The process stops when the photon exits the medium. Thus, the information about the photon fluence within the medium comes from photon weights recorded at all the nodes belonging to elements crossed by the photon. The last leg of the path is the detector position, where the algorithm returns the exiting photon flux. At the end, this quantity is divided by the total number of simulated photons, in order to be calibrated. The final photon fluence is corrected imposing the sum of exiting photon flux and absorbed photons equal to the total number of simulated photons (Boas et al., 2002).

We launched 10^8 photons at both sources and detectors positions. To each node of the tetrahedral mesh is associated a value of absorption and scattering coefficient, specified in Table 2. We run this process in MATLAB using a Mesh-based Monte Carlo software package (MMC, v2016.1) (Fang, 2010). The great advantage of MMC, when compared to other similar solvers, is the capability to handle complex heterogeneous domains and meshes with complex element shapes, such as tetrahedral ones. Moreover, the method guarantees high efficiency in producing accurate solutions in objects with curved boundaries, for instance the human head model. The refractive index was set equal to 1.3 for all tissues.

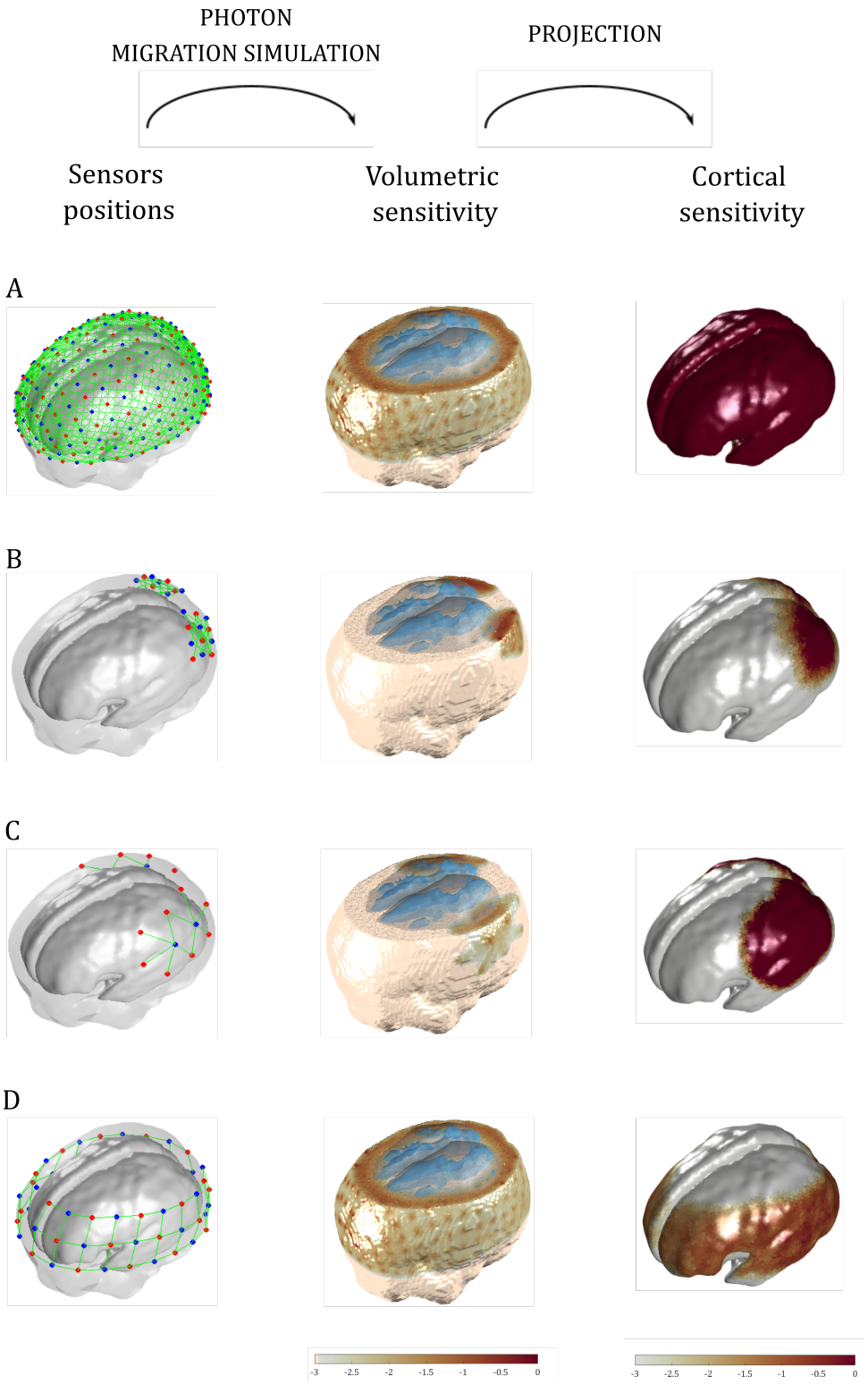

Figure 4.4 From source and detector positions to cortical sensitivities. Starting from the optodes coordinates onto the scalp of the Atlas (40th weeks), the Monte Carlo simulations were run. Resulting volumetric sensitivities were obtained and are reported in the second column. The cut aims to show in a clear way how light diffuses into the brain, from the scalp to the cortical layer. The volumetric information is then projected onto the cortex, as shown in the third column. The representations are reported for the different probes of 997 channels (A), 32 channels (B), 20 channels (C) and 94 channels (D). The maps of volumetric and cortical sensitivities are logarithmic.

4.2.5 Sensitivity maps

As extensively explained in section 2.6.1 and 2.6.2, by simulating photons migration from each optodes coordinates we could estimate the Green's functions (see Eq. 19) of the photon fluence for sources and detectors position (Custo et al., 2010). Sensitivity profiles of every fNIRS channel were computed as the normalized[6] node-wise product of relative sources and detectors corrected fluence distributions.

Thus, from the resulting contributes, we obtained the complete Jacobian – usually referred to as sensitivity matrix. Rows of the sensitivity matrix represented single measurements profiles and provided information on the spreading of light, ascribed to a specific channel; on the other hand, columns represented sensitivity of the whole brain to a specific node of the head mesh. At the end, four different sensitivity matrices were estimated, one for each probe configuration.

The resulting Jacobian matrix gives volumetric information. However, from this stage forward, we constrained the process to the cortex, projecting the three-dimensional map onto the superficial grey matter mesh. To this end, we associated each node of the volumetric head mesh to the node of the grey matter mesh placed at the minimum distance. This mapping was at the basis of the projection process. Indeed, the sensitivity of the superficial mesh was defined, in each point, as the sum of the sensitivity values of the correspondent three-dimensional mesh nodes. The choice of constraining the analysis the surface allowed to improve the quality of the final reconstruction (Boas & Dale, 2005) and decreased the computational cost. In fact, the number of nodes of grey matter mesh of the Atlas, for a term neonate, is almost 70 times smaller than the number of head mesh nodes. Resulting sensitivity matrices, expressed as the product of number of channels per number of grey matter mesh's nodes, are definitely more manageable (Figure 4.4).

[6] First, the single fluences have been corrected by dividing each one for the total number of photons used for the simulation. The sensitivity profiles have been obtained by dividing the product of the corrected fluences by half of the sum of the maximum values, respectively, of relative source and detector corrected fluences.

4.2.6 Synthetic cortical activations

In general, evaluating the goodness of a reconstruction without knowledge of the spatial origin of hemodynamic responses is a challenging process. Thus, a solid ground-truth reference is necessary to compare the results of the reconstruction. Since our research interest focused on the emergence of DMN in newborns, we created a synthetic pattern of correlated activations, which resembles the network under investigation. To do this, a time course simulating the absorption changes has to be associated with each point of the grey matter mesh in regions corresponding to the DMN.

First, we localized the foci of activation, representing the center of regions involved in the spatial pattern. We manually selected six symmetrical *reference points* - three for each hemisphere - respectively in the prefrontal, in the lateral parietal and over the precuneus areas of the grey matter mesh. Cortical nodes involved in our synthetic network were located inside spheres, centered on the reference points. Sphere radii were set to 3 mm for parietal and prefrontal nodes and to 1.5 mm for sulcus activations.
We simulated synthetic absorption changes using NeuroSim (Welvaert, Durnez, Moerkerke, Verdoolaege, & Rosseel, 2011), a R package generally adopted for simulating fMRI BOLD time series (Bordier, Nicolini, & Bifone, 2017). This tool generates time series, discerning two major components of the signal that are separately modeled: noise and activation. The latter can be obtained from an experimental design or a resting state condition. To every node involved in the pattern of activations, we assigned the same resting state signal – created using the *simTSrestingstate* function. Our artificial DMN is now mapped out, resulting in correlation $= 1$ (resulting from identical time courses) between involved mesh points and correlation $= 0$ elsewhere. In order to reproduce realistic experimental conditions, we injected, in each node of the mesh, noise time series that were independently generated from a mixture of system and physiological noise contributions. In detail, a physiological noise source is responsible for possible artifacts due to respiratory rate and heartbeat. Thus, it is defined by sine and cosine functions, modulated with respiratory and cardiac frequencies - respectively at 0.65 and 2 Hz in neonates. On the other hand, system's noise is modeled as Gaussian distributed noise. A visual representation of the time series allocation in each node of the mesh is reported in Figure 4.5. Noise and resting state time series consisted both of 12.000 time points, at a

sample frequency of 15.625 Hz (~ 13 min), to replicate the duration of a real successful resting state acquisition on neonate (based on the experiment presented in Chapter 3). The resulting pattern of correlations is illustrated in Figure 4.6.

Deciphering to what extent the existence of anticorrelated signals could affect the inverse reconstruction process is crucial to assess the reliability of the method for functional connectivity studies. Therefore, we created a second pattern of activations, in particular simulating the competitive relationship between DMN and part of dorsal attention network (DAN). To obtain this, we added to the previous spatial pattern the contributions of areas showing a negative correlation with DMN regions. Two new foci of activation were individuated on the grey matter mesh, one for each hemisphere, localized in cortical regions corresponding to intra parietal sulcus (IPS). Absorption perturbation involved all cortical nodes within a sphere of 2 mm radius, centered on the new reference points. Resting state and noise time series were introduced with the procedure described above. However, with the aim to produce anticorrelations, here we injected a resting state time course in exact phase opposition with respect to the one previously used (pattern of correlation and anticorrelation illustrated in Figure 4.6).

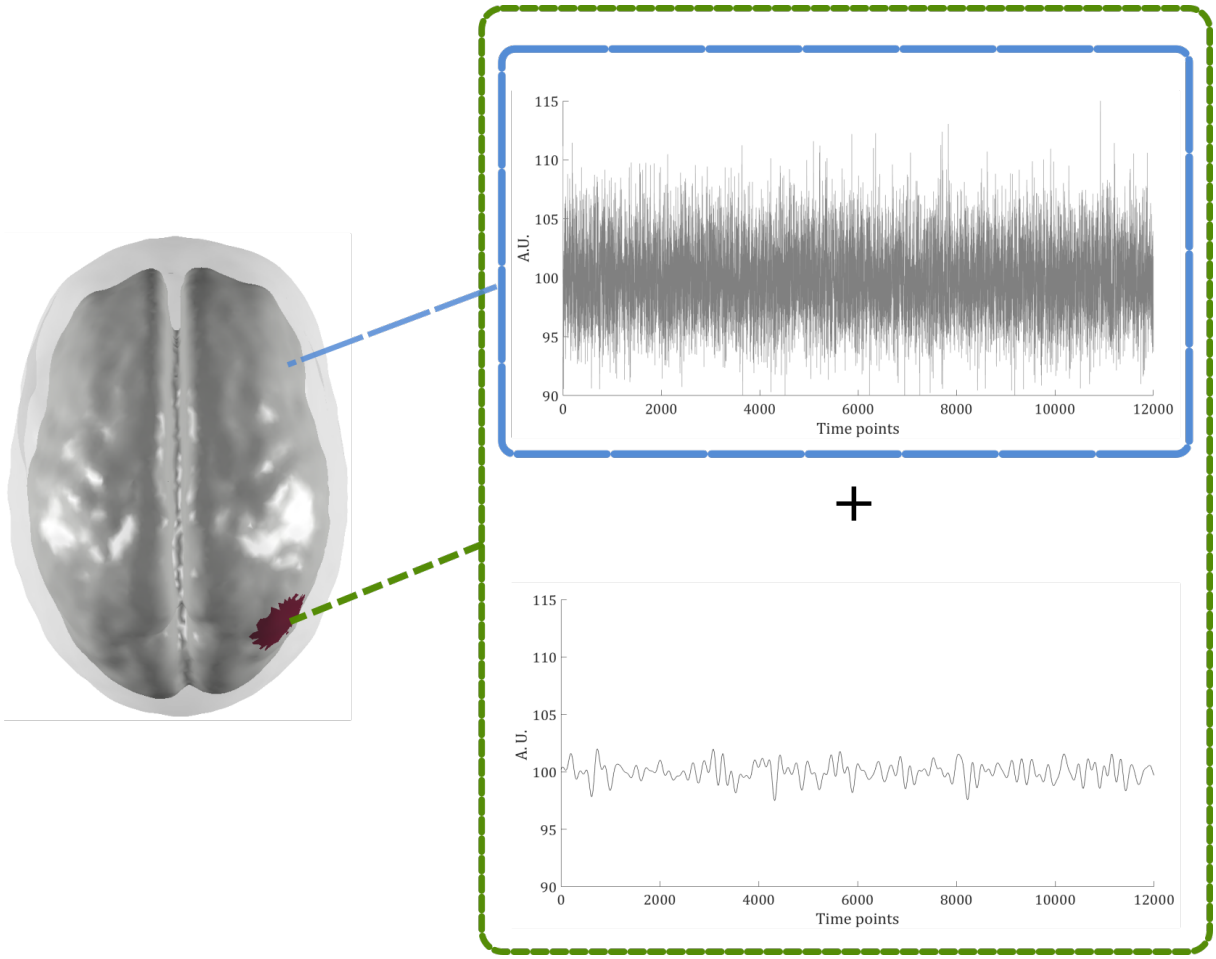

Figure 4.5 Generation of a synthetic set of activations in a term neonate's brain (4D Atlas). Noise (in the blue rectangle) and resting state time series of 12000 time points were generated using Neurosim R package. The noise time course has been associated to each node of the grey matter mesh; only in correspondence of the nodes involved in the correlation pattern we added the resting state time course to the noise (the resulting time series, at SNR = 30, is framed in green). The baseline of both noise and signal time series were set at 100. On the left, the red area represents a localized activation (set of adjacent nodes to which correlated time series were associated).

In order to explore effects of level of system noise, we modulated the Signal to Noise Ratio (SNR) of the total time course, which is defined as the ratio between the average magnitude of the signal (resting state time course) and the standard deviation of the noise (Figure 4.5). We created absorption variations at several levels of noise, but only three of them were considered for the analyses – as they are the most representative. We showed how the quality of resulting reconstruction of functional connectivity maps might vary in presence of high quality of source's signal (SNR = 30), realistic signals (SNR = 10) and very noisy signals (SNR = 1).

To sum up, in order to assess the reliability of the process we chose probe geometry, pattern configuration and level of noise as variable parameters for our model.

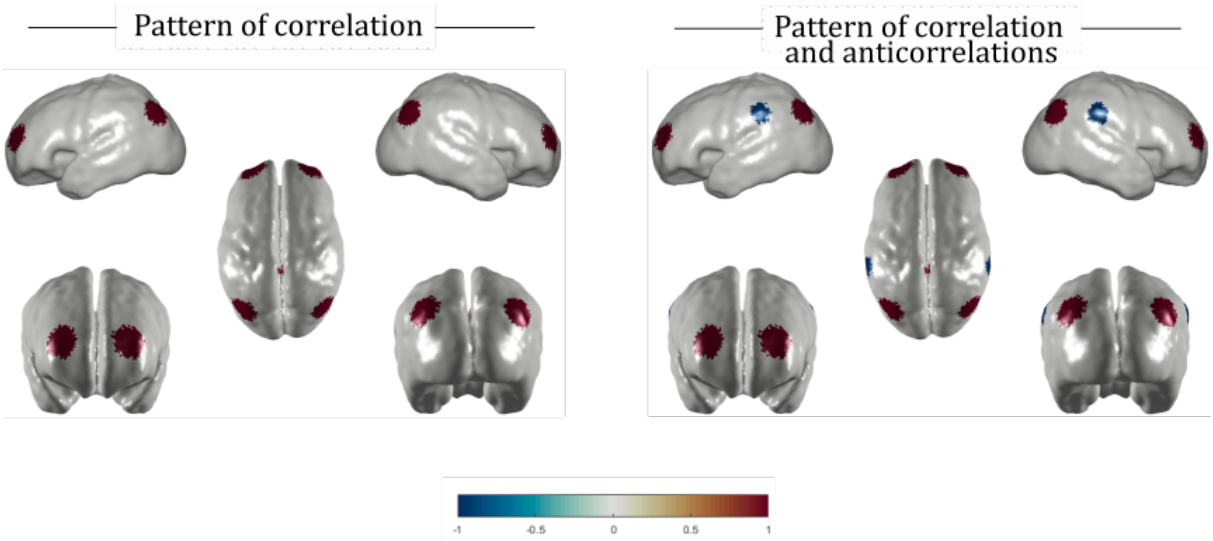

Figure 4.6 Patterns of synthetic positive and negative correlations. On the left, the first set of correlated activations reproduces the characteristic spatial pattern of Default Mode Network, with distinct and symmetric clusters of activations localized above the prefrontal, parietal and precuneus cortical regions. On the right, the second pattern includes two additional regional of interest above the intra-parietal sulcus of the Dorsal Attentional Network, emulating the relationship (in the form of negative correlations) between the two different networks.

4.2.7 Real data

In addition to the validation of the method in a synthetic environment, we tested the inverse reconstruction method using real acquisitions on newborns.

First real dataset

The first dataset consisted of eight resting state measurements, acquired on term infants with the 20-channels probe and has been thoroughly described in Chapter 3. It is worth recalling that the set of time courses admitted to final connectivity analyses met rigorous inclusion criteria. Good positioning of the probe, quietness and low ambient light conditions were guaranteed during the acquisitions. Moreover, time-courses with minimal artifacts were selected and processed, in order to avoid motion artifacts. The

relationship between DMN and DAN at rest was explored using a seed-based connectivity analysis in the sensor space on representative oxy- and deoxy- hemoglobin time series, obtained from the concatenation of the single z-scored signals, within the sample of eight participants. Results obtained from the analyses in the space of channels are reported in section 3.7.

Second real dataset

Collaborators from University of Tokyo provided the second dataset. Results of channel-based analyses performed on these subjects have been already discussed in a published work (Homae et al., 2010). The sample consisted of fifteen neonates, with age ranging from 2 to 11 days (mean 4.3 days). They were scanned in Tokyo Women's Medical University during natural sleep, with a multichannel continuous-wave instrumentation using two NIRS wavelengths (785 and 830 nm). Signals underwent band-pass filtering in the frequency range of [0.005 – 1 Hz]. For each subject's acquisition, time series of the duration of 3 minutes were extracted and used to obtain seed-based correlation analyses (r-Pearson value) in the sensor space. In the description of the dataset acquisition, it is well specified that no motion artifacts were detected. In addition, behavioral factors confirmed the deep sleep of the infants (not disturbed by sudden movements or non-nutritive sucking). All these elements together suggested a reliable quality of the dataset.

4.2.8 Inverse image reconstruction problem

Dealing with synthetic absorption variations, we needed to implement the simulated fluence measurements at the scalp, combining the sensitivity matrix and absorption variations. For small changes of absorption coefficient, small changes in fluences at the scalp level can be calculated using the linear equation (see Eq. 21):

$$\underset{(m \times 1)}{\Delta \mathbf{OD}} = \underset{(m \times n)}{\mathbf{J}} \; \underset{(n \times 1)}{\Delta \boldsymbol{\mu}_a}$$

where *m* is the number of channel, depending on the probe configuration in use and *n* is the total number of nodes of the atlas mesh. We constrained the process to the cortical

surface, thus n here refers to the size of the grey matter mesh (a superficial mesh) of the 4D Atlas for the 40th week.
In order to generate as realistic synthetic time series as possible, we introduced system and physiological noise components. For this reason, we filtered the data obtained at optodes level to the frequency band of 0.01 – 0.1 Hz, as we did in the case of real data.

On the other hand, starting from real raw intensity signals collected at the scalp, it was necessary to extract absorbance variations. For the first dataset, the values were extracted, for both wavelengths, from individual signals, using the relationships:

$$\Delta A_{\lambda_1} = \varepsilon_{oxy}(\lambda_1) \cdot \Delta C'_{oxy} + \varepsilon_{deoxy}(\lambda_1) \cdot \Delta C'_{deoxy}$$
$$\Delta A_{\lambda_2} = \varepsilon_{oxy}(\lambda_2) \cdot \Delta C'_{oxy} + \varepsilon_{deoxy}(\lambda_2) \cdot \Delta C'_{deoxy}$$

where λ_1 and λ_2 are the specific NIRS wavelengths of the instrumentation in use, in this case, 830 nm and 690 nm, respectively ; $\Delta C'$ indicates changes in concentration we estimated from attenuation of light recorded at the scalp; values of extinction coefficients are tabulated in (Prahl, 1999) and , specifically, $\varepsilon_{oxy}(\lambda_1) = 415$, $\varepsilon_{deoxy}(\lambda_1) = 2141.8$, $\varepsilon_{oxy}(\lambda_2)$=1008, $\varepsilon_{deoxy}(\lambda_2) = 778$ (molar extinction coefficients are expressed in $\mathrm{l} \cdot \mathrm{cm}^{-1} \cdot \mathrm{mol}^{-1}$).
In the case of Japanese dataset, absorbance measures were obtained directly from the machine.

Once we obtained the simulated raw fluences at the scalp or the real absorbance variations, at the level of the sensor space, we were able to solve the inverse model to reconstruct original elements of the source space. The inversion of the $\mathbf{J}$ matrix has been accomplished using the regularization methods reported in Chapter 2.
Thus, cortical activations are reconstructed from the relation expressed in Eq. 22:

$$\Delta\hat{\boldsymbol{\mu}}_{\mathrm{a}} = \mathbf{J}^{\mathbf{T}} (\mathbf{J}\,\mathbf{J}^{\mathbf{T}} + \mathrm{k}\boldsymbol{\sigma}^2_{\Delta\mathbf{OD}})^{-1}\Delta\mathbf{OD}$$

in which $\boldsymbol{\sigma}^2_{\Delta\mathbf{OD}}$ is the diagonal measurement covariance matrix and the parameter k is defined as $\alpha \cdot \max(diag(\mathbf{J}\mathbf{J}^{\mathrm{T}}))$, where α=0.01 (Boas & Dale, 2005). At the end, we were

able to define a map of absorption variations, which theoretically reflects the neural activity.

4.2.9 Reconstructions comparison: quantitative metrics

Exploiting the availability of the ground-truth pattern, we defined some quantitative metrics to describe more accurately the influence of different experimental factors on the results. We chose to investigate the variations in the position, extension and shape of the reconstructed pattern with respect to the ones defined in the ground-truth, with or without anticorrelations.

First, considering one component of the correlation pattern at a time, we computed the Euclidean distance in the 3D space between the centroids of original (ground-truth) and reconstructed components, in order to detect potential shifts due to the reconstruction process.

The extension of the regions was evaluated computing the sum of the areas of the mesh including nodes that showed a correlation higher than the threshold. In the count, mesh triangles were included only if all the three component nodes satisfied this condition. The difference between each original component and the corresponding reconstructed one was considered. Moreover, we estimated the ratio of nodes in common between ground-truth and reconstructed components by calculating the Jaccard index (Jaccard & Zurich, 1901). This index measures the similarity between finite sets of nodes and is defined as the size of the intersection of the two sets of interest divided by the size of their union (the index varies in the range [0,1]).

Alterations in the shape of reconstructed areas with respect to the original ones were estimated by computing the Hausdorff distance (Huttenlocher, Klanderman, & Rucklidge, 1993), which is defined as the largest distance of the first set of points to the nearest point of the second set.

The average of the quantitative metrics over the different components was used to assess the reliability of the reconstruction of the whole pattern.

We note that the reconstructed correlation patterns depended on the choice of threshold, as they include a set of nodes exhibiting correlation above a certain value. Thus, to investigate the effect of the threshold choice on the connectivity maps, we computed the metrics for 20 different values of threshold.

4.2.10 Functional connectivity maps

The reliability of the process was evaluated by comparing the synthetic spatial patterns that were originally injected and the reconstructed ones. Functional connectivity maps were defined using a seed-based analysis. Above the regions of interest, we localized reference points that became the centers of a sphere with radius 1.5 mm. Seed time courses, for each region of interest, were derived from the average of all the time series associated to cortical nodes in this sphere.

Connectivity maps were computed from the correlations between seed and all time courses associated to cortical nodes. We obtained functional maps from original activations (we injected directly into the cortex) and reconstructed activations. The former represented the ground-truth we used for assessing the goodness of the method.

The reconstruction of real data allowed the comparison between the sensor-based description, reported in Chapter 3, and the source-based representation here implemented.

The rationale of the process is briefly schematized in Figure 4.7.

4.3 Results

In the present section, outcomes of the process of reconstruction will be illustrated.

Four different probes were defined onto the scalp of the Atlas (40^{th} week): a 997 channels with full coverage of the brain with a high, although impractical, density of sensors; a 32 channel probe with the same geometry of the extended one, in term of density of channels, but with coverage of parietal areas of DMN; a 20-channels probe designed to cover the LP regions of DMN and IPS within DAN; a 94 channels array, original employed for the investigation of frontal, temporal, parietal and occipital areas. A clear representation of the available configurations is reported in Figure 4.8.

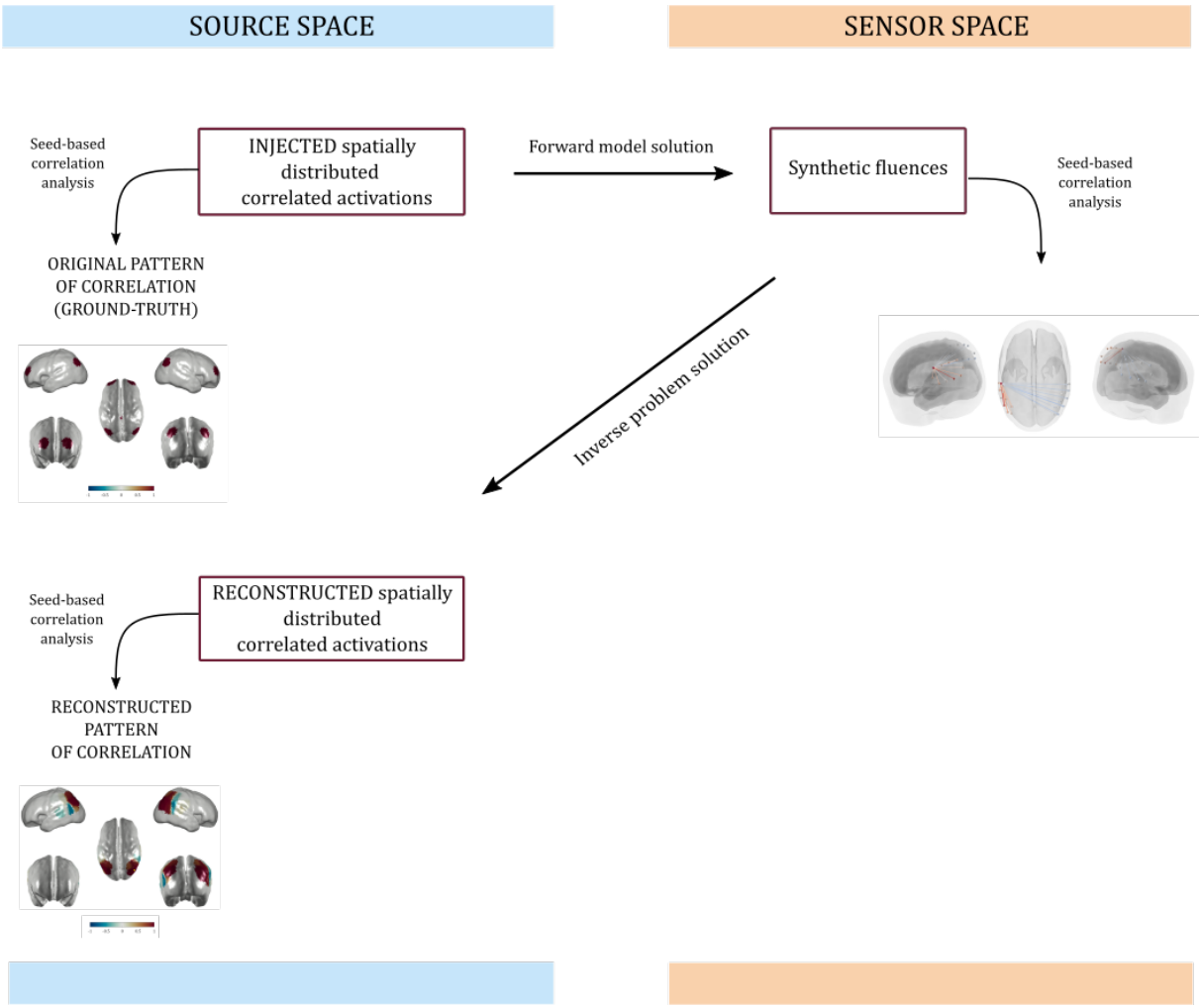

Figure 4.7 Schematics of the process of functional connectivity maps reconstruction using the 20-channels probe.

For the four probe configurations, we computed the volumetric spatial sensitivity (Figure 4.9). At each node of the head mesh, the map gives information on the amount of photons that have passed through that specific position on their way to the detector. This representation is powerful because it provides a visualization of the light diffusion into the brain. In particular, the top view highlights the inability of fNIRS light to reach deep cortical regions. On the other hand, the projection of the sensitivity matrix onto the cortex emphasizes the actual region under investigation with the specific optodes arrangement in use (Figure 4.10).

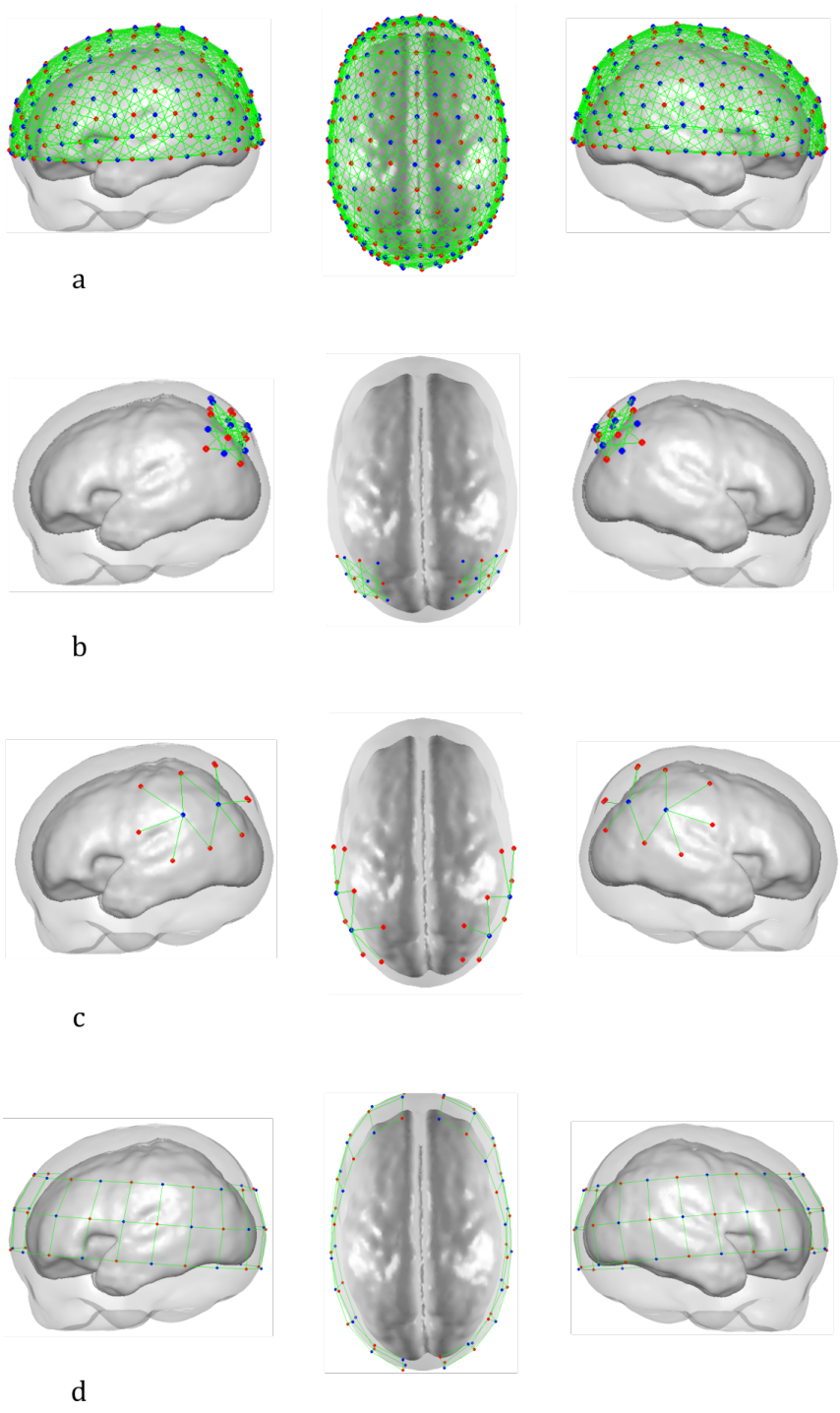

Figure 4.8 The four probe configurations used to test the reconstructions reliability on synthetic and real data. Sources and detectors positions are shown, respectively, in red and blue onto the scalp of the Atlas. The a) is formed of 997 channels, arranged in a dense and extended array able to cover the whole brain using overlapping and multidistance source-detector pairs. With 12 sources and 12 detectors densely packed in 32 channels, the b) covers only the parietal regions of the DMN. The c) reproduces the 20 channels probe employed to investigate the DMN in term newborns. Source – detector distance is fixed at 20 mm. Lastly, the d) reflects characteristics of probe used to collect data from the University of Tokyo (Homae et al., 2010).

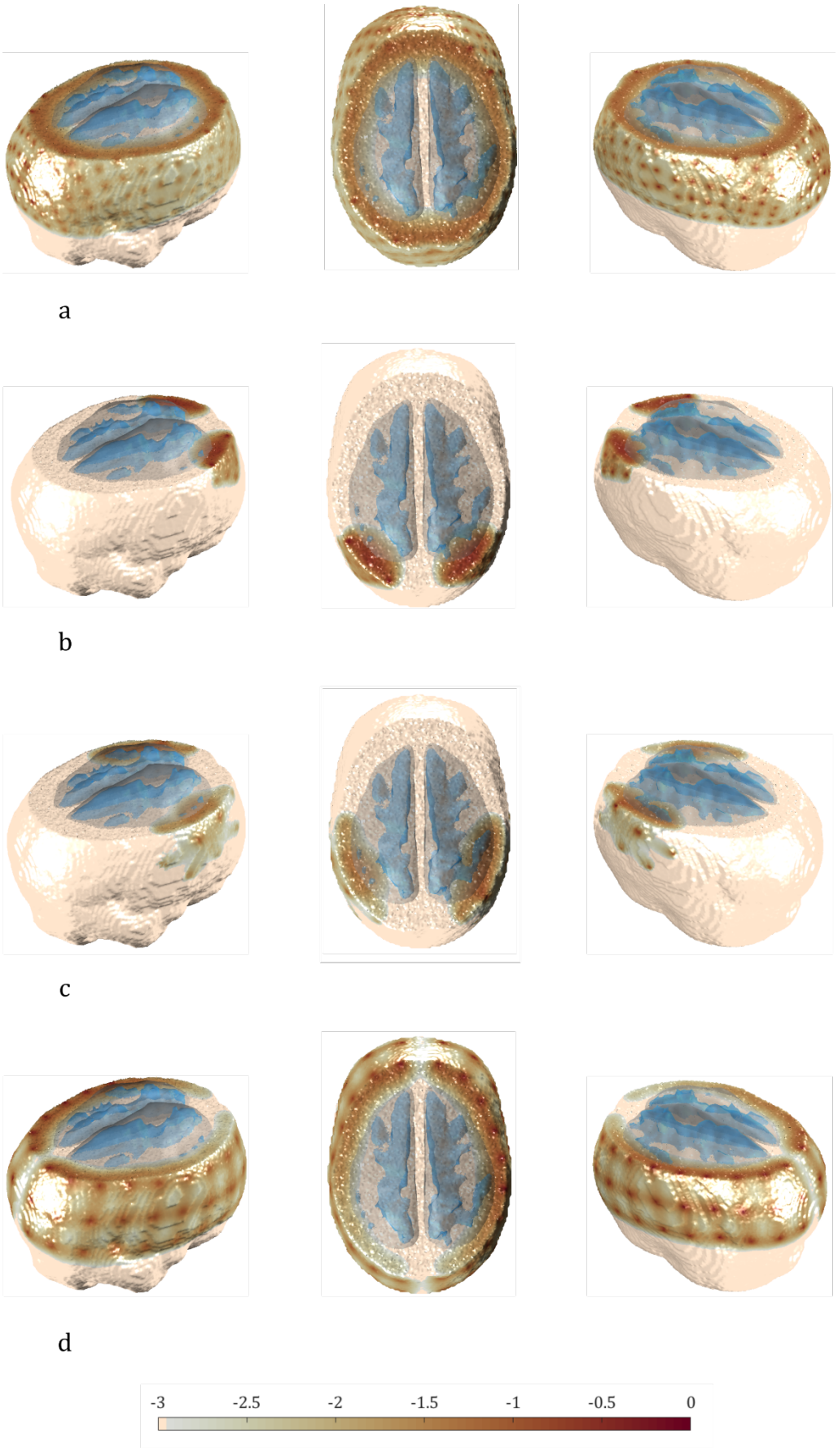

Figure 4.9 Logarithmic representation of the volumetric sensitivity for the four probes: 997 channels (a), 32 channels (b), 20 channels (c), 94 channels (d).

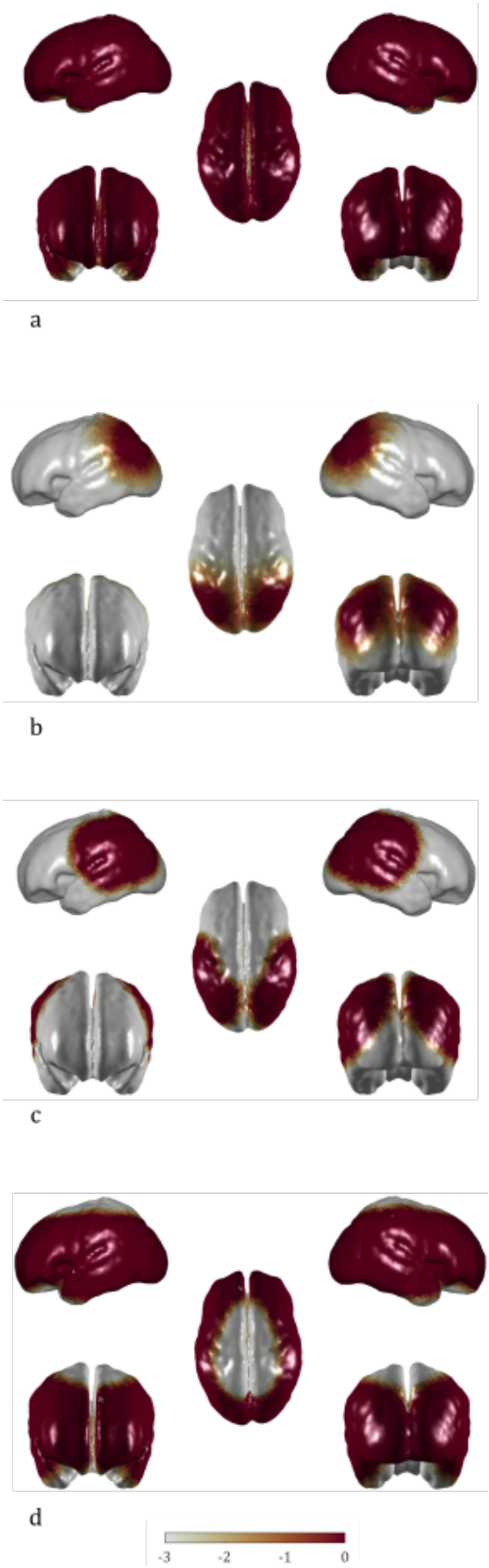

Figure 4.10 Logarithmic representation of the cortical sensitivity for the four probes: 997 channels (a), 32 channels (b), 20 channels (c), 94 channels (d).

4.3.1 Reconstruction of synthetic data

Synthetic absorption variations were spatially organized in order to emulate the DMN pattern. All of the available arrangements were able to cover, at least partially, regions of the network of interest. It is worth noting that beyond the spatial extension, a major difference between the four arrangements that we used is the source-detector separation (that can vary within a range of distances or can be set at a fixed value) and the existence (or not) of overlapping channels.

In Figure 4.11, we show the reconstruction of the original pattern of correlation injected into the cortex at different levels of SNR, with the largest arrangement of sources and detectors. The correlation was estimated using a seed placed in the right parietal region. As highlighted by the projection of the volumetric sensitivity onto the grey matter, the probe allowed investigating the whole brain uniformly. With SNR 30, we obtained an accurate reconstruction of the ground-truth pattern. It was possible to discern different loci of activations, which maintained their original shape and position, even though they appeared enlarged, if compared to the original ones. Interestingly, a halo of negative correlations surrounded the distinct correlated regions. In the rest of the brain, random spots of extremely weak correlation and anticorrelation accounted for the presence of a very low noise. Observing the reconstructed correlations pattern from signals at SNR 10, the effect of the noise was notable. In any case, the entire simulated DMN was still fully recognizable, but the value of average correlation was lower. In the case of a very high contribution of noise, we observed a resulting random pattern of positive and negative correlations. Here, original characteristics of the network were completely buried under the noise.

Figure 4.12 presents outcomes of the process, when specific cerebral regions were investigated with a high density but spatially limited probe, positioned exactly above the area of interest (in this case, lateral parietal components of the synthetic DMN). With SNR $= 30$, it appeared clear that the different arrangement had an effect on the reconstruction. Despite the clear presence of the two correlated sources of activation, the shape was no longer entirely preserved. Indeed, borders became irregular and fuzzy. This time, the negative artefactual correlations did not encircle systematically the activations, but

appeared fragmented. We observed similar dynamics in reconstructions at SNR = 10, except that the higher weight of the noise led to a decrease of the average value of correlation and a weaker effect of negative correlations. Again, the sharp decrease of the SNR, in the last case, prevented detection, even partially, of the original pattern.

The synthetic pattern was also reconstructed with the probe geometry used for our experiment (Figure 4.13). The probe covered, by a large margin, the parietal activations, which were roughly reconstructed. It was still possible to recognize the presence of two main correlated contributions, but, in the resulting maps, the shape of activations was consistently enlarged, in both SNR = 30 and SNR = 10. Even at high SNR, it should be noted the presence of a compact band of negative correlations, adjacent to the set of positive correlated nodes. The effect of noise is critical in the last case where, at SNR = 1, image reconstruction failed. Indeed, the outcome seems to suggest the emergence of a spatial pattern of correlation (negative and positive) that did not reflect, at all, the original one.

The 94 –channels probe was designed to cover the prefrontal cortex and a large part of the parietal cortex, including most of the LP and the IPS (Figure 4.14). This configuration allowed testing the combination of an extended coverage with a low-density distribution of sources and detectors, without overlapping channels. This probe configuration was used to acquire resting state data in 4 day old babies (Homae et al., 2010) by Prof. Taga's group, and its simulation will make it possible to attempt reconstruction of this dataset (see section 4.3.3). If compared to the outcomes obtained with the ideal probe (see Figure 4.11), an enlargement of the reconstructed correlation foci is apparent, especially in the frontal region. Similarly, the spurious negative correlations arise, in particular at SNR 30, closely localized around the cluster of nodes positively correlated.

We tested the process of image reconstruction keeping intact the modalities above described, but introducing at the scalp a different synthetic configuration of spatially distributed activations. We simulated the competitive relationship between DMN and DAN, adding to the previous pattern two symmetric foci of activations, anticorrelated with the rest of the network. The summary table in Figure 4.15 illustrates the resulting connectivity maps obtained with different probes, and varying the level of noise. The

extended coverage of the brain confirmed its capability to reconstruct correctly the original activations, preserving not only the position and the shape but also the sign of correlation. Indeed, negative contributions appeared clearly distinguishable at acceptable levels of noise. It is worth noting that at SNR = 30 systematic spots of positive correlations appeared around the cluster of negative correlations, in addition to the opposite behavior already noted with the previous configuration. Again, working with minimum SNR, the reconstruction of random noise is observed. As expected, the 32-channels probe is unable to detect changes in absorption coefficient located in IPS area, thus the outcome in this case is comparable to the one showed in Figure 4.12. The last row of the chart shows effects of a low-density arrangement on the process. At maximum SNR, the map of functional connections seemed to be characterized by a sharp bimodal behavior. Indeed, positive correlated structures permeated the posterior half part of the entire area to which probe is sensitive. On the other hand, an extended component of negative correlations expanded in the superior anterior side. The original shape and size of activations were not recognizable anymore and it was evident a decrease of accuracy in the final reconstruction. Interestingly, the resulting pattern obtained with very low SNR is highly consistent with the previous computed without anticorrelations in the starting configuration.

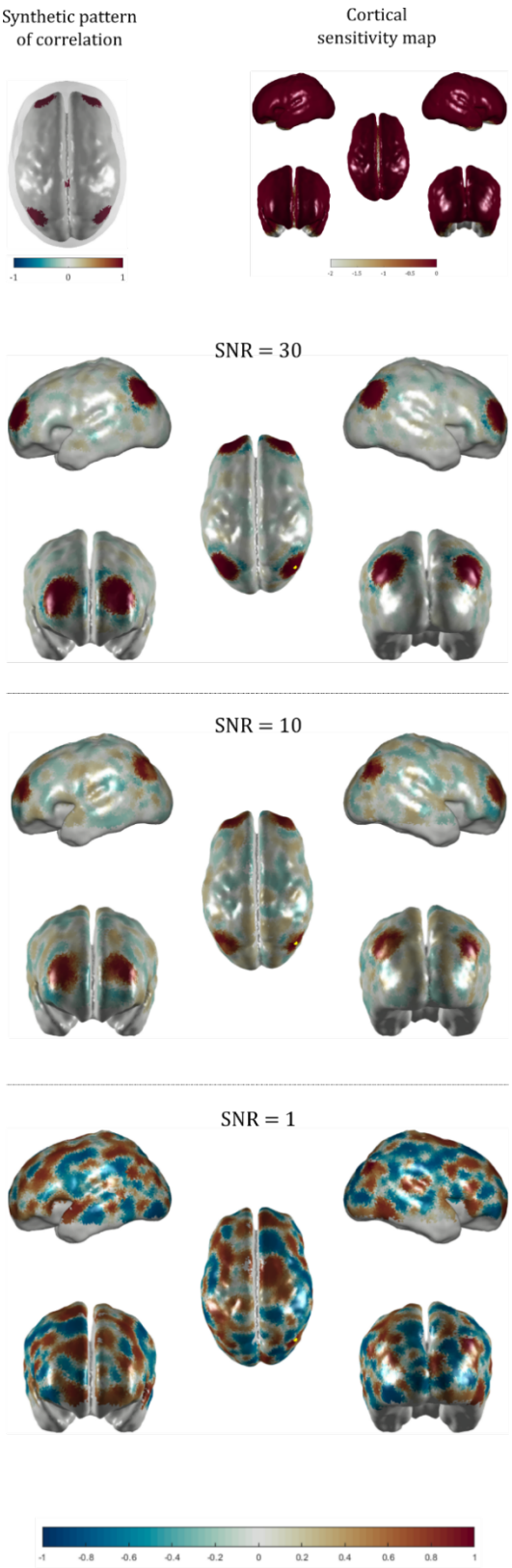

Figure 4.11 Spatial maps of reconstructed pattern of correlations obtained at different levels of SNR, using a probe of 997 channels. At the top on the left, the original configuration introduced in the cortex represents the ground-truth for comparisons. The pattern clearly emulates the DMN. On the right, a logarithmic map of the cortical sensitivity of the probe is illustrated. Note that logarithmic sensitivity below 100 is shown in white. Each connectivity map has been masked in the same way. Parietal seed used for correlation analysis is indicated in yellow.

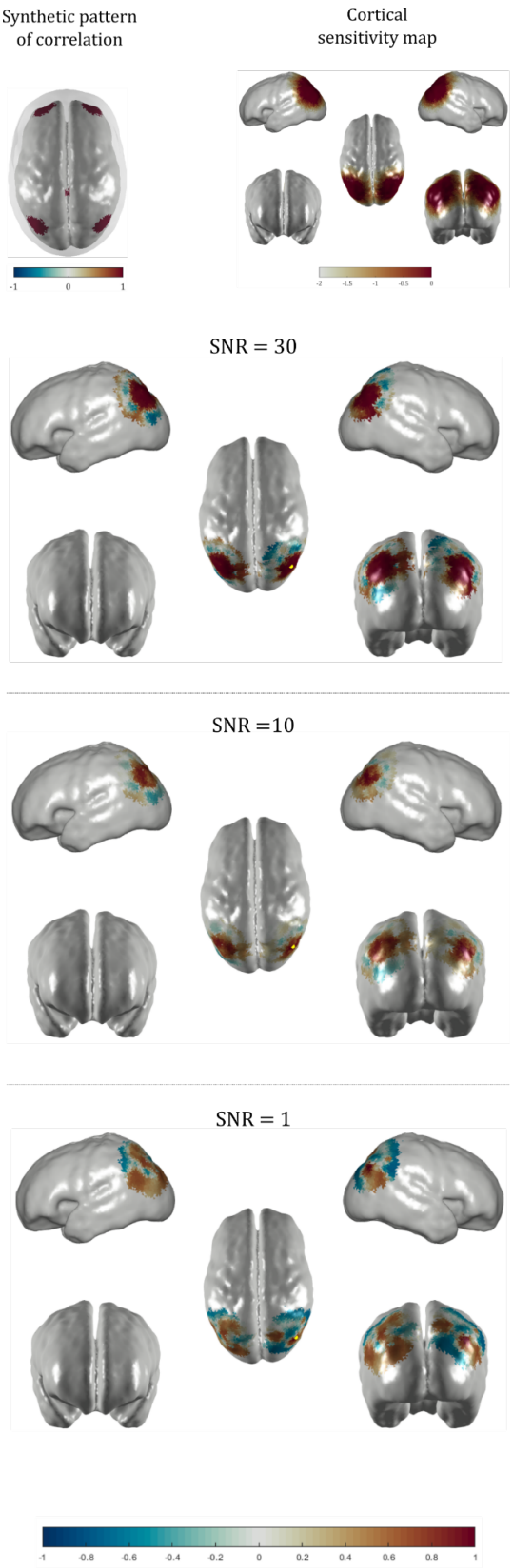

Figure 4.12 Spatial maps of reconstructed pattern of correlations obtained at different levels of SNR using a probe of 32 channels. At the top on the left, the original configuration introduced in the cortex represents the ground-truth for comparisons. The pattern clearly emulates the DMN. On the right, a logarithmic map of the cortical sensitivity of the probe is illustrated. Note that logarithmic sensitivity below 100 is shown in white. Each connectivity map has been masked in the same way. Parietal seed used for correlation analysis is indicated in yellow.

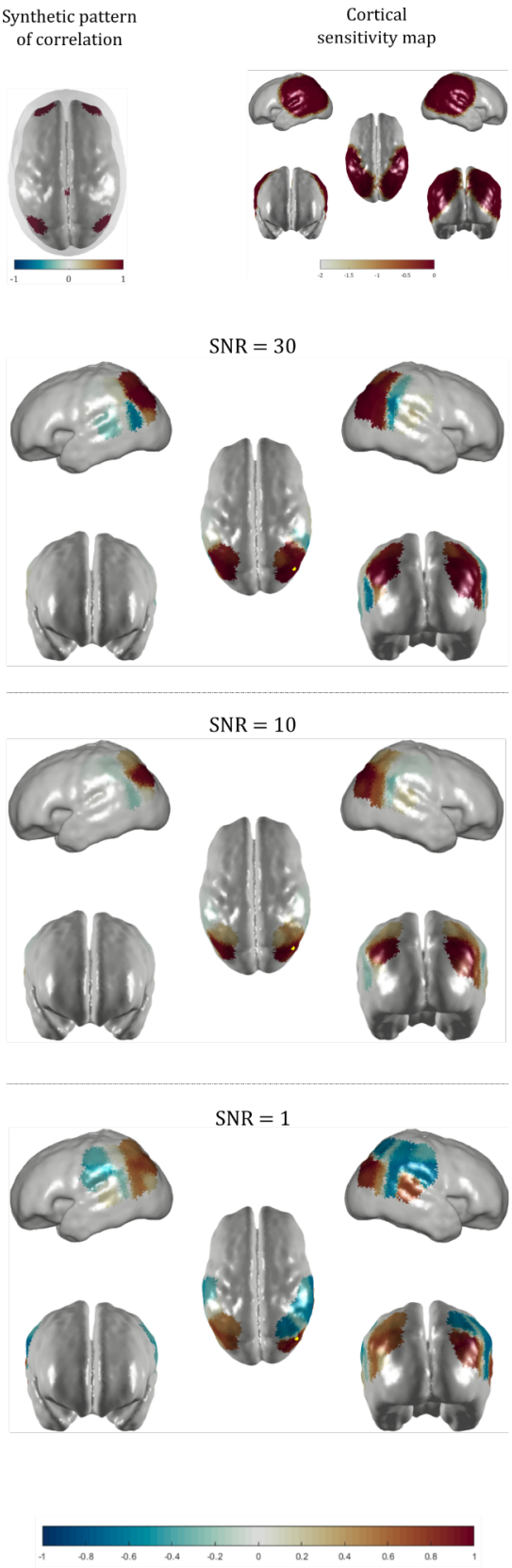

Figure 4.13 Spatial maps of reconstructed pattern of correlations obtained at different levels of SNR using a probe of 20 channels. At the top on the left, the original configuration introduced in the cortex represents the ground-truth for comparisons. The pattern clearly emulates the DMN. On the right, a logarithmic map of the cortical sensitivity of the probe is illustrated. Note that logarithmic sensitivity below 100 is shown in white. Each connectivity map has been masked in the same way. Parietal seed used for correlation analysis is indicated in yellow.

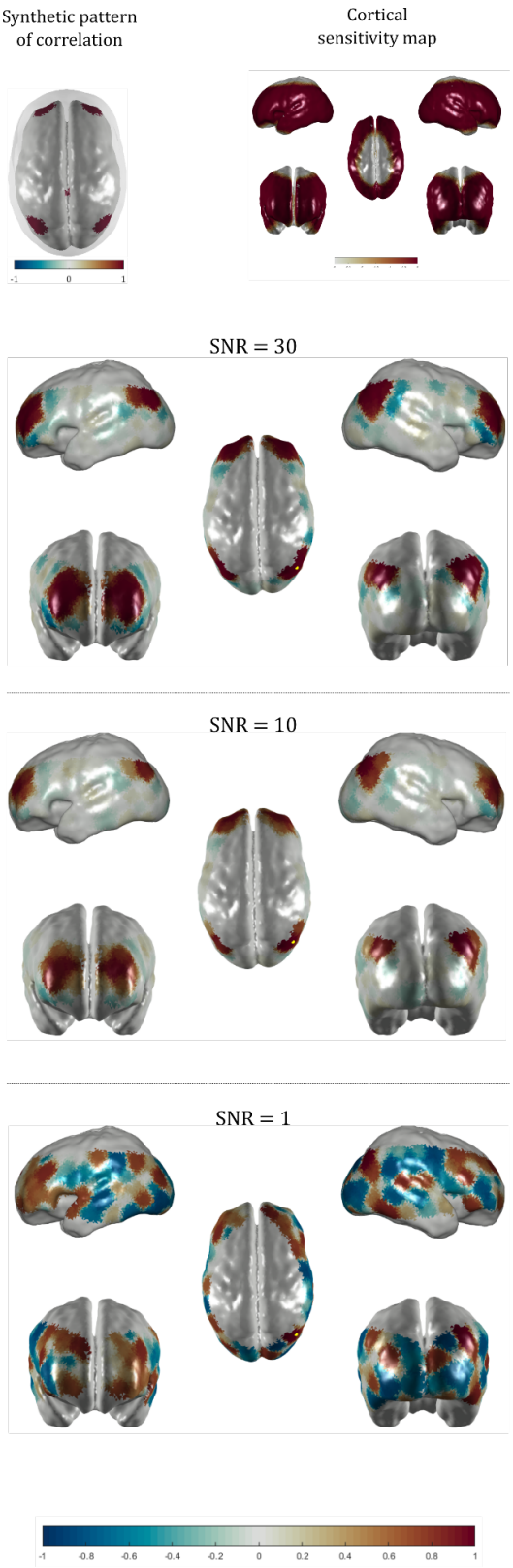

Figure 4.14 Spatial maps of reconstructed pattern of correlations obtained at different levels of SNR using a probe of 94 channels. At the top on the left, the original configuration introduced in the cortex represents the ground-truth for comparisons. The pattern clearly emulates the DMN. On the right, a logarithmic map of the cortical sensitivity of the probe is illustrated. Note that logarithmic sensitivity below 100 is shown in white. Each connectivity map has been masked in the same way. Parietal seed used for correlation analysis is indicated in yellow.

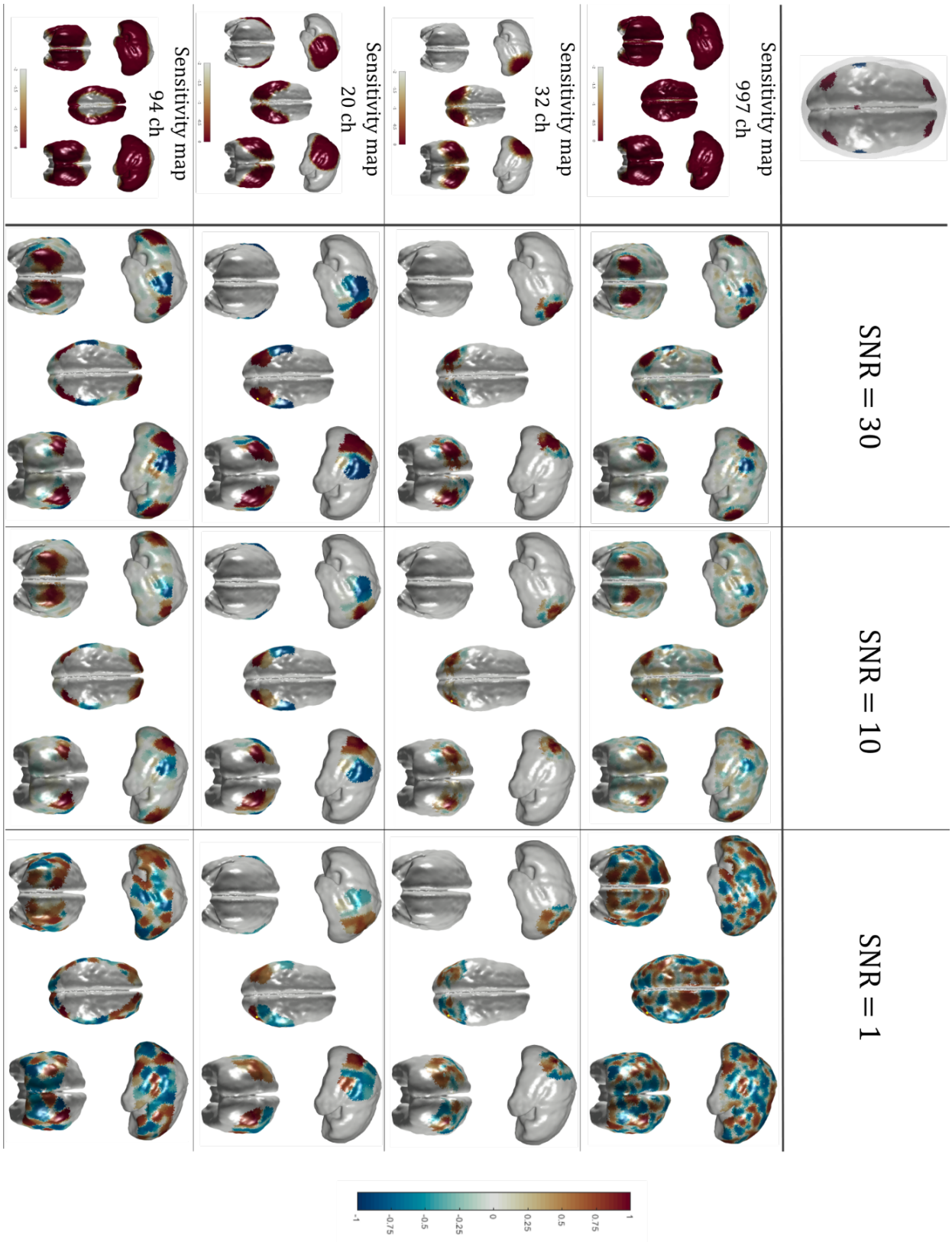

Figure 4.15 Overview of resulting connectivity maps, reconstructed from a ground-truth of correlated and anticorrelated activations. The outcomes varying probe size and geometry and SNR levels are shown.

4.3.2 Quantitative metrics

In order to test the goodness of the reconstruction process, we quantitatively compared the reconstructed functional connectivity maps with the ground-truth pattern, originally introduced at cortical level. Considering one activation at a time, we computed the distance between original and reconstructed regions' centroids and the difference between correspondent areas. Moreover, Hausdorff distance and Jaccard index were estimated. All the previously described metrics depend on the correlation threshold in use. For this reason, we conducted a preliminary exploration of the effects of the threshold choice on results. Here, these are reported in the case of the optimal largest probe (997 channels), investigating the ground-truth pattern without negative correlations. For each metric and each threshold, we showed the average value calculated among all the activations within the pattern.

It can be noted that metrics at SNR 30 and SNR 10 showed similar behaviors. In this cases, the reconstructed activations preserved their original positions (Figure 4.16), if the correlation threshold was greater than 0.4. The suboptimal performances below this threshold, shown in Figure 4.16, were also noticed computing the difference between areas of original and reconstructed activations (Figure 4.17). It can be noted that for thresholds greater than 0.6, at SNR 10, negative values are registered, suggesting a considerable area's reduction of the reconstructed activation. The observation of the Jaccard index trade (Figure 4.18) confirmed this peculiarity of data at SNR 10: indeed the percentage of nodes in common between original and reconstructed regions decreased at very low or very high threshold values. Lastly, the shape variation is relatively independent of the threshold in the range [0.4 – 0.7] (Figure 4.19). On the contrary, at SNR 1 all metrics showed stable but uninformative reconstruction, due to the high noise level.

This is consistent with the idea that there exists a range of thresholds whereby the optimal trade-off between removal of spurious correlations and preservation of informative correlations is achieved. Indeed, weak correlations are strongly affected by noise, and may confound reconstruction. Hence, thresholding is expected to improve the ability to delineate genuine activations. However, excessive thresholding may remove informative correlations as well, thus negatively affecting reconstruction. In our preliminary analysis,

we found that the optimal threshold falls in the range [0.4-0.7]. Importantly, within this range, the results do not critically depend on the specific value of threshold. In the light of these observations, we computed the metrics of Table 3, applying a threshold of 0.5. We noted that this is the same threshold used in previous papers (Homae et al., 2010) – for positive correlation patterns.

Also, we only show results for the case SNR=10, which is the closest to realistic experimental conditions.

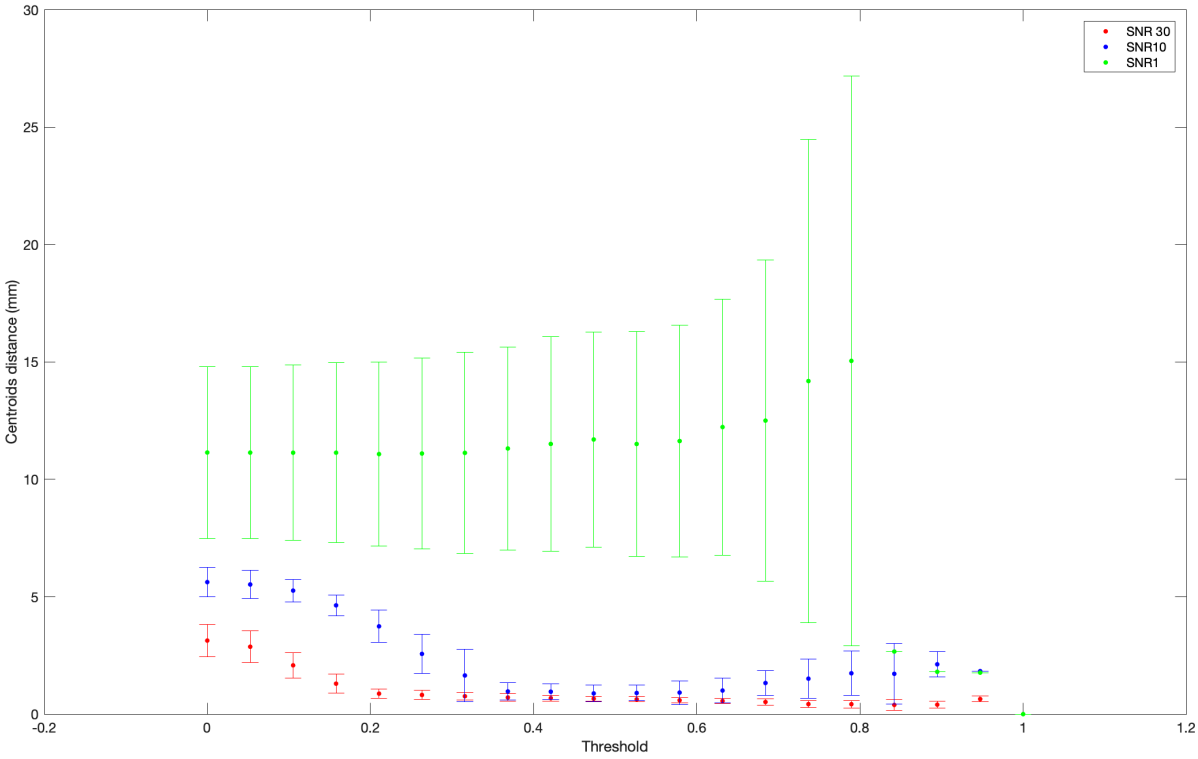

Figure 4.16 Euclidean distance between centroids of original and reconstructed activations, reported at different SNR values. The results refer to the ground-truth pattern without negative correlations, detected from the largest probe of 997 channels.

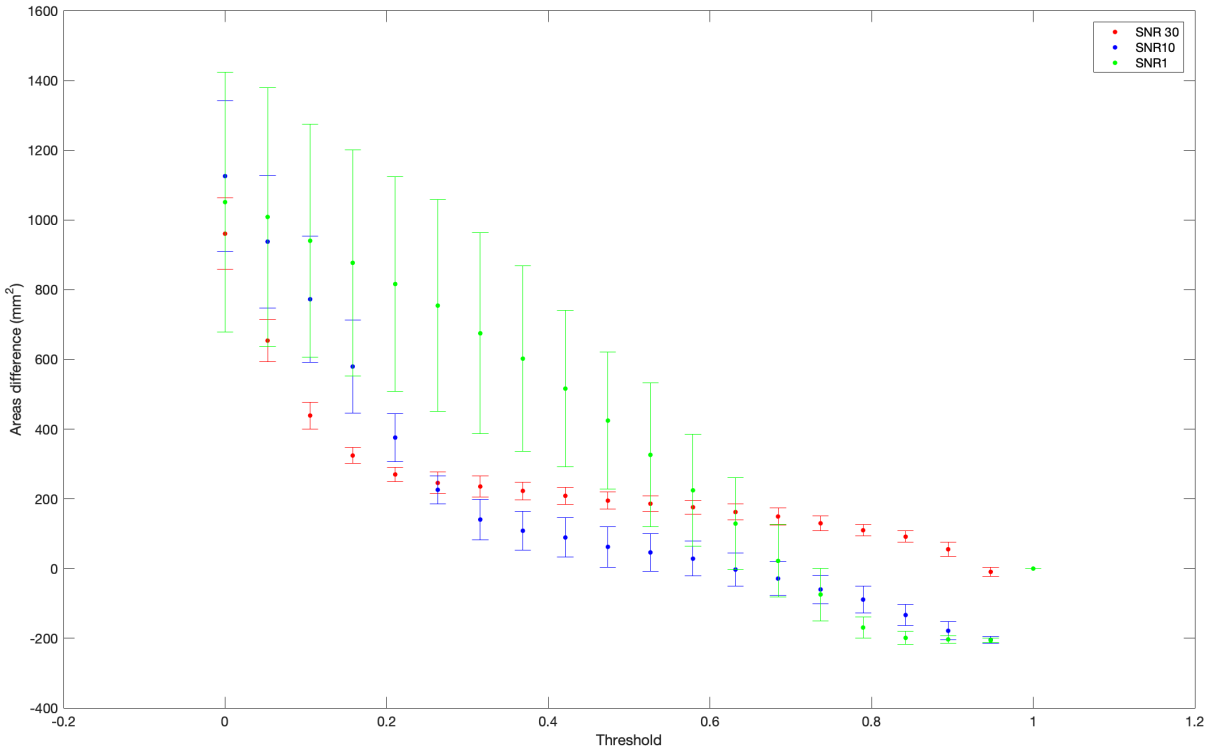

Figure 4.17 Differences between areas of original activations and correspondent reconstructed ones, reported at different SNR values. The results refer to the ground-truth pattern without negative correlations, detected from the largest probe of 997 channels.

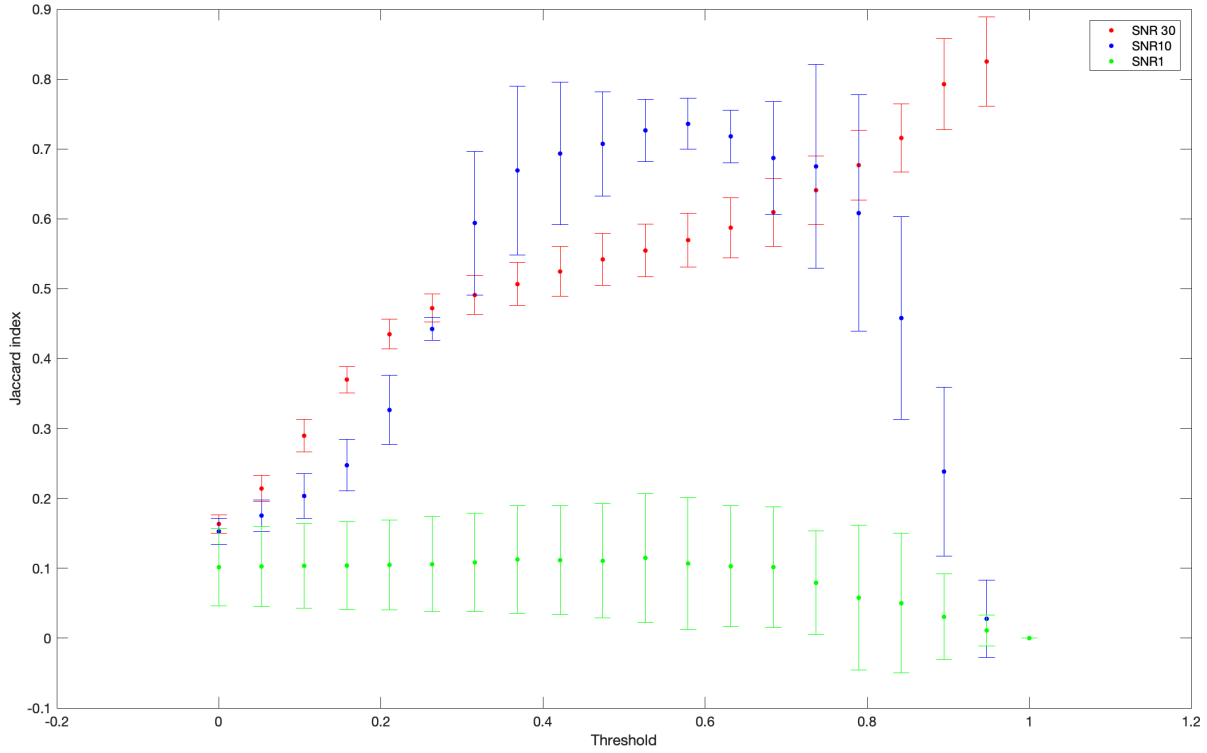

Figure 4.18 Jaccard index variation estimated, at different SNR values, on the sets of nodes included in the original and reconstructed correspondent activations. The results refer to the ground-truth pattern without negative correlations, detected from the largest probe of 997 channels.

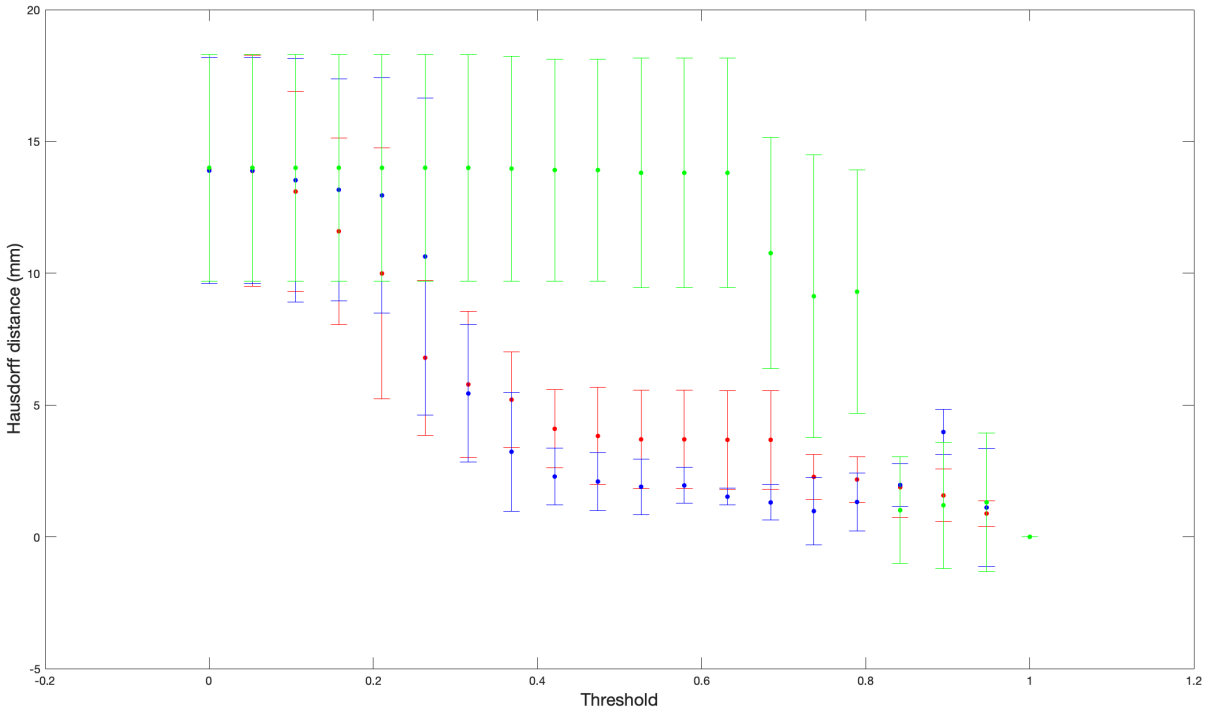

Figure 4.19 Hausdorff distance estimated, at different SNR values, between correspondent original and reconstructed activations. The results refer to the ground-truth pattern without negative correlations, detected from the largest probe of 997 channels.

Table 4 shows the same metrics for the reconstruction of the anticorrelated activations. In the case of the 32-channels probe, the area of sensitivity did not cover the IPS region, and it was not possible to define reconstructed negative correlated regions.

Table 3 – Results of quantitative metrics obtained using different probe configurations for SNR 10 data at threshold 0.5. The pattern formed of positive correlated areas represented the ground truth.

	Centroids distance (mm)	**Δ Areas (mm^2)**	**Hausdorff distance (mm)**	**Jaccard Index**
997 channels	0.88 ± 0.17	46.38 ± 27.15	1.9 ± 0.52	0.7 ± 0.02
32 channels	0.93 ± 0.67	33.20 ± 28.18	6.21 ± 3.24	0.7 ± 0.01
20 channels	2.65 ± 1.98	251.87 ± 156.52	3.65 ± 1.77	0.51 ± 0.22
94 channels	2.56 ± 0.38	208.44 ± 82.78	3.8 ± 1.28	0.46 ± 0.03

Table 4 Results of quantitative metrics obtained using different probe configurations for SNR 10 data at threshold 0.5.

	Centroids distance (mm)	Δ Areas (mm^2)	Hausdorff distance (mm)	Jaccard Index
997 channels	1.39 ± 0.05	45.73 ± 14.39	2.41 ± 0.07	0.54 ± 0.01
32 channels	-	-	-	-
20 channels	5.73 ± 0.38	446.31 ± 9.85	9.12 ± 0.30	0.2 ± 0.02
94 channels	2.32 ± 0.98	159.11 ± 81.6	3.61 ± 1.92	0.3 ± 0.03

4.3.3 Dataset reconstructions

Combining the variation of concentrations in both HbO and HHb, weighted by the relative extinction coefficients, we could infer the reconstruction of connectivity maps in the source space, starting from real fNIRS data acquired on term neonates and described in the previous chapter. The information was projected onto the cortex of the 40^{th} week of the Atlas, which reflects the examined population. A seed-based analysis was performed in order to characterize the connectivity between all cortical nodes with a small region of interest (or seed).

Figure 4.20 and Figure 4.21 show a direct comparison of the two approaches using data from the first dataset of eight subjects, using a probe of 20 channels. Observing the representation of spatially distributed functional contributions, the remarkable similarity between the maps referring to the two different wavelengths is evident. However, each one is affected differently by the HbO and HHb components, even if it is difficult to differentiate rigorously the contributions. Considering the research question guiding the experimental measurements, we presented outcomes using two representative seeds of interest in the right hemisphere: one above the parietal area of DMN (Figure 4.21) and the other over the IPS within the DAN (Figure 4.20). The cortical representation clearly showed the absence of communication between the two hemispheres. Moreover, it is able to account for a very weak correlation of the seed with one channel of the opposite

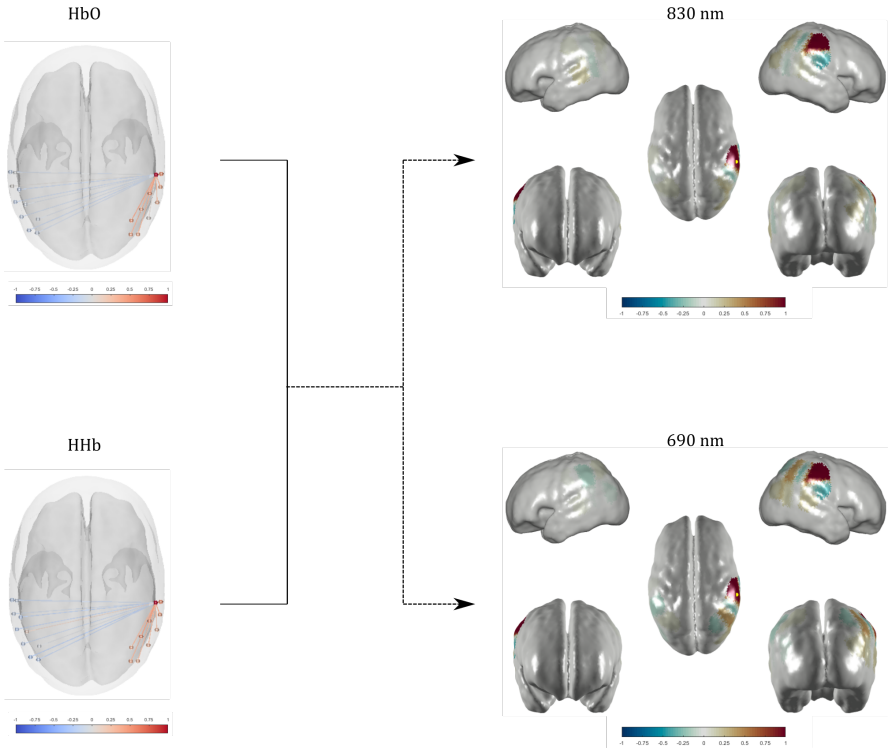

Figure 4.20 Comparison between channels-based maps from concentration values and source space maps. The seed is placed above the intra parietal sulcus area.

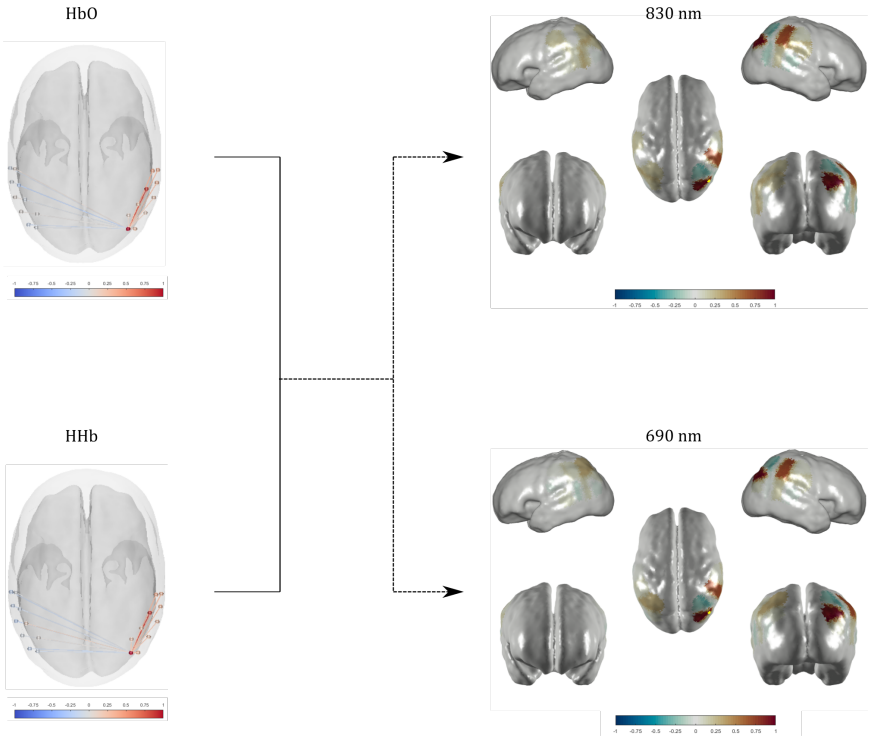

Figure 4.21 Comparison between channels-based maps from concentration values and source space maps. The seed is placed above the parietal region.

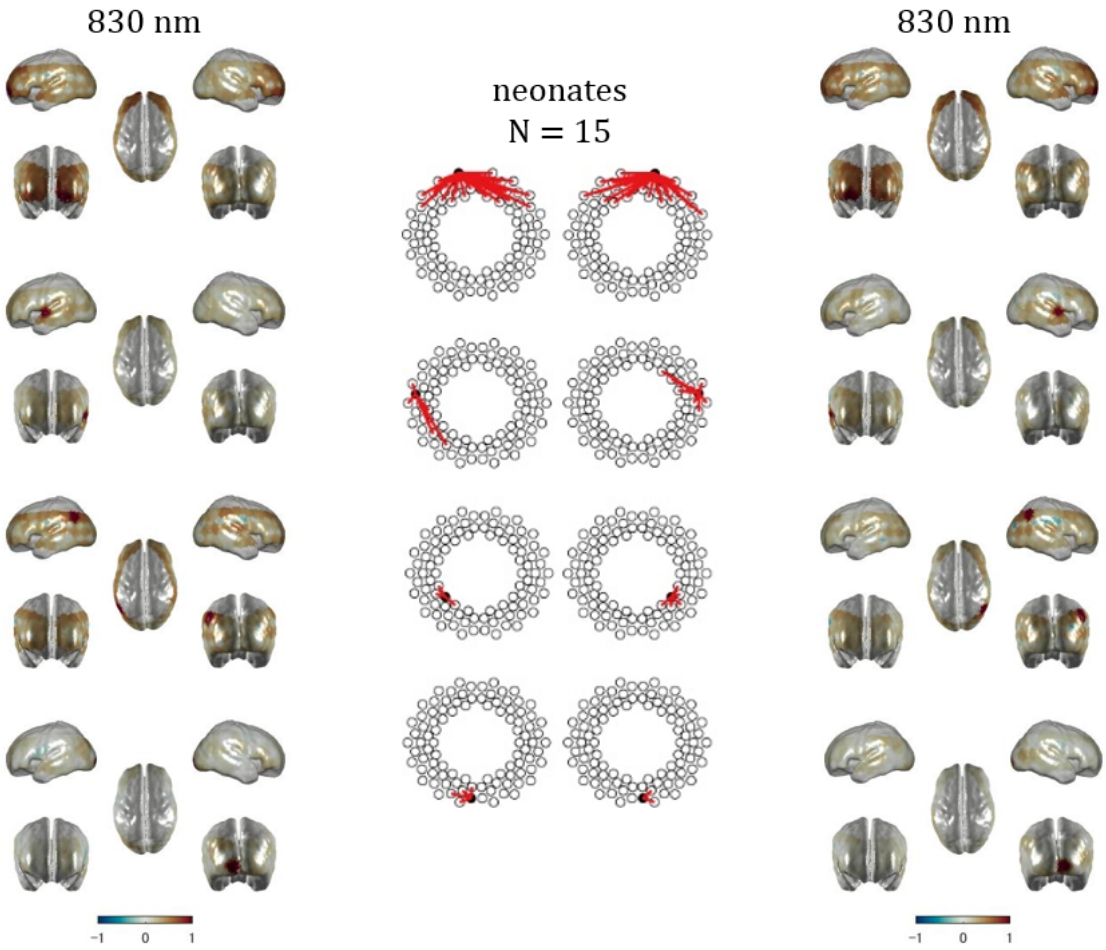

Figure 4.22 Comparison between sensor (center) and source based analysis of the second dataset at 830 nm wavelength. The panel in the center shows results of the correlation analysis for 4 distinct seed for hemisphere. The seeds we used are, from the top: (left column) Fp1, T3, P3, (right column) Fp2, T4, P4 and inion. Red lines in the sensor analysis indicate only correlations – averaged in the entire sample- higher than 0.5. No correlation threshold has been applied to volumetric maps.

Courtesy of Prof. Fumitaka Homae that ran the reconstruction using our software.

hemisphere, visible in the HHb map in Figure 4.21. Surprisingly, in the Figure 4.20 the effect of the low anticorrelation between the seed and the majority of the channels in left hemisphere appeared reduced in the reconstructed sources. On the other hand, the strong correlation between the two channels in both HbO and HHb in Figure 4.21 is defined with good localization. Independently of the seed used, we registered a recurrent emergence

of areas of spurious anticorrelation in the proximity of the seed region, where the value of positive correlation is higher.

In Figure 4.22 and Figure 4.23, results of the connectivity analyses in the sensor and source space for the second dataset are illustrated. Volumetric maps obtained using seeds in Fp1 and Fp2 were both able to return the compact area of positive correlations above the frontal region.

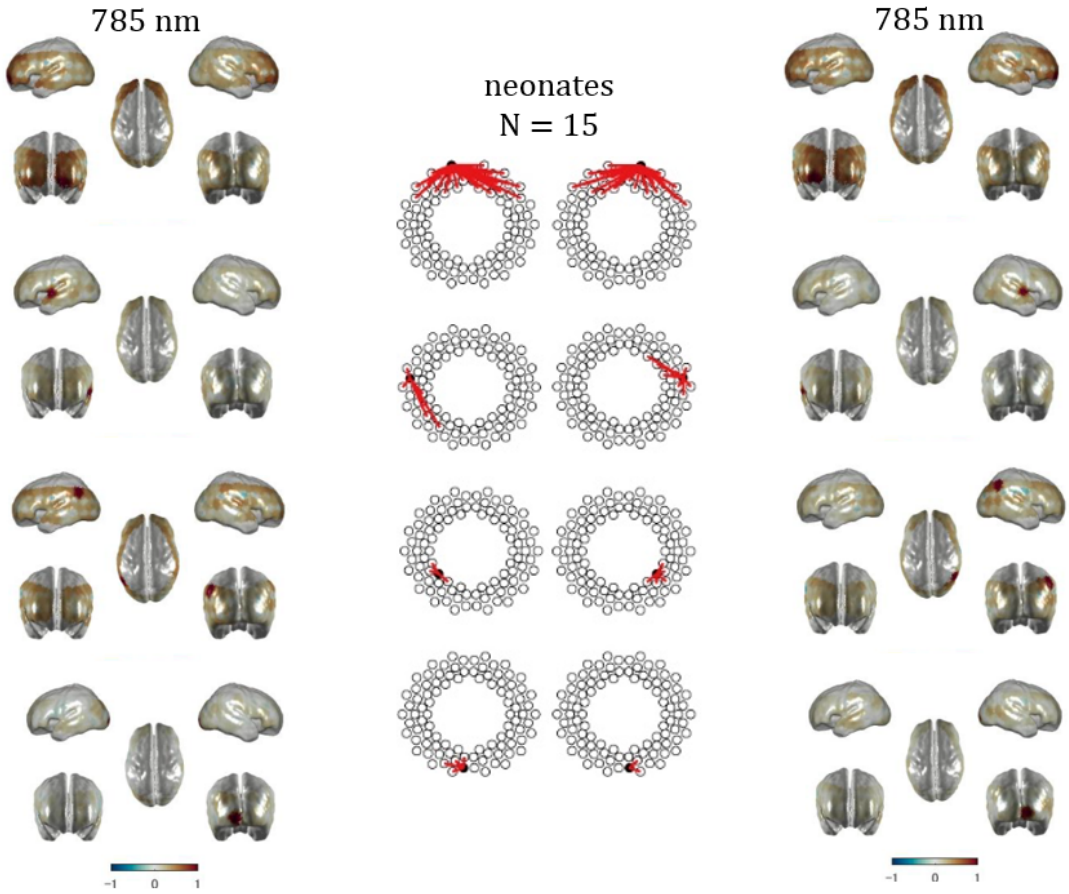

Figure 4.23 Comparison between sensor (center) and source based analysis of the second dataset at 785 nm wavelength. The panel in the center shows results of the correlation analysis for 4 distinct seed for hemisphere. Seeds used are, in order from the top: (left column) Fp1, T3, P3, (right column) Fp2, T4, P4 and inion. Red lines in the sensor analysis indicate only correlations – averaged in the entire sample- higher than 0.5. No correlation threshold has been applied to volumetric maps.

Courtesy of Prof. Fumitaka Homae that run the analyses using our software.

Specifically, in the case of temporal and occipital seeds the lack of interhemispheric connectivity was well represented also in the reconstructed maps. When seeds were chosen in the parietal areas, the three-dimensional descriptions accounted for a more extended correlated regions. This could be partially due to a different correlation threshold between sensor and source space representations: in the sensor space red lines indicated only correlation with the chosen seed higher than 0.5. As we expected, results at 785 nm and 830 nm were very similar.

4.4 Discussion

In recent years, fNIRS has been established as a powerful mean to investigate brain dynamics, in particular in vulnerable and non-verbal populations, such as neonates. Specifically, the technique is ideal to perform, at a very early stage of life, resting-state studies that require, among others, a silent environment and a total non-invasiveness. However, functional connectivity in neonates is usually inferred from a discrete channel-based analysis, using optical signals collected at the scalp. This provides a coarse description of the phenomenon, limiting a global visualization of the cortical dynamics. Moreover, direct comparisons with connectivity maps obtained from fMRI, which remains the main reference for resting state studies, are also hampered. Therefore, recovering as much as possible of the available spatial information is a critical issue to improve the efficacy of the technique. To this purpose, the enhancement of the sensor space analysis with a volumetric description in the source space should be promoted. However, to what extent the variability of different experimental conditions may influence the computation of functional connectivity from reconstructed sources remains unclear.

In this study, we validated the procedure for the reconstruction of spatially distributed functional signals onto a dedicated anatomical template for newborns. As with other neuroimaging inverse problems (such as in electro- or magneto- encephalography), in fNIRS we do not have the capability to know the real distribution of sources and original emerging patterns. To remedy the lack of knowledge of the ground-truth, we generated simulated data for assessing the reliability of the method. We associated the variability in experimental conditions to the changes of specific parameters. The amount of noise in the signal (expressed in form of SNR), pattern of correlation and probe geometry were all

modulated through synthetic processes. We varied one parameter at time to estimate the influence of each condition on the image reconstruction.

At first, we assessed the impact of different sensor arrangement on the reconstruction of a spatial pattern of positive correlations, which emulates the DMN. To this purpose, the first configuration contemplated was highly unrealistic, because capable to cover the whole brain using almost one thousand channels. Indeed, the state of art for neonates measurements is represented by a cap positioned onto only occipital, temporal and parietal cortices with approximately 300 channels (Ferradal et al., 2015). Nonetheless, our ideal arrangement aimed to test the method in the best-case scenario, to disclose the potentiality of the procedure. Focusing on results from injected signals with a very high and acceptable SNR (respectively, 30 and 10) it is evident that the estimation of cortical connectivity maps was highly precise and reliable. The final functional description appeared remarkably comparable to the ground-truth functional map, in terms of position, shape and total areas of activations. This observation was confirmed by the quantitative metrics we computed, which showed, in this case, minimal shift of the reconstructed activations, low variation in shape and high ratio of nodes shared with the ground-truth. If compared with the other probe configurations, the 997 channel array showed lowest values of centroid and Hausdorff distances. The 32 channels probe seems to result in a smaller difference in area, but it should be noted that the standard error of the mean is much larger for this probe. We might associate the goodness of the result mainly to the presence of overlapping and multi-distance source-detector pairs that, as already demonstrated (Boas & Dale, 2005; Durduran, Choe, Baker, & Yodh, 2010), generally improve the image reconstruction, also because it facilitates depth localization. A large coverage of the head plays a key role on the quality of the reconstruction. However, this condition is not sufficient, as suggested by the outcomes in the case of an extended probe with low-density optodes arrangement (using 94 measurements). Here, the reconstruction presented a larger shift of the position with respect to the 997-channelss probe and a general worsening of the quantitative metrics, due to the lack of overlapping channels. Surprisingly, we did not register a strong improvement from 20 channels to 94 channels array: this may be associated to a suboptimal coverage of the areas of interest from the 94 probe, which in origin was not specifically designed to study the DMN.

In general, reducing the actual area under investigation had an impact on the accuracy of the reconstruction process. The 32-sensors array, in fact, preserved an adequate density of channels per unit of space, but it was able to investigate precisely only the lateral areas of the DMN. In this case, the disposition of optodes was still valid to return a reliable functional connectivity map, but we observed a less precise localization of the two lateral activations. Moreover, their shape was less accurate, as confirmed from the highest Hausdorff distance, showing blurred edges. We referred to this phenomenon as a sort of *edge effect* to highlight the dependence on the size of the probe, but it is still difficult to comment on the physical origin of this result. At last, we tested the impact of a low-density channel structure, keeping limited the brain coverage. This time, channel disposition corresponded to those used in previous experimental acquisitions. Here, as it often happens, the need of the arrangement to be sensitive to specific areas of interest – to capture the relationship between DMN and DAN - and the small number of available sources and detectors prevented the use of overlapping and multi-distance measurements. The lower spatial resolution affected noticeably the results, further reducing the specificity of the connectivity dynamics description in the source space. In Figure 4.13, the emergence of a symmetric pattern of correlated regions was still very clear, but the localization of spatial information was inaccurate. The effect was evident from the strong increase in the difference of areas computed for the 20 channels probe. This suggests a remarkable enlargement of the average activations areas and a suboptimal reconstructed functional connectivity map. In the last case, the map of functional connectivity, reconstructed in the source space, derived from a sparse system of sensors. Consequently, due to the lack of the measurements' overlapping, the same information coming from a single channel is spread to a substantial number of nodes of the grey matter mesh. A clear example is showed in the Figure 4.13, where at $SNR = 10$ the contributions projected from two distinct channels looked well separated. The same effect is observable in Figure 4.15, in correspondence of LP region. In the four different probes, further evidences about the issue emerged observing the outcomes at very disadvantageous conditions ($SNR = 1$). In this case, the detected signal is almost completely hidden under the noise component. Therefore, the method returned reconstructions of Gaussian noise patterns, in the form of alternate positive and negative small clusters of correlations. In our interpretation, size and randomness of these arrays might be linked directly to the features of the probe. The unreliability of the

reconstruction was confirmed by the metrics, which indicate a completely uninformative reconstruction, independently of the chosen threshold.

It is important to specify that, although the reconstruction was projected on the surface, it did take into account depth information. Hence, the performance of probes enabling multi-distance and overlapping channels measurements was better, with DOT probes providing more accurate and informative results.

The final map indicated that with disadvantageous conditions – such as noisy time series and sparse limited probe – results could be misleading and, without a knowledge of the ground-truth, might be considered as a functional pattern of connectivity *per se*. In this direction, our study stressed the critical role of experimental factors for a reliable interpretation of source space descriptions.

Regardless of the differences in sensors' array, we observed the appearance of artifactual negative correlations, in the largest probes in form of a well-defined halo around the positive activations, and with a sparser distribution and diffused shape in the others. Initially, we hypothesized that the localized inversion of the sign of correlation could be attributed to the sharp form of step function, which defines absorption coefficient changes and, consequently, spatial distribution of correlated signals. This effect was evident especially in the case of very high SNR signal and became attenuated by the noise in SNR $= 10$. Its presence is consistent in the close proximity to compact set of nodes with highly correlated activity. In order to test the impact of spurious anticorrelations, we computed quantitative metrics specifically on the negative correlated activations. As expected, we registered a sharp worsening of the values especially for the 20 channels probe, as already observed in functional connectivity maps. However, the particular localization made these spurious contributions highly recognizable, reducing the risk of a misinterpretation. Especially in fMRI-based works, the detection of negative correlations is an essential component in the study of functional connectivity. Its emergence in the reconstructed sources, from the original positive correlated pattern, raised our interest in understanding the capability of the method to discern the negative correlations in the ground-truth, when present. To this end, we generated a second spatial configuration, which simulated the competitive relationship between DMN and DAN, already

investigated in Chapter 3. We observed that the anticorrelations are well- preserved in the reconstruction, with a level of accuracy that varies in a similar way than the positive ones above described. As expected, with the 32 channels probe, no new effect was found, confirming the very confined sensitivity of this array. This leads us to comment on the crucial choice of optodes disposition in the process of probe design. Of course, the decision on the final arrangement of sources and detectors depends on a trade-off between the necessity to cover specific areas and the attempt to realize a structure as compact as possible, preferably equipped with overlapping channels. On the other hand, increasing the density at the cost of the size could be risky. For these reasons, a detailed knowledge of the brain regions actually investigated is necessary. The cortical sensitivity maps resulting from Monte Carlo simulations represented a powerful means in this regard, providing prior information on the brain regions probed and facilitating the stage of design of the experiment. Further improvements could be certainly made - such as a more intuitive way to define the probe onto the atlas. In any case, probe optimization is one of the most pivotal challenges that recently involved the fNIRS community – the number of dedicated tools released in the last years represents a practical confirmation (to name but a few (Aasted et al., 2015; Brigadoi, Salvagnin, Fischetti, & Cooper, 2018; Zimeo Morais, Balardin, & Sato, 2018)).

The core of the present study is represented by the computational approach used to validate the reconstruction process. The test involved synthetic data and a dedicated head model, which is a procedure widely established in literature (Brigadoi et al., 2015; Cooper et al., 2012; Leamy, Ward, & Sweeney, 2011; Pinti et al., 2017). However, the efficacy of the model also depends on the reliability of the simulated elements. In our case, we used an atlas that specifically reflects the characteristic of the population of interest. The 4D Atlas is today's most valid alternative for information on anatomical structures to the subject-specific fMRI. Indeed, the latter is an impractical solution for monitoring studies on healthy newborns and its use would undermine all the advantages offered by the optical imaging. An accurate head model is necessary to solve the forward model, but also the assignment of optical properties to each layer of the segmented atlas could have an impact on the result. In our case, we worked with simulated data (and, subsequently, we proposed the same model for real data) using optical properties at only one wavelength (800 nm). This choice does not represent a limitation because, as already demonstrated (Custo et al., 2010; G. Strangman, Franceschini, & Boas, 2003), the small variation of

optical properties due to different wavelengths results in negligible effects compared to other factors, such as the probe geometry and the probe placement.

Finally, after having obtained encouraging results using simulated data, we applied the pipeline for image reconstruction on two different datasets of real resting state measurements on newborns. The first one was formed by the cohort of term neonates we acquired at the Hospital of Rovereto, presented in detail in Chapter 3. The second dataset was consistent with the first one for age of subjects and modality of acquisitions (even though the subjects were slightly older), but offered the possibility to examine reconstruction of functional connectivity maps using a more extended probe. For both neonates' samples, only analyses in the sensor space - performed with a seed-based method - were available and, in the second case, already published. It is worth pointing out that real data showed good quality overall. To this regard, the factors taken in consideration were different. For each sample, we extracted time courses without motion artifacts, acquired on subjects in a deep sleep stage (ensured on the basis of behavioral parameters) in a dim lit environment, with the probe well-positioned above the head. These observations persuaded us of the reliability of the data. As the previous tests suggested, the prerequisite for the application of the method is not dealing with highly noisy time series. The reconstructed functional connectivity maps confirmed the capability of the source analysis to accurately provide anatomical reference to the connectivity obtained in the sensor space. The visualization was improved, facilitating the interpretation of the connectivity distribution and the comparison with other techniques. However, especially in the distribution of reconstructed sources of the first dataset, we observed the emergence of spurious anticorrelations, not detected in the sensor space. While their origin is not completely clear, they may arise from the limited coverage of the probe and the sparsity of its channels. These artefacts may substantially confound interpretation of the data. In the future, we aim to expand the study by including more probe configurations and adding different pattern configurations, to improve the specificity of the method. Moreover, we intend to define a procedure to identify specific user-defined anatomical references. Of course, in the seed-based correlation analysis, the seed is defined by the average time series among a set of adjacent nodes, and therefore the error is reduced. However, we would like to better exploit the advantage of the choice of a specific node onto the cortex, enabled by source space representation.

In conclusion, evaluation of source localization accuracy, using both synthetic and real data, confirmed the reliability of the reconstruction method for functional connectivity studies in infants, but only under specific conditions. The assessment of the impact of distinct external factors on the process should make it possible to establish criteria for the anatomical reconstruction in order to promote an enrichment of the sensor based description with the analysis in the source space.

5 Conclusions and future directions

In the last decade, optical systems based on fNIRS principles have been established as powerful tools to explore the brain functional architecture. Thanks to its technical characteristics, this technique is extremely suitable for cognitive and clinical investigations in developmental neuroscience. Indeed, the possibility to perform quiet and totally non-invasive measurements, as well as portability and good spatial and temporal resolution tradeoffs, are highly advantageous features for vulnerable and non-verbal populations, such as newborns. Despite the urgent quest to understand the mechanisms underlying inception and evolution of brain functional connectivity at the very first stage of life, the field is still in its infancy. This entire dissertation focused on the application of fNIRS technique to study functional organization of healthy term neonate's brain. The topic of interest has been addressed from two main standpoints.

On one side, a peculiar aspect of resting state functional connectivity has been investigated. Indeed, for the first time, optical imaging has been exploited to study specifically the emergence of Default Mode Network within the first two days of life. In this thesis, the state of the network after birth has been explored capitalizing on a specific signature, which has been consistently observed in adults. This approach, which takes into account both positive and negative correlations, could be implemented using the limited number of channels available on our instrument, which did not allow coverage of the entire DMN. Channel-based analysis clearly showed the lack of homotopic correlations in the parietal components of the DMN. Moreover, no intrahemispheric anticorrelation between the LP and IPS cortices was observed, thus corroborating the idea that a mature DMN has not yet developed at birth. Importantly, our analysis was performed in a small but selected group of subjects, avoiding potential sources of artifacts that might introduce spurious correlations and confound the interpretation. Given the small number of subjects included in our study, we did not perform additional analyses –

for instance, of the potential dependence of functional connectivity on the sex of the subjects or on their age (expressed in days).

On the other side, a consistent section of the thesis has been dedicated to the validation of a method for the reconstruction of functional maps in the space of sources. This study has been prompted by the need to enrich the description of the typical channel-based connectivity, popular in resting state works on infants. Indeed, shifting the analysis from a sensor to a source space can improve the anatomical description of functional connectivity and facilitate comparison with previous studies performed with different techniques, such as fMRI. One of the aims of this work was to clarify to what extent the process of image reconstruction from signals collected at the scalp is influenced by external factors, like noise or probe design. In order to provide a ground-truth for the assessment of the reconstruction, we generated synthetic datasets mimicking features of the DMN, including both positive and negative correlations. This analysis defined useful guidelines for reliable reconstruction of the data. We found that the both density and extension of the optical probe dramatically impact the source reconstruction. Indeed, low density of optodes or lack of overlapping channels can substantially blur the reconstructed data. Moreover, partial coverage of the scalp can cause massive artifacts, with the emergence of spurious negative correlations and edge effects. However, results obtained with synthetic data showed that, with a judicious choice of probe design and sufficient SNR, reliable patterns of positive and negative correlations can be reconstructed, thus providing a means to study homotopic connectivity and the relationship between DMN and DAN.

We applied this source reconstruction scheme to independent real datasets, acquired on two groups of term neonates with different probes, to obtain anatomically resolved functional connectivity maps. These maps improved visualization and confirmed our sensor-space analysis, showing no evidence of interhemispheric correlations in the parietal cortices, and no anticorrelations between LP and IPS at this age. These observations, derived from our dataset of 2 days-old subjects, were confirmed by an independent dataset acquired on 4-days old neonates and suggest that the DMN is still immature at birth. It is worth recalling that the interest towards the investigation of the early emergence of the DMN was induced by the confounding scenario offered by the fMRI

literature on the topic. Our work corroborates previous observations, on term newborns, of a fragmented network that includes only medial prefrontal cortex and posterior cingulate (Gao, Alcauter, Elton, et al., 2015; Gao et al., 2009; Smyser et al., 2010b). Other studies have shown that interhemispheric communication and synchronization between anatomically distant regions within the DMN, as well as within DAN, increases after birth, reaching a mature state only at one year of age (Gao, Alcauter, Elton, et al., 2015; Gao, Alcauter, Smith, Gilmore, & Lin, 2015). These results suggest that developmental trajectories of functional connectivity are closely connected to the development of the underlying cognitive functions. Indeed, complete configurations of visual, sensorimotor and auditory networks have been detected at birth. Conversely, networks involved in higher order cognitive functions, like the salience network, responsible for the integration of complex functions associated with social behavior and communication, show incomplete spatial patterns until the beginning of the second year of age. Thus, it is plausible that the DMN, which is thought to be involved in self-awareness and sense of consciousness, is not fully developed at birth and reaches full maturation only later in the development.

In light of the results presented in this thesis, several follow-up investigations can be envisaged. Longitudinal monitoring of the very early stage of development, with repeated sessions in the weeks after birth and up to the first year of life, would enable carefully tracing the developmental trajectory of the DMN. Moreover, a longitudinal study could address the question as to whether extrinsic features of the DMN, like its interplay with the DAN, mature independently of its intrinsic features, like homotopic parietal correlations and long-distance connectivity. Ultimately, accurate mapping of this maturation process could provide a benchmark for studies aimed at understanding neurodevelopmental conditions, in which the developmental trajectory goes awry. While some of the work presented in this dissertation may help pave the way to pursue such an ambitious project, is also clearly shows that employment of DOT instrumentation with a large number of channels, enabling ample coverage of the scalp, would be crucial to avoid confounding artifacts and to improve the reliability of source-space functional connectivity maps. To set these conclusions on firmer bases, we plan to extend and refine the computational model, in order to provide guidance to tailor and optimize probes for specific purposes.

Finally, we note that the field suffers from a lack of standardization in acquisition and analysis processes, which substantially hampers comparison of different studies. It is therefore desirable that the entire scientific community strives to build solid methodological guidelines, in order to facilitate data reproducibility and shared procedures. From this perspective, we hope that the present work may provide tools to assist optimal probe design and for the anatomical reconstruction of functional connectivity derived from fNIRS.

References

Aasted, C. M., Yücel, M. A., Cooper, R. J., Dubb, J., Tsuzuki, D., Becerra, L., … Boas, D. A. (2015). Anatomical guidance for functional near-infrared spectroscopy: AtlasViewer tutorial. *Neurophotonics*, *2*(2), 020801. https://doi.org/10.1117/1.NPh.2.2.020801

Apgar, V. (2015). A proposal for a new method of evaluation of the newborn infant. In *Anesthesia and Analgesia* (Vol. 120, pp. 1056–1059). https://doi.org/10.1213/ANE.0b013e31829bdc5c

Arridge, S. R., & Hebden, J. C. (1997). Optical imaging in medicine: II. Modelling and reconstruction. *Physics in Medicine and Biology*, *42*(5), 841–853. https://doi.org/10.1088/0031-9155/42/5/008

Arridge, S. R., & Schotland, J. C. (2009). Optical tomography: forward and inverse problems. *Inverse Problems*, *25*(12), 123010. https://doi.org/10.1088/0266-5611/25/12/123010

Arridge, S. R., & Schweiger, M. (1997). Image reconstruction in optical tomography. *Philosophical Transactions of the Royal Society of London. Series B, Biological Sciences*, *352*, 717–726.

Arridge, S. R., Schweiger, M., Hiraoka, M., & Delpy, D. T. (1993). A finite element approach for modeling photon transport in tissue. *Medical Physics*, *20*(2), 299–309. https://doi.org/10.1118/1.597069

Aslin, R. N., & Mehler, J. (2005). Near-infrared spectroscopy for functional studies of brain activity in human infants: promise, prospects, and challenges. *Journal of Biomedical Optics*, *10*(1), 011009. https://doi.org/10.1117/1.1854672

Aslin, R. N., Shukla, M., & Emberson, L. L. (2015). Hemodynamic Correlates of Cognition in Human Infants. *Annual Review of Psychology*, *66*(1), 349–379. https://doi.org/10.1146/annurev-psych-010213-115108

Beardslee, W. R., Chien, P. L., & Bell, C. C. (2011). Prevention of Mental Disorders, Substance Abuse, and Problem Behaviors: A Developmental Perspective. *Psychiatric Services*, *62*(3), 247–254. https://doi.org/10.1176/ps.62.3.pss6203_0247

Becerra, L., Pendse, G., Chang, P.-C., Bishop, J., & Borsook, D. (2011). Robust Reproducible Resting State Networks in the Awake Rodent Brain. *PLoS ONE*, *6*(10). https://doi.org/10.1371/journal.pone.0025701

Beckmann, C. F., DeLuca, M., Devlin, J. T., & Smith, S. M. (2005). Investigations into resting-state connectivity using independent component analysis. *Philosophical Transactions of the Royal Society B: Biological Sciences*, *360*(1457), 1001–1013. https://doi.org/10.1098/rstb.2005.1634

Biswal, B., Yetkin, F. Z., Haughton, V. M., & Hyde, J. S. (1995). Functional connectivity in the motor cortex of resting human brain using echo-planar MRI. *Magnetic Resonance in Medicine*, *34*(4), 537–541. Retrieved from http://www.ncbi.nlm.nih.gov/pubmed/8524021

Boas, D. A., Culver, J. P., Stott, J. J., & Dunn, A. K. (2002). Three dimensional Monte Carlo code for photon migration through complex heterogeneous media including the adult human head. *Optics Express*, *10*(3), 159. https://doi.org/10.1364/OE.10.000159

Boas, D. A., & Dale, A. M. (2005). Simulation study of magnetic resonance imaging-guided cortically constrained diffuse optical tomography of human brain function. *Applied Optics*, *44*(10), 1957–1968.

Retrieved from http://www.ncbi.nlm.nih.gov/pubmed/15813532

Bordier, C., Nicolini, C., & Bifone, A. (2017). Graph Analysis and Modularity of Brain Functional Connectivity Networks: Searching for the Optimal Threshold. *Frontiers in Neuroscience*, *11*, 441. https://doi.org/10.3389/fnins.2017.00441

Brigadoi, S., Aljabar, P., Kuklisova-Murgasova, M., Arridge, S. R., & Cooper, R. J. (2014). A 4D neonatal head model for diffuse optical imaging of pre-term to term infants. *NeuroImage*, *100*, 385–394. https://doi.org/10.1016/j.neuroimage.2014.06.028

Brigadoi, S., & Cooper, R. J. (2015). How short is short? Optimum source-detector distance for short-separation channels in functional near-infrared spectroscopy. https://doi.org/10.1117/1.NPh.2.2.025005

Brigadoi, S., Powell, S., Cooper, R. J., Dempsey, L. A., Arridge, S., Everdell, N., … Gibson, A. P. (2015). Evaluating real-time image reconstruction in diffuse optical tomography using physiologically realistic test data. *Biomedical Optics Express*, *6*(12), 4719. https://doi.org/10.1364/BOE.6.004719

Brigadoi, S., Salvagnin, D., Fischetti, M., & Cooper, R. J. (2018). Array Designer: automated optimized array design for functional near-infrared spectroscopy. *Neurophotonics*, *5*(03), 1. https://doi.org/10.1117/1.NPh.5.3.035010

Buckner, R. L., Andrews-Hanna, J. R., & Schacter, D. L. (2008). The brain's default network: Anatomy, function, and relevance to disease. *Annals of the New York Academy of Sciences*, *1124*, 1–38. https://doi.org/10.1196/annals.1440.011

Buckner, R. L., & Carroll, D. C. (2007). Self-projection and the brain. *Trends in Cognitive Sciences*, *11*(2), 49–57. https://doi.org/10.1016/j.tics.2006.11.004

Bunce, S. C., Izzetoglu, M., Izzetoglu, K., Onaral, B., & Pourrezaei, K. (2006). Functional near-infrared spectroscopy. *IEEE Engineering in Medicine and Biology Magazine*, *25*(4), 54–62. https://doi.org/10.1109/MEMB.2006.1657788

Buxton, R. B., Wong, E. C., & Frank, L. R. (1998). Dynamics of blood flow and oxygenation changes during brain activation: the balloon model. *Magnetic Resonance in Medicine*, *39*(6), 855–864. Retrieved from http://www.ncbi.nlm.nih.gov/pubmed/9621908

Bystron, I., Blakemore, C., & Rakic, P. (2008). Development of the human cerebral cortex: Boulder Committee revisited. *Nature Reviews Neuroscience*, *9*(2), 110–122. https://doi.org/10.1038/nrn2252

Caffini, M. (2009). *Diffuse Optical Tomography. Development and Validation of a Medical Device and of Physical Models for Brain Activation Studies*. Politecnico di Milano.

Cai, L., Dong, Q., & Niu, H. (2018). The development of functional network organization in early childhood and early adolescence: A resting-state fNIRS study. *Developmental Cognitive Neuroscience*, *30*, 223–235. https://doi.org/10.1016/J.DCN.2018.03.003

Calderon-Arnulphi, M., Alaraj, A., & Slavin, K. V. (2009). Near infrared technology in neuroscience: past, present and future. *Neurological Research*, *31*(6), 605–614. https://doi.org/10.1179/174313209X383286

Castellanos, F. X., & Aoki, Y. (2016). Intrinsic Functional Connectivity in Attention-Deficit/Hyperactivity Disorder: A Science in Development. *Biological Psychiatry: Cognitive Neuroscience and*

Neuroimaging, *1*(3), 253–261. https://doi.org/10.1016/j.bpsc.2016.03.004

Chai, X. J., Ofen, N., Gabrieli, J. D. E., & Whitfield-Gabrieli, S. (2014). Selective Development of Anticorrelated Networks in the Intrinsic Functional Organization of the Human Brain. *Journal of Cognitive Neuroscience*, *26*(3), 501–513. https://doi.org/10.1162/jocn_a_00517

Chance, B., Zhuang, Z., UnAh, C., Alter, C., & Lipton, L. (1993). Cognition-activated low-frequency modulation of light absorption in human brain. *Proceedings of the National Academy of Sciences of the United States of America*, *90*(8), 3770–3774. Retrieved from http://www.ncbi.nlm.nih.gov/pubmed/8475128

Choi, J., Wolf, M., Toronov, V., Wolf, U., Polzonetti, C., Hueber, D., … Gratton, E. (2004). Noninvasive determination of the optical properties of adult brain: near-infrared spectroscopy approach. *Journal of Biomedical Optics*, *9*(1), 221. https://doi.org/10.1117/1.1628242

Cole, D. M., Smith, S. M., & Beckmann, C. F. (2010). Advances and pitfalls in the analysis and interpretation of resting-state FMRI data. *Frontiers in Systems Neuroscience*, *4*, 8. https://doi.org/10.3389/fnsys.2010.00008

Cooper, R. J., Caffini, M., Dubb, J., Fang, Q., Custo, A., Tsuzuki, D., … Boas, D. A. (2012). Validating atlas-guided DOT: A comparison of diffuse optical tomography informed by atlas and subject-specific anatomies. *NeuroImage*, *62*(3), 1999–2006. https://doi.org/10.1016/J.NEUROIMAGE.2012.05.031

Cope, M., & Delpy, D. T. (1988). System for long-term measurement of cerebral blood and tissue oxygenation on newborn infants by near infra-red transillumination. *Medical & Biological Engineering & Computing*, *26*(3), 289–294. https://doi.org/10.1007/BF02447083

Corbetta, M., & Shulman, G. L. (2002). Control of Goal-Directed and Stimulus-Driven Attention in the Brain. *Nature Reviews Neuroscience*, *3*(3), 215–229. https://doi.org/10.1038/nrn755

Cui, W., Kumar, C., & Chance, B. (2005). Experimental study of migration depth for the photons meaured at sample surface. In Britton Chance (Ed.), *Time-Resolved Spectroscopy and Imaging of Tissues* (Vol. 1431, pp. 180–191). International Society for Optics and Photonics. https://doi.org/10.1117/12.44189

Custo, A., Boas, D. A., Tsuzuki, D., Dan, I., Mesquita, R., Fischl, B., … Wells, W. (2010). Anatomical atlas-guided diffuse optical tomography of brain activation. *NeuroImage*, *49*(1), 561–567. https://doi.org/10.1016/j.neuroimage.2009.07.033

Damoiseaux, J. S., Rombouts, S. A. R. B., Barkhof, F., Scheltens, P., Stam, C. J., Smith, S. M., & Beckmann, C. F. (2006). Consistent resting-state networks across healthy subjects. *Proceedings of the National Academy of Sciences of the United States of America*, *103*(37), 13848–13853. https://doi.org/10.1073/pnas.0601417103

de Lacy, N., Doherty, D., King, B. H., Rachakonda, S., & Calhoun, V. D. (2017). Disruption to control network function correlates with altered dynamic connectivity in the wider autism spectrum. *NeuroImage. Clinical*, *15*, 513–524. https://doi.org/10.1016/j.nicl.2017.05.024

De Luca, M., Beckmann, C. F., De Stefano, N., Matthews, P. M., & Smith, S. M. (2006). fMRI resting state networks define distinct modes of long-distance interactions in the human brain. *NeuroImage*, *29*(4), 1359–1367. https://doi.org/10.1016/j.neuroimage.2005.08.035

De Luca, M., Smith, S., De Stefano, N., Federico, A., & Matthews, P. M. (2005). Blood oxygenation level

dependent contrast resting state networks are relevant to functional activity in the neocortical sensorimotor system. *Experimental Brain Research*, *167*(4), 587–594. https://doi.org/10.1007/s00221-005-0059-1

Dehaes, M., Kazemi, K., Pélégrini-Issac, M., Grebe, R., Benali, H., & Wallois, F. (2013). Quantitative effect of the neonatal fontanel on synthetic near infrared spectroscopy measurements. *Human Brain Mapping*, *34*(4), 878–889. https://doi.org/10.1002/hbm.21483

Delpy, D. T., & Cope, M. (1997). Quantification in tissue near–infrared spectroscopy. *Philosophical Transactions of the Royal Society of London. Series B: Biological Sciences*, *352*(1354), 649–659. https://doi.org/10.1098/rstb.1997.0046

Delpy, D. T., Cope, M., Zee, P. van der, Arridge, S., Wray, S., & Wyatt, J. (1988). Estimation of optical pathlength through tissue from direct time of flight measurement. *Physics in Medicine and Biology*, *33*(12), 1433–1442. https://doi.org/10.1088/0031-9155/33/12/008

Dixon, M. L., Andrews-Hanna, J. R., Spreng, R. N., Irving, Z. C., & Christoff, K. (2016). Anticorrelation between default and dorsal attention networks varies across default subsystems and cognitive states. *BioRxiv*, *147*(July 2016), 056424. https://doi.org/10.1101/056424

Doria, V., Beckmann, C. F., Arichi, T., Merchant, N., Groppo, M., & Turkheimer, F. E. (2010). Emergence of resting state networks in the preterm human brain. https://doi.org/10.1073/pnas.1007921107

Duncan, A., Meek, J. H., Clemence, M., Elwell, C. E., Tyszczuk, L., Cope, M., & Delpy, D. (1995). Optical pathlength measurements on adult head, calf and forearm and the head of the newborn infant using phase resolved optical spectroscopy. *Physics in Medicine and Biology*, *40*(2), 295–304. https://doi.org/10.1088/0031-9155/40/2/007

Durduran, T., Choe, R., Baker, W. B., & Yodh, A. G. (2010). Diffuse Optics for Tissue Monitoring and Tomography. *Reports on Progress in Physics. Physical Society (Great Britain)*, *73*(7). https://doi.org/10.1088/0034-4885/73/7/076701

Eggebrecht, A. T., Ferradal, S. L., Robichaux-Viehoever, A., Hassanpour, M. S., Dehghani, H., Snyder, A. Z., … Culver, J. P. (2014). Mapping distributed brain function and networks with diffuse optical tomography. *Nature Photonics*, *8*(6), 448–454. https://doi.org/10.1038/nphoton.2014.107

Eggebrecht, A. T., White, B. R., Ferradal, S. L., Chen, C., Zhan, Y., Snyder, A. Z., … Culver, J. P. (2012). A quantitative spatial comparison of high-density diffuse optical tomography and fMRI cortical mapping. *NeuroImage*, *61*(4), 1120–1128. https://doi.org/10.1016/j.neuroimage.2012.01.124

Engl, H. W., Hanke, M., & Neubauer, A. (1996). *Regularization of inverse problems*. Kluwer Academic Publishers.

Engstro, M., Hallberg, B., Mosskin, M., Åden, U., Fransson, P., Skio, B., … Al, F. E. T. (2009). Spontaneous Brain Activity in the Newborn Brain During Natural Sleep — An fMRI Study in Infants Born at Full Term, *66*(3), 301–305.

Fang, Q. (2010). Mesh-based Monte Carlo method using fast ray-tracing in Plücker coordinates. *Biomedical Optics Express*, *1*(1), 165. https://doi.org/10.1364/BOE.1.000165

Fang, Q., & Boas, D. A. (2009). Monte Carlo Simulation of Photon Migration in 3D Turbid Media Accelerated by Graphics Processing Units. *Optics Express*, *17*(22), 20178. https://doi.org/10.1364/OE.17.020178

Fantini, S. (1995). Frequency-domain multichannel optical detector for noninvasive tissue spectroscopy

and oximetry. *Optical Engineering*, *34*(1), 32. https://doi.org/10.1117/12.183988

Ferradal, S. L., Liao, S. M., Eggebrecht, A. T., Shimony, J. S., Inder, T. E., Culver, J. P., & Smyser, C. D. (2015). Functional Imaging of the Developing Brain at the Bedside Using Diffuse Optical Tomography, 1–11. https://doi.org/10.1093/cercor/bhu320

Ferrari, M., de Marchis, C., & Giannini, I. (1986). Cerebral blood volume and haemoglobin oxygen saturation monitoring in neonatal brain by near infrared spectroscopy. *Advances in Experimental Medicine and Biology*. Retrieved from http://www.ncbi.nlm.nih.gov/pubmed/3799308

Ferrari, M., Giannini, I., Sideri, G., & Zanette, E. (1985). Continuous non invasive monitoring of human brain by near infrared spectroscopy. *Advances in Experimental Medicine and Biology*, *191*, 873–882. Retrieved from http://www.ncbi.nlm.nih.gov/pubmed/3008520

Ferrari, M., & Quaresima, V. (2012). A brief review on the history of human functional near-infrared spectroscopy (fNIRS) development and fields of application. *NeuroImage*, *63*(2), 921–935. https://doi.org/10.1016/j.neuroimage.2012.03.049

Fox, M. D., Corbetta, M., Snyder, A. Z., Vincent, J. L., & Raichle, M. E. (2006). Spontaneous neuronal activity distinguishes human dorsal and ventral attention systems. *Proceedings of the National Academy of Sciences of the United States of America*, *103*(26), 10046–10051. https://doi.org/10.1073/pnas.0604187103

Fox, M. D., & Greicius, M. (2010). Clinical applications of resting state functional connectivity. *Frontiers in Systems Neuroscience*, *4*(June), 19. https://doi.org/10.3389/fnsys.2010.00019

Fox, M. D., & Raichle, M. E. (2007). Spontaneous fluctuations in brain activity observed with functional magnetic resonance imaging. *Nature Reviews Neuroscience*, *8*(9), 700–711. https://doi.org/10.1038/nrn2201

Fox, M. D., Snyder, A. Z., Vincent, J. L., Corbetta, M., Van Essen, D. C., & Raichle, M. E. (2005). The human brain is intrinsically organized into dynamic, anticorrelated functional networks. *Proceedings of the National Academy of Sciences of the United States of America*, *102*(27), 9673–9678. https://doi.org/10.1073/pnas.0504136102

Fox, M. D., Zhang, D., Snyder, A. Z., & Raichle, M. E. (2009). The global signal and observed anticorrelated resting state brain networks. *Journal of Neurophysiology*, *101*(6), 3270–3283. https://doi.org/10.1152/jn.90777.2008

Fox, P. T., & Raichle, M. E. (1986). Focal physiological uncoupling of cerebral blood flow and oxidative metabolism during somatosensory stimulation in human subjects. *Proceedings of the National Academy of Sciences of the United States of America*, *83*(4), 1140–1144. Retrieved from http://www.ncbi.nlm.nih.gov/pubmed/3485282

Fransson, P. (2005). Spontaneous low-frequency BOLD signal fluctuations: An fMRI investigation of the resting-state default mode of brain function hypothesis. *Human Brain Mapping*, *26*(1), 15–29. https://doi.org/10.1002/hbm.20113

Fransson, P., Skiöld, B., Engström, M., Hallberg, B., Mosskin, M., Åden, U., … Blennow, M. (2009). Spontaneous Brain Activity in the Newborn Brain During Natural Sleep—An fMRI Study in Infants Born at Full Term. *Pediatric Research*, *66*(3), 301–305. https://doi.org/10.1203/PDR.0b013e3181b1bd84

Fransson, P., Skiöld, B., Horsch, S., Nordell, A., Blennow, M., Lagercrantz, H., & Aden, U. (2007). Resting-state

networks in the infant brain. *Proceedings of the National Academy of Sciences of the United States of America*, *104*(39), 15531–15536. https://doi.org/10.1073/pnas.0704380104

Friston, K. J. (2011). Functional and Effective Connectivity: A Review. *Brain Connectivity*, *1*(1), 13–36. https://doi.org/10.1089/brain.2011.0008

Fuchino, Y., Naoi, N., Shibata, M., Niwa, F., Kawai, M., Konishi, Y., … Myowa-Yamakoshi, M. (2013). Effects of Preterm Birth on Intrinsic Fluctuations in Neonatal Cerebral Activity Examined Using Optical Imaging. *PLoS ONE*, *8*(6), e67432. https://doi.org/10.1371/journal.pone.0067432

Fukui, Y., Ajichi, Y., & Okada, E. (2003). Monte Carlo prediction of near-infrared light propagation in realistic adult and neonatal head models. *Applied Optics*, *42*(16), 2881–2887. Retrieved from http://www.ncbi.nlm.nih.gov/pubmed/12790436

Galderisi, A., Brigadoi, S., Cutini, S., Moro, S. B., Lolli, E., Meconi, F., … Dell'Acqua, R. (2016). Long-term continuous monitoring of the preterm brain with diffuse optical tomography and electroencephalography: a technical note on cap manufacturing. *Neurophotonics*, *3*(4), 045009. https://doi.org/10.1117/1.NPh.3.4.045009

Gao, W., Alcauter, S., Elton, A., Hernandez-Castillo, C. R., Smith, J. K., Ramirez, J., & Lin, W. (2015). Functional Network Development During the First Year: Relative Sequence and Socioeconomic Correlations. *Cerebral Cortex*, *25*(9), 2919–2928. https://doi.org/10.1093/cercor/bhu088

Gao, W., Alcauter, S., Smith, J. K., Gilmore, J. H., & Lin, W. (2015). Development of human brain cortical network architecture during infancy. *Brain Structure and Function*, *220*(2), 1173–1186. https://doi.org/10.1007/s00429-014-0710-3

Gao, W., Elton, A., Zhu, H., Alcauter, S., Smith, J. K., Gilmore, J. H., & Lin, W. (2014). Intersubject Variability of and Genetic Effects on the Brain's Functional Connectivity during Infancy. *Journal of Neuroscience*, *34*(34), 11288–11296. https://doi.org/10.1523/JNEUROSCI.5072-13.2014

Gao, W., Gilmore, J. H., Giovanello, K. S., Smith, J. K., Shen, D., Zhu, H., & Lin, W. (2011). Temporal and spatial evolution of brain network topology during the first two years of life. *PLoS ONE*, *6*(9). https://doi.org/10.1371/journal.pone.0025278

Gao, W., Gilmore, J. H., Shen, D., Smith, J. K., Zhu, H., & Lin, W. (2013). The synchronization within and interaction between the default and dorsal attention networks in early infancy. *Cerebral Cortex*, *23*(3), 594–603. https://doi.org/10.1093/cercor/bhs043

Gao, W., Lin, W., Grewen, K., & Gilmore, J. H. (2017). Functional connectivity of the infant human brain: Plastic and modifiable. *Neuroscientist*, *23*(2), 169–184. https://doi.org/10.1177/1073858416635986

Gao, W., Zhu, H., Giovanello, K. S., Smith, J. K., Shen, D., Gilmore, J. H., & Lin, W. (2009). Evidence on the emergence of the brain's default network from 2-week-old to 2-year-old healthy pediatric subjects. *Proceedings of the National Academy of Sciences of the United States of America*, *106*(16), 6790–6795. https://doi.org/10.1073/pnas.0811221106

Giannini, I., Ferrari, M., Carpi, A., & Fasella, P. (1982). Rat brain monitoring by near-infrared spectroscopy: an assessment of possible clinical significance. *Physiological Chemistry and Physics*, *14*(3), 295–305. Retrieved from http://www.ncbi.nlm.nih.gov/pubmed/7185063

Greicius, M. (2008). Resting-state functional connectivity in neuropsychiatric disorders. *Current Opinion in*

Neurology, *24*(4), 424–430. https://doi.org/10.1097/WCO.0b013e328306f2c5

Greicius, M. D., Krasnow, B., Reiss, A. L., & Menon, V. (2003). Functional connectivity in the resting brain: A network analysis of the default mode hypothesis. *Proceedings of the National Academy of Sciences*, *100*(1), 253–258. https://doi.org/10.1073/pnas.0135058100

Grigg-damberger, M. M. (2016). Visual scoring of sleep in infants. *Journal of Clinical Sleep Medicine*, *12*(3). https://doi.org/10.5664/jcsm.5600

Guven, M., Yazici, B., Intes, X., & Chance, B. (2005). Diffuse optical tomography with *a priori* anatomical information. *Physics in Medicine and Biology*, *50*(12), 2837–2858. https://doi.org/10.1088/0031-9155/50/12/008

Hassanpour, M. S., White, B. R., Eggebrecht, A. T., Ferradal, S. L., Snyder, A. Z., & Culver, J. P. (2014). Statistical analysis of high density diffuse optical tomography. *NeuroImage*, *85*, 104–116. https://doi.org/10.1016/J.NEUROIMAGE.2013.05.105

Homae, F., Watanabe, H., Konishi, Y., Go, T., Taga, G., Nakano, T., & Otobe, T. (2010). Development of Global Cortical Networks in Early Infancy. *Journal of Neuroscience*, *30*(14), 4877–4882. https://doi.org/10.1523/jneurosci.5618-09.2010

Homae, F., Watanabe, H., Nakano, T., & Taga, G. (2007). Prosodic processing in the developing brain. *Neuroscience Research*, *59*(1), 29–39. https://doi.org/10.1016/j.neures.2007.05.005

Horovitz, S. G., Braun, A. R., Carr, W. S., Picchioni, D., Balkin, T. J., Fukunaga, M., & Duyn, J. H. (2009). Decoupling of the brain's default mode network during deep sleep. *Proceedings of the National Academy of Sciences*, *106*(27), 11376–11381. https://doi.org/10.1073/pnas.0901435106

Hoshi, Y., & Tamura, M. (1993). Detection of dynamic changes in cerebral oxygenation coupled to neuronal function during mental work in man. *Neuroscience Letters*, *150*(1), 5–8. Retrieved from http://www.ncbi.nlm.nih.gov/pubmed/8469403

Huang H., Huppi P., He Y., L. J. (2019). Imaging Baby Brain Development [Special Issue]. *NeuroImage*, *185*. Retrieved from https://www.sciencedirect.com/journal/neuroimage/special-issue/107GFHJHMRH

Huppert, T. J., Diamond, S. G., Franceschini, M. A., & Boas, D. A. (2009). HomER: a review of time-series analysis methods for near-infrared spectroscopy of the brain. *Applied Optics*, *48*(10), D280-98. Retrieved from http://www.ncbi.nlm.nih.gov/pubmed/19340120

Huppert, T. J., Hoge, R. D., Diamond, S. G., Franceschini, M. A., & Boas, D. A. (2006). A temporal comparison of BOLD, ASL, and NIRS hemodynamic responses to motor stimuli in adult humans. *NeuroImage*, *29*(2), 368–382. https://doi.org/10.1016/j.neuroimage.2005.08.065

Huttenlocher, D. P., Klanderman, G. A., & Rucklidge, W. J. (1993). Comparing images using the Hausdorff distance - Pattern Analysis and Machine Intelligence, IEEE Transactions on, *15*(9), 850–863.

Ijichi, S., Kusaka, T., Isobe, K., Okubo, K., Kawada, K., Namba, M., … Itoh, S. (2005). Developmental changes of optical properties in neonates determined by near-infrared time-resolved spectroscopy. *Pediatric Research*, *58*(3), 568–573. https://doi.org/10.1203/01.PDR.0000175638.98041.0E

Jaccard, P., & Zurich, E. (1901). Article in Bulletin de la Societe Vaudoise des Sciences Naturelles, (June). https://doi.org/10.5169/seals-266450

Jöbsis-vanderVliet, F. F. (1999). Discovery of the Near-Infrared Window into the Body and the Early Development of Near-Infrared Spectroscopy. *Journal of Biomedical Optics*, *4*(4), 392.

https://doi.org/10.1117/1.429952

Jobsis, F. (1977). Noninvasive, infrared monitoring of cerebral and myocardial oxygen sufficiency and circulatory parameters. *Science*, *198*(4323). Retrieved from http://science.sciencemag.org/content/198/4323/1264.long

Joel, S. E., Caffo, B. S., van Zijl, P. C. M., & Pekar, J. J. (2011). On the relationship between seed-based and ICA-based measures of functional connectivity. *Magnetic Resonance in Medicine*, *66*(3), 644–657. https://doi.org/10.1002/mrm.22818

Joseph, D. K., Huppert, T. J., Franceschini, M. A., & Boas, D. A. (2006). Diffuse optical tomography system to image brain activation with improved spatial resolution and validation with functional magnetic resonance imaging. *Applied Optics*, *45*(31), 8142–8151. Retrieved from http://www.ncbi.nlm.nih.gov/pubmed/17068557

Jurcak, V., Tsuzuki, D., & Dan, I. (2007). 10/20, 10/10, and 10/5 systems revisited: Their validity as relative head-surface-based positioning systems. *NeuroImage*, *34*, 1600–1611. https://doi.org/10.1016/j.neuroimage.2006.09.024

Kabdebon, C., Leroy, F., Simmonet, H., Perrot, M., Dubois, J., & Dehaene-Lambertz, G. (2014). Anatomical correlations of the international 10-20 sensor placement system in infants. *NeuroImage*, *99*(99), 342–356. Retrieved from https://www.infona.pl//resource/bwmeta1.element.elsevier-e2ed5e61-13d7-3e71-9402-77844bb5f2e8

Kato, T., Kamei, A., Takashima, S., & Ozaki, T. (1993). Human Visual Cortical Function during Photic Stimulation Monitoring by Means of near-Infrared Spectroscopy. *Journal of Cerebral Blood Flow & Metabolism*, *13*(3), 516–520. https://doi.org/10.1038/jcbfm.1993.66

Keller, J. B., Hedden, T., Thompson, T. W., Anteraper, S. A., Gabrieli, J. D. E., & Whitfield-Gabrieli, S. (2015). Resting-state anticorrelations between medial and lateral prefrontal cortex: Association with working memory, aging, and individual differences. *Cortex*, *64*, 271–280. https://doi.org/10.1016/j.cortex.2014.12.001

Kelly, A. M. C., Uddin, L. Q., Biswal, B. B., Castellanos, F. X., & Milham, M. P. (2008). Competition between functional brain networks mediates behavioral variability. *NeuroImage*, *39*(1), 527–537. https://doi.org/10.1016/J.NEUROIMAGE.2007.08.008

Keunen, K., Counsell, S. J., & Benders, M. J. (2017). The emergence of functional architecture during early brain development. *NeuroImage*. https://doi.org/10.1016/j.neuroimage.2017.01.047

Koch, S. P., Habermehl, C., Mehnert, J., Schmitz, C. H., Holtze, S., Villringer, A., … Obrig, H. (2010). High-resolution optical functional mapping of the human somatosensory cortex. *Frontiers in Neuroenergetics*, *2*, 12. https://doi.org/10.3389/fnene.2010.00012

Kuklisova-Murgasova, M., Aljabar, P., Srinivasan, L., Counsell, S. J., Doria, V., Serag, A., … Rueckert, D. (2011). A dynamic 4D probabilistic atlas of the developing brain. *NeuroImage*, *54*(4), 2750–2763. https://doi.org/10.1016/j.neuroimage.2010.10.019

Leamy, D. J., Ward, T. E., & Sweeney, K. T. (2011). Functional Near Infrared Spectroscopy (fNIRS) synthetic data generation. In *2011 Annual International Conference of the IEEE Engineering in Medicine and Biology Society* (Vol. 2011, pp. 6589–6592). IEEE. https://doi.org/10.1109/IEMBS.2011.6091625

Liang, M., Zhou, Y., Jiang, T., Liu, Z., Tian, L., Liu, H., & Hao, Y. (2006). Widespread functional disconnectivity

in schizophrenia with resting-state functional magnetic resonance imaging. *Neuroreport*, *17*(2), 209–213. Retrieved from http://www.ncbi.nlm.nih.gov/pubmed/16407773

Liu, W. C., Flax, J. F., Guise, K. G., Sukul, V., & Benasich, A. A. (2008). Functional connectivity of the sensorimotor area in naturally sleeping infants. *Brain Research*, *1223*, 42–49. https://doi.org/10.1016/j.brainres.2008.05.054

Lloyd-Fox, S., Blasi, A., & Elwell, C. E. (2010). Illuminating the developing brain: The past, present and future of functional near infrared spectroscopy. *Neuroscience & Biobehavioral Reviews*, *34*(3), 269–284. https://doi.org/10.1016/j.neubiorev.2009.07.008

Lloyd-Fox, S., Papademetriou, M., Darboe, M. K., Everdell, N. L., Wegmuller, R., Prentice, A. M., … Elwell, C. E. (2015). Functional near infrared spectroscopy (fNIRS) to assess cognitive function in infants in rural Africa. *Scientific Reports*, *4*(1), 4740. https://doi.org/10.1038/srep04740

Logothetis, N. K., & Pfeuffer, J. (2004). On the nature of the BOLD fMRI contrast mechanism. *Magnetic Resonance Imaging*, *22*(10), 1517–1531. https://doi.org/10.1016/j.mri.2004.10.018

Lowe, M. J., Phillips, M. D., Lurito, J. T., Mattson, D., Dzemidzic, M., & Mathews, V. P. (2002). Multiple Sclerosis: Low-Frequency Temporal Blood Oxygen Level–Dependent Fluctuations Indicate Reduced Functional Connectivity—Initial Results. *Radiology*, *224*(1), 184–192. https://doi.org/10.1148/radiol.2241011005

Lu, C.-M., Zhang, Y.-J., Biswal, B. B., Zang, Y.-F., Peng, D.-L., & Zhu, C.-Z. (2010). Use of fNIRS to assess resting state functional connectivity. *Journal of Neuroscience Methods*, *186*(2), 242–249. https://doi.org/10.1016/j.jneumeth.2009.11.010

Lv, X. H., Wang, X. Z., Tong, X. E., Williams, X. L. M., Zaharchuk, X. G., Zeineh, X. M., … Wintermark, X. M. (2018). Resting-State Functional MRI: Everything That Nonexperts Have Always Wanted to Know. https://doi.org/10.3174/ajnr.A5527

Madsen, S. J. (2013). *Optical methods and instrumentation in brain imaging and therapy*. Springer.

McCormick, E. M., & Telzer, E. H. (2018). Contributions of default mode network stability and deactivation to adolescent task engagement. *Scientific Reports*, *8*(1), 18049. https://doi.org/10.1038/s41598-018-36269-4

Mohammadi-Nejad, A. R., Mahmoudzadeh, M., Hassanpour, M. S., Wallois, F., Muzik, O., Papadelis, C., … Nasiriavanaki, M. (2018). Neonatal brain resting-state functional connectivity imaging modalities. *Photoacoustics*, *10*, 1–19. https://doi.org/10.1016/j.pacs.2018.01.003

Murphy, K., Birn, R. M., Handwerker, D. A., Jones, T. B., & Bandettini, P. A. (2009). The impact of global signal regression on resting state correlations: Are anti-correlated networks introduced? *NeuroImage*, *44*(3), 893–905. https://doi.org/10.1016/j.neuroimage.2008.09.036

Murphy, K., & Fox, M. D. (2017). Towards a consensus regarding global signal regression for resting state functional connectivity MRI. *NeuroImage*, *154*(November), 169–173. https://doi.org/10.1016/j.neuroimage.2016.11.052

Neumaier, A. (1998). Solving Ill-Conditioned and Singular Linear Systems: A Tutorial on Regularization. *SIAM Review*, *40*(3), 636–666. https://doi.org/10.1137/S0036144597321909

Niu, H., & He, Y. (2014). Resting-State Functional Brain Connectivity. *The Neuroscientist*, *20*(2), 173–188. https://doi.org/10.1177/1073858413502707

Oostenveld, R., & Praamstra, P. (2001). The five percent electrode system for high-resolution EEG and ERP measurements. *Clinical Neurophysiology : Official Journal of the International Federation of Clinical Neurophysiology*, *112*(4), 713–719. Retrieved from http://www.ncbi.nlm.nih.gov/pubmed/11275545

Orekhova, E. V, Elsabbagh, M., Jones, E. J., Dawson, G., Charman, T., & Johnson, M. H. (2014). EEG hyper-connectivity in high-risk infants is associated with later autism. *Journal of Neurodevelopmental Disorders*, *6*(1), 40. https://doi.org/10.1186/1866-1955-6-40

Padmanabhan, A., Lynch, C. J., Schaer, M., & Menon, V. (2017). The Default Mode Network in Autism. *Biological Psychiatry. Cognitive Neuroscience and Neuroimaging*, *2*(6), 476–486. https://doi.org/10.1016/j.bpsc.2017.04.004

Perdue, K. L., Fang, Q., & Diamond, S. G. (2012). Quantitative assessment of diffuse optical tomography sensitivity to the cerebral cortex using a whole-head probe. *Physics in Medicine and Biology*, *57*(10), 2857–2872. https://doi.org/10.1088/0031-9155/57/10/2857

PERINATAL CARE PERINATAL CARE Seventh Edition Guidelines for Guidelines for. (2012). Retrieved from https://www.healthplan.org/sites/default/files/documents/resources/quality-measures/GuidelinesforPerinatalCare.pdf

Perutz, M. (1995). Hoppe-Seyler, Stokes and haemoglobin. *Biological Chemistry Hoppe-Seyler*, *376*(8), 449–450. Retrieved from http://www.ncbi.nlm.nih.gov/pubmed/7576244

Pinti, P., Merla, A., Aichelburg, C., Lind, F., Power, S., Swingler, E., … Tachtsidis, I. (2017). A novel GLM-based method for the Automatic IDentification of functional Events (AIDE) in fNIRS data recorded in naturalistic environments. https://doi.org/10.1016/j.neuroimage.2017.05.001

Pogue, B. W., Patterson, M. S., Jiang, H., & Paulsen, K. D. (1995). Initial assessment of a simple system for frequency domain diffuse optical tomography. *Physics in Medicine and Biology*, *40*(10), 1709–1729. https://doi.org/10.1088/0031-9155/40/10/011

Prahl, S. (1999). Optical absorption of Hemoglobin (http://omlc.ogi.edu/spectra/hemoglobin/index.html). Retrieved from https://omlc.org/spectra/hemoglobin/

Raichle, M. E., MacLeod, A. M., Snyder, A. Z., Powers, W. J., Gusnard, D. A., & Shulman, G. L. (2001). A default mode of brain function. *Proceedings of the National Academy of Sciences*, *98*(2), 676–682. https://doi.org/10.1073/pnas.98.2.676

Raichle, M. E., & Mintun, M. A. (2006). BRAIN WORK AND BRAIN IMAGING. *Annual Review of Neuroscience*, *29*(1), 449–476. https://doi.org/10.1146/annurev.neuro.29.051605.112819

Redcay, E., Moran, J. M., Mavros, P. L., Tager-Flusberg, H., Gabrieli, J. D. E., & Whitfield-Gabrieli, S. (2013). Intrinsic functional network organization in high-functioning adolescents with autism spectrum disorder. *Frontiers in Human Neuroscience*, *7*, 573. https://doi.org/10.3389/fnhum.2013.00573

Rosazza, C., & Minati, L. (2011). Resting-state brain networks: literature review and clinical applications. *Neurological Sciences*, *32*(5), 773–785. https://doi.org/10.1007/s10072-011-0636-y

Rothbart, M. K., & Posner, M. (2001). Mechanism and variation in the development of attentional networks. *Handbook of Developmental Cognitive Neuroscience*, (January 2001), p.353-363. Retrieved from http://faculty.oxy.edu/clint/physio/article/MechanismsandvariatinintheDevelopmentofAttentionalNetworks.pdf

Sasai, S., Homae, F., Watanabe, H., Sasaki, A. T., Tanabe, H. C., Sadato, N., & Taga, G. (2012). A NIRS–fMRI study of resting state network. *NeuroImage*, *63*(1), 179–193. https://doi.org/10.1016/j.neuroimage.2012.06.011

Scholkmann, F., Kleiser, S., Metz, A. J., Zimmermann, R., Mata Pavia, J., Wolf, U., & Wolf, M. (2014). A review on continuous wave functional near-infrared spectroscopy and imaging instrumentation and methodology. *NeuroImage*. https://doi.org/10.1016/j.neuroimage.2013.05.004

Schöpf, V., Kasprian, G., Brugger, P. C., & Prayer, D. (2012). Watching the fetal brain at 'rest.' *International Journal of Developmental Neuroscience*, *30*(1), 11–17. https://doi.org/10.1016/j.ijdevneu.2011.10.006

Seeley, W. W., Crawford, R. K., Zhou, J., Miller, B. L., & Greicius, M. D. (2009). Neurodegenerative diseases target large-scale human brain networks. *Neuron*, *62*(1), 42–52. https://doi.org/10.1016/j.neuron.2009.03.024

Shine, J. M., & Breakspear, M. (2018). Understanding the Brain, By Default. *Trends in Neurosciences*, *41*(5), 244–247. https://doi.org/10.1016/j.tins.2018.03.004

Singh, H., Cooper, R. J., Wai Lee, C., Dempsey, L., Edwards, A., Brigadoi, S., … Austin, T. (2014). Mapping cortical haemodynamics during neonatal seizures using diffuse optical tomography: A case study. *NeuroImage: Clinical*, *5*, 256–265. https://doi.org/10.1016/J.NICL.2014.06.012

Smith, J. K., Hernandez-Castillo, C. R., Lin, W., Elton, A., Ramirez, J., Alcauter, S., & Gao, W. (2014). Functional Network Development During the First Year: Relative Sequence and Socioeconomic Correlations. *Cerebral Cortex*, *25*(9), 2919–2928. https://doi.org/10.1093/cercor/bhu088

Smith, S. M., Fox, P. T., Miller, K. L., Glahn, D. C., Fox, P. M., Mackay, C. E., … Beckmann, C. F. (2009). Correspondence of the brain's functional architecture during activation and rest. *Proceedings of the National Academy of Sciences of the United States of America*, *106*(31), 13040–13045. https://doi.org/10.1073/pnas.0905267106

Smyser, C. D., Inder, T. E., Shimony, J. S., Hill, J. E., Degnan, A. J., Snyder, A. Z., & Neil, J. J. (2010a). Longitudinal analysis of neural network development in preterm infants. *Cerebral Cortex*, *20*(12), 2852–2862. https://doi.org/10.1093/cercor/bhq035

Smyser, C. D., Inder, T. E., Shimony, J. S., Hill, J. E., Degnan, A. J., Snyder, A. Z., & Neil, J. J. (2010b). Longitudinal Analysis of Neural Network Development in Preterm Infants. https://doi.org/10.1093/cercor/bhq035

Souweidane, M. M., Kim, K. H. S., McDowall, R., Ruge, M. I., Lis, E., Krol, G., & Hirsch, J. (1999). Brain Mapping in Sedated Infants and Young Children with Passive-Functional Magnetic Resonance Imaging. *Pediatric Neurosurgery*, *30*(2), 86–92. https://doi.org/10.1159/000028768

Sporns, O., Tononi, G., & Kötter, R. (2005). The Human Connectome: A Structural Description of the Human Brain. *PLoS Computational Biology*, *1*(4), e42. https://doi.org/10.1371/journal.pcbi.0010042

Stefanski, M., Schulze, K., Bateman, D., Kairam, R., Pedley, T. A., Masterson, J., & James, L. S. (1984). A scoring system for states of sleep and wakefulness in term and preterm infants. *Pediatric Research*, *18*(1), 58–62. Retrieved from http://www.ncbi.nlm.nih.gov/pubmed/6701035

Stiles, J., & Jernigan, T. L. (2010). The basics of brain development. *Neuropsychology Review*, *20*(4), 327–348. https://doi.org/10.1007/s11065-010-9148-4

Strangman, G. E., Li, Z., & Zhang, Q. (2013). Depth Sensitivity and Source-Detector Separations for Near Infrared Spectroscopy Based on the Colin27 Brain Template. *PLoS ONE*, *8*(8), e66319. https://doi.org/10.1371/journal.pone.0066319

Strangman, G., Franceschini, M. A., & Boas, D. A. (2003). Factors affecting the accuracy of near-infrared spectroscopy concentration calculations for focal changes in oxygenation parameters. *NeuroImage*, *18*(4), 865–879. Retrieved from http://www.ncbi.nlm.nih.gov/pubmed/12725763

Supekar, K., Menon, V., Rubin, D., Musen, M., & Greicius, M. D. (2008). Network Analysis of Intrinsic Functional Brain Connectivity in Alzheimer's Disease. *PLoS Computational Biology*, *4*(6), e1000100. https://doi.org/10.1371/journal.pcbi.1000100

Taga, G., Konishi, Y., Maki, A., Tachibana, T., Fujiwara, M., & Koizumi, H. (2000). Spontaneous oscillation of oxy- and deoxy- hemoglobin changes with a phase difference throughout the occipital cortex of newborn infants observed using non-invasive optical topography. *Neuroscience Letters*, *282*(1–2), 101–104. https://doi.org/10.1016/S0304-3940(00)00874-0

Tak, S, Uga, M., Flandin, G., Dan, I., & Penny, W. D. (2016). Sensor space group analysis for fNIRS data. *Journal of Neuroscience Methods*, *264*, 103–112. https://doi.org/10.1016/j.jneumeth.2016.03.003

Tak, Sungho, & Ye, J. C. (2013). Statistical analysis of fNIRS data: A comprehensive review. https://doi.org/10.1016/j.neuroimage.2013.06.016

Thomason, M. E., Dassanayake, M. T., Shen, S., Katkuri, Y., Alexis, M., Anderson, A. L., … Romero, R. (2013). Cross-hemispheric functional connectivity in the human fetal brain. *Science Translational Medicine*, *5*(173), 173ra24. https://doi.org/10.1126/scitranslmed.3004978

Thomason, M. E., Grove, L. E., Lozon, T. A., Vila, A. M., Ye, Y., Nye, M. J., … Romero, R. (2015). Age-related increases in long-range connectivity in fetal functional neural connectivity networks in utero. *Developmental Cognitive Neuroscience*, *11*, 96–104. https://doi.org/10.1016/j.dcn.2014.09.001

Thorngren-Jerneck, K., Ohlsson, T., Sandell, A., Erlandsson, K., Strand, S.-E., Ryding, E., & Svenningsen, N. W. (2001). Cerebral Glucose Metabolism Measured by Positron Emission Tomography in Term Newborn Infants with Hypoxic Ischemic Encephalopathy. *Pediatric Research*, *49*(4), 495–501. https://doi.org/10.1203/00006450-200104000-00010

Tikhonov, A. N., Goncharsky, A. V., Stepanov, V. V., & Yagola, A. G. (1995). Numerical methods for the approximate solution of ill-posed problems on compact sets. In *Numerical Methods for the Solution of Ill-Posed Problems* (pp. 65–79). Dordrecht: Springer Netherlands. https://doi.org/10.1007/978-94-015-8480-7_3

Tokariev, A., Videman, M., Palva, J. M., & Vanhatalo, S. (2016). Functional Brain Connectivity Develops Rapidly Around Term Age and Changes Between Vigilance States in the Human Newborn. *Cerebral Cortex*, *26*(12), 4540–4550. https://doi.org/10.1093/cercor/bhv219

Tong, Y., Bergethon, P. R., & Frederick, B. D. (2011). An improved method for mapping cerebrovascular reserve using concurrent fMRI and near-infrared spectroscopy with Regressor Interpolation at Progressive Time Delays (RIPTiDe). *NeuroImage*, *56*(4), 2047–2057. https://doi.org/10.1016/j.neuroimage.2011.03.071

Torricelli, A., Contini, D., Pifferi, A., Caffini, M., Re, R., Zucchelli, L., & Spinelli, L. (2014). Time domain functional NIRS imaging for human brain mapping. *NeuroImage*, *85*, 28–50.

https://doi.org/10.1016/j.neuroimage.2013.05.106

Tremblay, J., Martínez-Montes, E., Vannasing, P., Nguyen, D. K., Sawan, M., Lepore, F., & Gallagher, A. (2018). Comparison of source localization techniques in diffuse optical tomography for fNIRS application using a realistic head model. *Biomedical Optics Express*, *9*(7), 2994. https://doi.org/10.1364/BOE.9.002994

Uddin, L. Q., Clare Kelly, A. M., Biswal, B. B., Xavier Castellanos, F., & Milham, M. P. (2009). Functional connectivity of default mode network components: Correlation, anticorrelation, and causality. *Human Brain Mapping*, *30*(2), 625–637. https://doi.org/10.1002/hbm.20531

van de Ven, V. G., Formisano, E., Prvulovic, D., Roeder, C. H., & Linden, D. E. J. (2004). Functional connectivity as revealed by spatial independent component analysis of fMRI measurements during rest. *Human Brain Mapping*, *22*(3), 165–178. https://doi.org/10.1002/hbm.20022

van den Heuvel, M. P., & Hulshoff Pol, H. E. (2010). Exploring the brain network: A review on resting-state fMRI functional connectivity. *European Neuropsychopharmacology*, *20*(8), 519–534. https://doi.org/10.1016/j.euroneuro.2010.03.008

van den Heuvel, M. P., Mandl, R. C. W., Kahn, R. S., & Hulshoff Pol, H. E. (2009). Functionally linked resting-state networks reflect the underlying structural connectivity architecture of the human brain. *Human Brain Mapping*, *30*(10), 3127–3141. https://doi.org/10.1002/hbm.20737

Vilain, E. (2014). *Near Infrared Spectroscopy Systems for Tissue Oximetry*.

Villringer, A., Planck, J., Hock, C., Schleinkofer, L., & Dirnagl, U. (1993). Near infrared spectroscopy (NIRS): a new tool to study hemodynamic changes during activation of brain function in human adults. *Neuroscience Letters*, *154*(1–2), 101–104. Retrieved from http://www.ncbi.nlm.nih.gov/pubmed/8361619

Vincent, J. L., Kahn, I., Snyder, A. Z., Raichle, M. E., & Buckner, R. L. (2008). Evidence for a Frontoparietal Control System Revealed by Intrinsic Functional Connectivity. *Journal of Neurophysiology*, *100*(6), 3328–3342. https://doi.org/10.1152/jn.90355.2008

Vincent, J. L., Patel, G. H., Fox, M. D., Snyder, A. Z., Baker, J. T., Van Essen, D. C., … Raichle, M. E. (2007). Intrinsic functional architecture in the anaesthetized monkey brain. *Nature*, *447*(7140), 83–86. https://doi.org/10.1038/nature05758

Wang, J., Dong, Q., & Niu, H. (2017). The minimum resting-state fNIRS imaging duration for accurate and stable mapping of brain connectivity network in children. *Scientific Reports*, *7*(1), 6461. https://doi.org/10.1038/s41598-017-06340-7

Wang, L., Jacques, S. L., & Zheng, L. (1995). MCML—Monte Carlo modeling of light transport in multi-layered tissues. *Computer Methods and Programs in Biomedicine*, *47*(2), 131–146. https://doi.org/10.1016/0169-2607(95)01640-F

Wang, L., Zhu, C., He, Y., Zang, Y., Cao, Q., Zhang, H., … Wang, Y. (2009). Altered small-world brain functional networks in children with attention-deficit/hyperactivity disorder. *Human Brain Mapping*, *30*(2), 638–649. https://doi.org/10.1002/hbm.20530

Wang, Lihong V., & Wu, H.-I. (2009). *Biomedical Optics*. Hoboken, NJ, USA: John Wiley & Sons, Inc. https://doi.org/10.1002/9780470177013

Webb, S. J., Monk, C. S., & Nelson, C. A. (2001). Mechanisms of Postnatal Neurobiological Development:

Implications for Human Development. *Developmental Neuropsychology*, *19*(2), 147–171. https://doi.org/10.1207/S15326942DN1902_2

Welvaert, M., Durnez, J., Moerkerke, B., Verdoolaege, G., & Rosseel, Y. (2011). **neuRosim** : An *R* Package for Generating fMRI Data. *Journal of Statistical Software*, *44*(10), 1–18. https://doi.org/10.18637/jss.v044.i10

Weng, S.-J., Wiggins, J. L., Peltier, S. J., Carrasco, M., Risi, S., Lord, C., & Monk, C. S. (2010). Alterations of resting state functional connectivity in the default network in adolescents with autism spectrum disorders. *Brain Research*, *1313*, 202–214. https://doi.org/10.1016/j.brainres.2009.11.057

White, B. R., & Culver, J. P. (2010). Quantitative evaluation of high-density diffuse optical tomography: <italic>in vivo</italic> resolution and mapping performance. *Journal of Biomedical Optics*, *15*(2), 026006. https://doi.org/10.1117/1.3368999

White, B. R., Liao, S. M., Ferradal, S. L., Inder, T. E., & Culver, J. P. (2012). Bedside optical imaging of occipital resting-state functional connectivity in neonates. *NeuroImage*, *59*(3), 2529–2538. https://doi.org/10.1016/j.neuroimage.2011.08.094

White, B. R., Snyder, A. Z., Cohen, A. L., Petersen, S. E., Raichle, M. E., Schlaggar, B. L., & Culver, J. P. (2009). Resting-state functional connectivity in the human brain revealed with diffuse optical tomography. *NeuroImage*, *47*(1), 148–156. https://doi.org/10.1016/j.neuroimage.2009.03.058

Wilson, B. C., & Adam, G. (1983). A Monte Carlo model for the absorption and flux distributions of light in tissue. *Medical Physics*, *10*(6), 824–830. https://doi.org/10.1118/1.595361

Wolf, M., Morren, G., Haensse, D., Karen, T., Wolf, U., Fauchère, J., & Bucher, H. (2008a). Near infrared spectroscopy to study the brain: an overview. *Opto-Electronics Review*, *16*(4), 413–419. https://doi.org/10.2478/s11772-008-0042-z

Wolf, M., Morren, G., Haensse, D., Karen, T., Wolf, U., Fauchère, J., & Bucher, H. (2008b). Near infrared spectroscopy to study the brain: an overview. *Opto-Electronics Review*, *16*(4), 413. https://doi.org/10.2478/s11772-008-0042-z

Yamada, H., Yonekura, Y., Sadato, N., Ishii, Y., Tanaka, M., Konishi, Y., & Kimura, K. (2003). A rapid brain metabolic change in infants detected by fMRI. *NeuroReport*, *8*(17), 3775–3778. https://doi.org/10.1097/00001756-199712010-00024

Zeff, B. W., White, B. R., Dehghani, H., Schlaggar, B. L., & Culver, J. P. (2007). Retinotopic mapping of adult human visual cortex with high-density diffuse optical tomography. *Proceedings of the National Academy of Sciences of the United States of America*, *104*(29), 12169–12174. https://doi.org/10.1073/pnas.0611266104

Zhang, H., Zhang, Y.-J., Lu, C.-M., Ma, S.-Y., Zang, Y.-F., & Zhu, C.-Z. (2010). Functional connectivity as revealed by independent component analysis of resting-state fNIRS measurements. *NeuroImage*, *51*(3), 1150–1161. https://doi.org/10.1016/j.neuroimage.2010.02.080

Zhao, J., Ding, H. S., Hou, X. L., Zhou, C. Le, & Chance, B. (2005). In vivo determination of the optical properties of infant brain using frequency-domain near-infrared spectroscopy. *Journal of Biomedical Optics*, *10*(2), 024028. https://doi.org/10.1117/1.1891345

Zimeo Morais, G. A., Balardin, J. B., & Sato, J. R. (2018). fNIRS Optodes' Location Decider (fOLD): a toolbox for probe arrangement guided by brain regions-of-interest. *Scientific Reports*, *8*(1), 3341.

https://doi.org/10.1038/s41598-018-21716-z

Zucchelli, L., Caffini, M., Cattarossi, L., Filippin, L., Fló, A., Torricelli, A., … Ferry, A. L. (2017). In vivo measure of neonate brain optical properties and hemodynamic parameters by time-domain near-infrared spectroscopy. *Neurophotonics*, *4*(04), 1. https://doi.org/10.1117/1.nph.4.4.041414